One and two photon excitation properties of selected biologically important molecules
by Bruce Eldon Anderson

A thesis submitted in partial fulfillment of the requirements for the degree of Doctor of Philosophy in Philosphy in Chemistry
Montana State University

Abstract:
5-Methyleytosine''s polarized fluorescence is observed in room temperature, aqueous solution. Intrinsic lifetimes, fluorescence lifetimes and quantum yields are calculated for the protonated neutral and deprotonated species of this molecule. Rotational correlation times times calculated from experimental polarization ratios, quantum yields and intrinsic lifetimes are compared with those predicted by sticking hydrodynamics and found to be, at most, three to four times shorter. Also, the cation of 5-methyl cytosine appears to rotationally diffuse twice as slowly as the natural and anion forms. In addition, possible sources of the wavelength of excitation dependence in the quantum yields of 5-methylcytosine and thymine in low temperature glasses are investigated. Thymine''s fluorescence excitation is seen nearly to match its absorption spectrum in ethano1-methanol glasses, supporting the idea that its wavelength of excitation dependent quantum yield is caused by the equilibrium of hydrogen and non-hydrogen bonded species in hydroxylic solvents. Investigations of the of SMC in neutral and acidic ethylene glycol-water glasses show that the cation of this molecule fluoresces with seven times greater efficiency at 143K than the neutral form. This, coupled with the observation that the pi* of 5-methyl cytosine shifts from 4.6 in room temperature aqueous solution to 7.0 in glass solution at 143K accounts for the wavelength of excitation dependence of 5-methyl cytosine''s quantum yield in hydroxylic solvent glasses. Cytidine''s and thymine''s pka''s are also seen to shift in ethyleneglycol water glasses at 143K, the latter by 2.6 pH units to 6.80. Finally, the two-photon fluorescence excitation spectrum (TPE) of benzimidazole is viewed for the first time. By comparison with the UV absorption spectrum of this molecule with that of indole and through use of circularly and linearly polarized two photon excitation, individual transitions in the TPE are identified. The La band, though predicted by CNDOS-CI to be very intense, is not seen in the TPE of benzimidazole. Lb''s Franck Condon transitions are clearly visible in the TPE, and two peaks, not seen in the one photon absorption are observed. These peaks are assigned to vibronic transitions within the manifold. Additionally, the La 0-0 transition of benzimidazole is identified in the one photon absorption spectrum.

ONE AND TWO PHOTON EXCITATION PROPERTIES OF SELECTED BIOLOGICALLY IMPORTANT MOLECULES

by

Bruce Eldon Anderson

A thesis submitted in partial fulfillment
of the requirements for the degree

of

Doctor of Philosophy

in

Chemistry

MONTANA STATE UNIVERSITY
Bozeman, Montana

July 1983

APPROVAL

of a thesis submitted by

Bruce Eldon Anderson

This thesis has been read by each member of the thesis committee and has been found to be satisfactory regarding content, English usage, format, citations, bibliographic style, and consistency, and is ready for submission to the College of Graduate Studies.

Aug 4, 1983
Date

Patrick R Callis
Chairperson, Graduate Committee

Approved for the Major Department

aug 4 1983
Date

Edwin H Abbott
Head, Major Department

Approved for the College of Graduate Studies

8-5-83
Date

Michael Malone
Graduate Dean

STATEMENT OF PERMISSION TO USE

In presenting this thesis in partial fulfillment of the requirements for a doctoral degree at Montana State University, I agree that the Library shall make it available to borrowers under rules of the Library. I further agree that copying of this thesis is allowable only for scholarly purposes, consistent with "fair use" as prescribed in the U.S. Copyright Law. Requests for extensive copying or reproduction of this thesis should be referred to University Microfilms International, 300 North Zeeb Road, Ann Arbor, Michigan 48106, to whom I have granted "the exclusive right to reproduce and distribute copies of the dissertation in and from microfilm and the right to reproduce and distribute by abstract in any format."

Signature Bruce Anderson

Date Aug 4, 1983

In memory of my father, John Pershing Anderson.

VITA

Bruce Eldon Anderson was born November 29, 1954 in Anniston, Alabama, to Iva F. and John P. Anderson. After receiving his diploma from Walter Wellborn High School in Anniston, he attended Auburn University and Jacksonville State University, receiving his B. S. degree in chemistry from Jacksonville State University in 1976. After roofing houses and building homes for a year, he enrolled as a graduate student in chemistry at Montana State University in the Fall of 1977. In June 1979 he married Kathleen Brunke, a fellow graduate student.

ACKNOWLEDGMENT

I wish to thank Profesor Patrik Callis for his teaching and moral support throughout my graduate stay. My appreciation is also extended to Dr. Richard Geer and Mr. Berk Knighton for their invaluable help with designing circuitry and in trouble-shooting electronic devices. Dr. Reed Howald and Dr. Eric Grimsrud are also due special thanks for helpful discussions and encouragement.

I also wish to express my gratitude to Tim Aoki, Berk Knighton and Richard Jones, my office partners, co-laborers and fishing buddies throughout my graduate career.

Finally, I wish to thank my wife, Kathleen Brunke, for her tremendous help in assembling this thesis and for her encouragement when my spirit waned.

TABLE OF CONTENTS

TABLE OF CONTENTS (continued)

LIST OF TABLES

LIST OF FIGURES

LIST OF FIGURES (continued)

LIST OF FIGURES (continued)

ABSTRACT

5-Methylcytosine's polarized fluorescence is observed in room temperature, aqueous solution. Intrinsic lifetimes, fluorescence lifetimes and quantum yields are calculated for the protonated neutral and deprotonated species of this molecule. Rotational correlation times times calculated from experimental polarization ratios, quantum yields and intrinsic lifetimes are compared with those predicted by sticking hydrodynamics and found to be, at most, three to four times shorter. Also, the cation of 5-methyl cytosine appears to rotationally diffuse twice as slowly as the netural and anion forms.

In addition, possible sources of the wavelength of excitation dependence in the quantum yields of 5-methylcytosine and thymine in low temperature glasses are investigated. Thymine's fluorescence excitation is seen nearly to match its absorption spectrum in ethanol-methanol glasses, supporting the idea that its wavelength of excitation dependent quantum yield is caused by the equilibrium of hydrogen and non-hydrogen bonded species in hydroxylic solvents.

Investigations of the ϕ_f of 5MC in neutral and acidic ethylene glycol-water glasses show that the cation of this molecule fluoresces with seven times greater efficiency at 143K than the neutral form. This, coupled with the observation that the pK_a of 5-methyl cytosine shifts from 4.6 in room temperature aqueous solution to 7.0 in glass solution at 143K accounts for the wavelength of excitation dependence of 5-methyl cytosine's quantum yield in hydroxylic solvent glasses. Cytidine's and thymine's pK_a's are also seen to shift in ethylene-glycol water glasses at 143K, the latter by 2.6 pH units to 6.80.

Finally, the two-photon fluorescence excitation spectrum (TPE) of benzimidazole is viewed for the first time. By comparison with the UV absorption spectrum of this molecule with that of indole and through use of circularly and linearly polarized two photon excitation, individual transitions in the TPE are identified. The L_a band, though predicted by CNDOS-CI to be very intense, is not seen in the TPE of benzimidazole. L_b's Franck Condon transitions are clearly visible in the TPE, and two peaks, not seen in the one photon absorption are observed. These peaks are assigned to vibronic transitions within the L_b manifold. Additionally, the L_a 0-0 transition of benzimidazole is identified in the one photon absorption spectrum.

INTRODUCTION

Pictured below are the four bases of DNA.

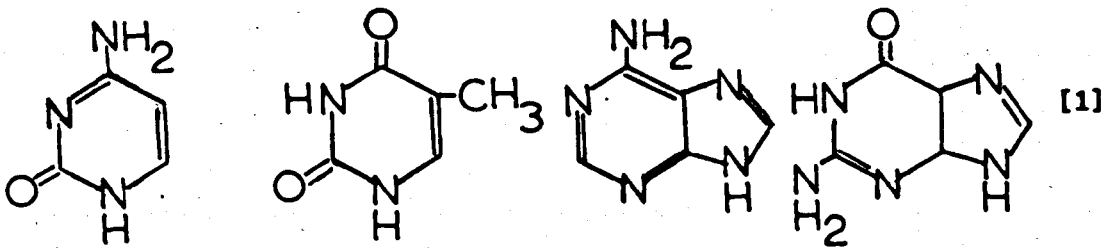

[1]

cytosine thymine adenine guanine

Research on the photophysical properties of these molecules has been an active field of endeavor for more than twenty years (for review, see reference 1). Their absorptions and emissions have been studied under varied conditions of temperature, pH, solvents and concentration. Through this accumulation of work, there now exists a partial understanding of the nature of the ground and excited states of the bases. There remains, however, a number of unexplained or, perhaps, unexplored questions in the area. The text of this thesis will address three such problems. The first section, entitled "Polarized Fluorescence of 5-Methylcytosine" examines the fluorescence and rotational lifetimes of this cytosine derivative in room temperature aqueous soltuion as calculated by two different methods.

The second part of this thesis details an investigation of the wavelength of excitation dependent fluorescence quantum yields of 5-methylcytosine, thymine and cytidine in low temperature ethylene glycol-water glasses.

Finally, in part three, the two-photon fluorescence excitation spectrum of benzimidazole, a molecule akin to the purine bases, is presented.

Polarized Fluorescence of 5-Methylcytosine

All the DNA bases are known to possess relatively low fluorescence quantum yields (on the order of 10^{-4} at 20°C), a factor which prevented the detection of their emissions at ambient temperatures until a decade ago (2). Quantum yields (ϕ_f) of 10^{-4} combined with calculated radiative lifetimes of 10^{-8}'s imply, through the relationship $\tau_f = \tau_0\phi_f$ (where τ_f and τ_0 are the fluorescence and radiative lifetimes, respectively), that the lifetime of the lowest excited singlets of the DNA bases are on the order of 10^{-12}s. Since the DNA bases are thought to possess absorption bands which are composite of more than one electronic transition, it is of some importance to know their fluorescence lifetimes.

If τ_f values are longer than those expected, emission is from weakly allowed states and not those giving rise to strongly allowed transitions seen in the typical UV absorption spectrum. Lifetimes found by use of the Strickler-Berg method (3) would not uncover such

abnormalities since they depend on integration of the entire first absorption band (4).

One way of measuring fluorescence lifetimes is through the use of the Perrins equation which is shown below,

$$\frac{1}{P} = \left(\frac{1}{P_o + .33}\right)\left(1 + \frac{\tau_f}{\tau_c}\right) \qquad [1]$$

where P is the measured fluorescence polarization $\{P_1 = (I_v - I_h)/(I_v + I_h)\}$, P_o is the polarization in the absence of rotational diffusion, and τ_c is the rotational correlation time which is a measure of the decay of fluorescence.

Since the τ_f values predicted for the bases are shorter than their expected rotational correlation times, their fluorescence should be highly polarized and indeed, polarization ratios for adenine, guanine, cytosine and thymine have been found to approach those seen in rigid media (5,6). An upper limit of τ_c can be calculated by Stokes-Einstein hydrodynamics (τ_c^{stick}) and comparisons can be made between τ_f from the Perrin equation above and τ_f^{SB} obtained through the Strickler-Berg equation to gain insight into the feasibility of either method. Conversly, τ_c^{stick} and τ_c^{SB} can be compared.

Morgan and Daniels (6) made use of the Perrin equation and the relationships discussed above to examine the τ_c^{SB} and of 5-methylcytosine (5MC). They found what was thought to be a unique property in this molecule, that of a pH dependent ϕ_f and τ_f. By plotting the inverse polarization ratio versus the ϕ_f of 5MC, they

obtained a linear graph, the slope of which indicated to them that τ_c^{stick} is about 50 times longer than τ_c^{SB}. Or, conversely, that τ_f^{stick} is 50 times longer than τ_f^{SB}.

Callis (5) obtained quite different results than those presented by Morgan and Daniels (6). Through polarized fluorescence studies at room temperature and low temperature (to obtain limiting polarization ratios), he concluded that τ_c^{SB} is only 3 to 4 times faster than τ_c^{stick} for the DNA bases.

Since the results of the two studies discussed above were in such blatant disagreement, we thought it necessary to study the hydrodynamics of these systems more carefully. In the work presented in chapter 3 of this thesis, a presentation of the quantum yields and polarization ratios of 5MC as a function of pH will appear. In addition, calculated τ_0's and τ_c^{stick} values for the cation, neutral and anion species of 5MC along with experimental lifetimes will be presented. The results of this work shows that rotational diffusion times calculated by Stokes-Einstein hydrodynamics are, at most, five times longer than those predicted by the Strickler-Berg equation and that the linear graph of 1/P vs. ϕ_f obtained by Morgan and Daniels is merely a fortuitous property of 5MC and its protonated and deprotonated species.

Wavelength Dependent Quantum Yields of 5-Methylcytosine, Cytidine and Thymine

In addition to the above study on the fluorescence and polarization of 5MC in room temperature aqueous solution, the

photophysical properties of this molecule, cytidine and thymine were examined at low temperature. Figure 1 shows the absorption (ABS) and fluorescence excitation spectrum (FES) of 5MC in neutral (pH = 7.0) ethylene glycol-water (EGW) at -130°C. You should note that the FES peak is shifted some 10 nm to longer wavelength than the ABS maximum. Close correlation is seen in both the onsets and minima of the two curves. However, the excitation is seen to be a factor of seven larger near the 0 - 0 transition with the ratio declining to 1 at 275 nm and to near .6 at the ABS minimum.

Fluorescence excitation spectra are merely the product of a molecule's fluorescence quantum efficiency and its absorption spectrum as a function of wavelength. If the quantum yield of a molecule is not constant across the absorption band, red-shifted FES will result. Indeed, experiments showed that ϕ_f = .35 for excitation in the 0 - 0 region dropping to 0.05 near the ABS minimum, which seemingly is a violation of Vavilov's law (a furtherr discussion of this law is contained within the text).

This behavior has been noted for all the DNA bases in low temperature solution (7-15). Wilson, Morgan and Callis (15) have studied the FES of the bases and nucleotides at low temperature in EGW. All ϕ_f's are seen to drop monotonically as excess energy is absorbed into the molecules. CMP (cytidine monophosphate) is especially noteworthy as its quantum yield is seen to decrease 15 fold as the excitation is increased 7000 cm^{-1} into the first band.

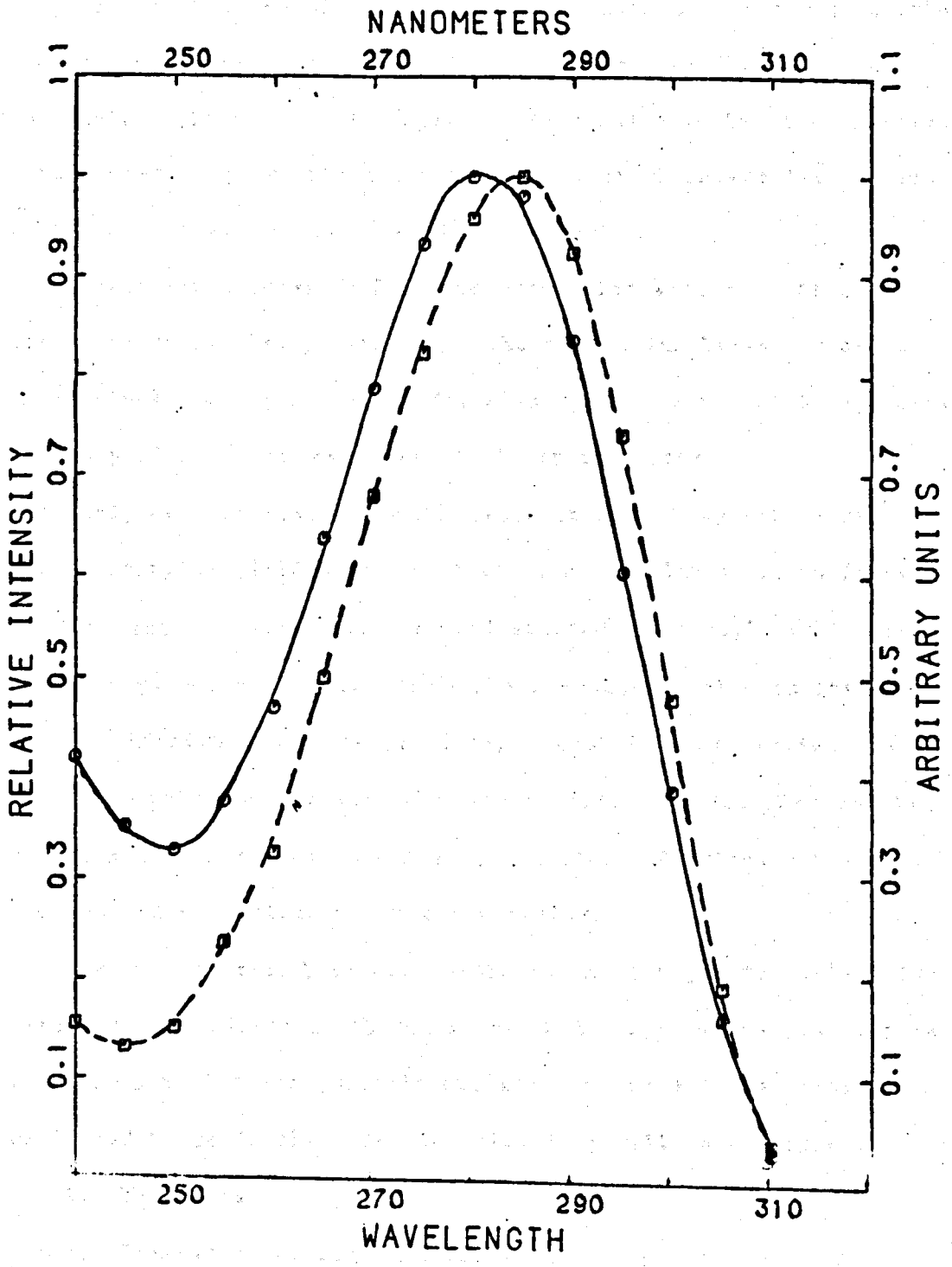

Figure 1. ABS (——) and FES (---) of 5MC in EGW at 143K λ_f = 330 nm.

The fact that wavelength dependent quantum yields exist for the DNA bases was first noted in 1965 by H.C. Borreson (8). From a study of the photophysical properties of guanine in low temperature methanol-water, this author presented data which showed its FES red-shifted and somewhat misshapen from its ABS.

Subsequent studies (7,9-15) reported that adenine, the other purine derivative base, along with the pyrimidine bases (cytosine and thymine) and their nucleotides also display wavelength dependent quantum yields in low temperature glassy solutions.

Early experiments on the DNA bases at room temperature in aqueous solution yielded somewhat the same results as those found in low temperature solutions, e.g. red-shifted FES's (2,16-18). Later studies have shown that thymine's FES correlates wel with its ABS (18,19). Adenine's room temperature, red-shifted excitation has been thoroughly investigated (20) and results show that tautomerism is responsible for this phenomenon. Guanine and cytosine have not been well characterized at room temperature.

Several theories have been explored in attempts to explain the wavelength dependency in the ϕ_f of the DNA bases in low temperature glasses. Six of these possible explanations were investigated and are listed below in the order in which they will be discussed.

1. Tautomers
2. Underlying or hidden transitions
3. Competitive deactivational pathways
4. Local heating

5. Solvent effects (hydrogen bonding, ionic strength)

6. pH dependence (speciation)

Tautomers

The excitation wavelength dependence in the quantum yields of adenine and guanine has been shown to be due to tautomeric activity (21). Crystallographic studies have established that adenine resides in the 9(H)-6-aminopurine (9HA) tautomer in the monohydrate crystal (22). Ab-initio calculations have shown that of the eight possible tautomeric forms, only 7HA has enough stability to coexist in solution with 9HA (23). All imino tautomers of adenine are considered too unstable.

Tautomers were first postulated as the source of adenine's anomalous FES by Eastman in an article emphasising this molecule's temperature dependent quantum yield (24). Wilson and Callis, acting on this clue, investigated and compared 7-methyladenine (7MA), 9-methyladenine (9MA) (shown below) and adenine's photophysical properties (11) and have presented arguments in support of adenine tautomerization. The authors constructed a hypothetical solution containing both 9HA and 7HA from which they produced expected experimental results. Their postulated outcome of 90% 9HA, 10% 7HA combinations shows good agreement with those found in adenine solutions.

If Callis and Wilson were correct in assuming that the differences between the emissive properties of 7MA and 9MA are representative of those between 7HA and 9HA, there can be little

doubt that the source of adenine's wavelength of excitation dependent quantum yield is the 7HA tautomer.

Guanine, like adenine, is composed of a parent purine ring with various substitutions as seen below. An ab-initio study by Mezig and Ladik (25) calculates that only four of the seventeen possible tautomers for guanine have sufficient stability to exist in aqueous solutions. Of the four, the following two are assumed to comprise > 99.9% of the total concentration.

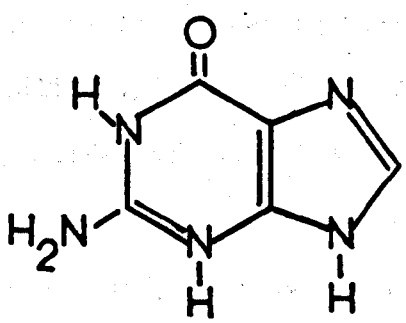

9-H Guanine

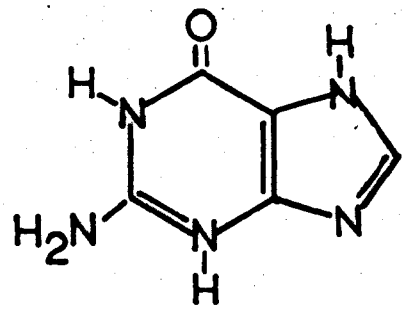

7-H Guanine

[3]

The proton residing on the five membered ring has been confirmed to be attached at the 9 position (15) a majority of the time and an equilibrium exists between the 9-H and 7-H tautomers though the extent of this is uncertain. Temperature jump thermodynamic studies have not been performed on guanine, so K_t and other various kinetic and thermodynamic information is unavailable.

Wilson and Callis, in the paper described above (21), have extended the tautomeric reasoning employed for the case of adenine to that of guanine. Along with the fact that guanine's FES resembles that of 7-methylguanine, they cite that guanine's ABS looks very much like that of guanine monophosphate. It was also

found that 7MG's quantum yield is about 10 times that of GMP in neutral EGW at 160K. From this, they concluded that guanine is also a victim of the tautomer syndrome.

Though some information is lacking and the case for guanine tautomerization cannot be said to be as strong as that for adenine, the anomalous fluorescence behavior of this molecule is satisfactorily explained through the 9-H —> 7-H equilibrium.

Tautomeric activity in the pyrimidine bases is not so easily realized as in the purine bases. Equilvalent protonating positions are available. However exchange of protons between the two lead to vastly different photophysical properties in both cytosine and thymine. A further discussion of this possibility will appear within the body of this work.

Hidden Transitions

The search for hidden or degenerate transitions in the pyrimidine bases has produced numerous publications involving varied experimental techniques. Polarized crystal absorption and reflectance of cytosine (26,27) has shown that two strongly allowed $\pi \longrightarrow \pi^*$ transitions comprise the ABS in the near UV. Transition moments of these states lie in plane and the absorption polarization is nearly constant throughout the bands.

Polarized fluorescence studies support the notion that band I in cytosine (5), 5MC (6,28) and cytidine (20) is strongly allowed. Polarization ratios are found to be high and constant throughout their respective FES's.

Linear dichroic (LD) (29,30), circular dichroic (CD)(31) and magnetic circular dichroic (MCD)(32) spectra of cytosine also show that transition I is probably pure and nondegenerate.

In the case of thymine, similar studies have been performed. Thymine, like cytosine, has two strongly allowed transitions in the near UV, as demonstrated by polarized absorption (33). Some evidence has been forwarded for a weakly absorbing band at 264 nm (34) with an oscillator strength of ca. .006, a factor of 200 to 300 less intense than band I. CD spectra (31) confirm the idea of a measureable underlying band, but position it at about 240 nm. A recent report on the polarized fluorescence of thymine proposes that a band is underlying Band I between 270 and 290 nm (35). However, no variation in the ϕ_f was seen in this area.

There is no doubt that undetected transitions exist in the pyrimidine bases. However, the presence of such band has yet to be proven in the case of wavelength of excitation dependent ϕ_f's. Due to this fact, this idea will not be explored in the text of this thesis.

Competitive Deactivational Pathways

Violations of Vavilov's law was postulated in early work by Hanswirth and Daniels (16). Wilson et al. (15), in a paper published previous to their conclusion that tautomerism is responsible for the wavelength dependence in adenine and guanine (21), logically explored this possibility for all the DNA bases. The form of these violations could either be internal conversion or

intersystem crossing occurring from vibrationally excited levels of the first excited singlet state with increased rates. Gas phase experiments on isolated molecules show that this occurs more often than not (36) and indeed pyrimidine, the parent compound of cytosine and thymine, shows a red-shifted FES under these conditions (37). Rates of internal conversion are speculated to be near 10^{12} sec^{-1} for the bases, (15) so competition between deactivation pathways could conceivably occur.

Local Heating

Quantum yields of cytosine and thymine display considerable temperature dependence, increasing by more than two orders of magnitude in going from room temperature aqueous solution to low temperature EGW glass. In fact, this Arrhenius type variation of fluorescence intensity with temperature has been found for all the neutral DNA bases. Having knowledge of this phenomenon and familiarity with the problem of noncoincidence in the ABS and FES curves of the DNA bases, Reed Howald (38) suggested that the two could be interrelated.

He proposed that when absorption is into the zero vibratonal level of the first excited state, no excess molecular energy is present so fluorescence will occur from a state in thermal equilibrium with the bulk solvent. When energy is present beyond the amount required to reach the fluorescent state (S1 with no vibrational quanta), this energy must be dissipated in vibrational motion, i.e., heat. If the thermal conductivity of the neighboring

molecules (usually solvent) is inefficient, then the effective temperature felt by the fluorescing molecule will be above that of the bulk thus lowering the probability that deactivation will occur through fluorescence.

Solvent Effects

The theory of solvent interaction with solute molecules to produce wavelength dependent ϕ_f's has already born fruit in the case of thymine in that this molecule was found to have a coincident FES and ABS in ethanol-methanol-glass at 77K (39).

Kogan and Becker (39) in a paper dealing with fluorescence properties of thymine and several methylated uracil derivatives, have invoked the following argument to explain the difference in their results for thymine in ethanol-methanol (EM) glasses and those found in our lab in rigid EGW. They proposed that in hydroxylic solvents, the following equilibrium is active,

$$N + nROH \rightleftharpoons N\cdots(ROH)_n \qquad [4]$$

where N is a DNA base, nucleoside or nucleotide. If N···ROH has a very high quantum yield, an absorption spectrum shifted slightly to the red of the non-hydrogen bonded species, and a negligible concentration, then the observed excitation spectrum of N would be red-shifted relative to the absorption spectrum. Logically, if solvents of low hydrogen bonding strength are used, little or no variation in the quantum yield will be found across the absorption bands. In support of this theory, they present excitation spectra

for the investigated molecules in EM and methyl tetrahydrofuran (MTHF) at 77K which are remarkably coincident with their respective absorption spectra.

pH Dependence

The last possibility to be explored is that of solution pH effects on the ionic distribution of molecular species. Equilibrium constants reported for the DNA bases are from room temperature aqueous solutions and probably are not correct for low temperature glassy solutions.

Adenine and guanine pKa's have been observed to shift to higher values in EGW at 77K (7). We discovered that 5MC, cytidine and 5-methyldeoxycytidine and thymine all displayed pKa's which were increased by 2 to 3 units. As the writing of this thesis was in progress, an untranslated article appeared in a Russian journal (40,41), which detailed the pKa change of cytidine at 77K. The acidic equilibrium constant of this molecule was shown to shift from the room temperature pH of 4.6 to 5.9 in EGW glass at 77K. Introduction of the highly fluorescent (at low temperature) cation is responsible, in part, for the red-shifted FES seen in that molecule. Residual wavelength dependency in the ϕ_f is explained by solvent interaction as described for the case of thymine in EM glass. Our results, obtained independently, support this contention but show slightly different values for the pKa.

Data and discussion presented in the second part of this thesis will examine each of these possible explanations for the wavelength

dependent ϕ_f's of the pyrimidine bases in low temperature glassy solutions. 5-methylcytosine was chosen to replace cytosine as a working model, since the latter cannot be obtained in a fluorescently pure form through the normal biochemical suppliers. The substitution of a methyl group for a hydrogen has been shown to introduce very little change in the resultant ABS and FES of molecules, so the results presented here for 5MC should be directly applicable to the base.

Two Photon Excitation of Benzimidazole

As was discussed to some degree earlier, there is much interest in the true nature of the state ordering in the DNA bases. The electronic states are not well understood and, in some cases, transition moment directions between the ground states and the lower excited states have not been agreed upon (1). Much of this uncertainty stems from the nature of the one photon absorption processes in the DNA bases. All display broad, intense absorption bands in the UV region of 200 nm to 300 nm. In addition, although purine and pyrimidine, the parent molecules of the bases, exhibit n $\longrightarrow \pi^*$ transitions of measureable intensity (42,43), such states are missing or are well hidden in the corresponding bases.

Attempts at modeling the electronic transitions in the bases have relied heavily on the Platt model (44) for benzene. This molecule has molecular orbital energies and symmetry patterns which result in the following electronic diagram,

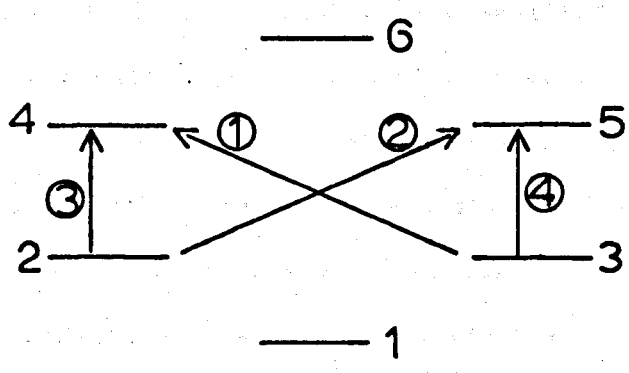

where uncircled numbers refer to molecular orbitals and circled numbers are transition of electrons between M.O.'s. Linear combinations of transitions 1 and 2 and transitions 3 and 4 give rise to states Lb, Bb, La and Ba according to Platt. States Ba and Bb are very intense in the UV spectrum of benzene indicating that they are strongly allowed. Lb is symmetry forbidden but gains weak intensity through vibrational coupling (45).

Pyrimidine, the parent of cytosine and thymine, reflects much of the features of benzene in its UV spectrum. It can be thought of as benzene with two meta hydrogens moved into the ring. The presence of the ring nitrogens however, give rise to n —> π^* transitions, one of which becomes the lowest energy transition in the UV spectrum.

When exocyclic heteroatoms are added to pyrimidine to form cytosine or thymine, analogy between the UV absorption of the former and the latter becomes very unclear. The two bases belong to the symmetry group Cs. Therefore, there are no symmetry restrictions on their electronic transitions so states which were forbidden in benzene for this reason are quite allowed in the bases. The lowest

energy transitions in these molecules have oscillator strengths of 0.1 - 0.2. At this point, it becomes clear that one photon UV absorption spectroscopy fails to yield the information necessary to identify and characterise the electronic states of the base.

As can be seen from the above, understanding of the electronic states of the pyrimidine bases through analogy with those of benzene using only the one photon absorption spectrum can be quite difficult. This difficulty is pressed to the limit, however, if one extends the benzene modeling to the cases of the purine basea, adenine and guanine. Even purine's one photon UV absorption is not well understood on this basis, since its structure represents a massive perturbation on that of benzene (1).

It is clear that further information is required to fully characterize the absorption of the DNA bases so we decided that two photon spectroscopy along with modified modeling techniques could provide much of the details which are missing in the UV absorption pictures of the DNA bases.

Two photon spectroscopy is a relatively new technique but has already shown great promise as an experimental tool (46,47). The possibility of a molecule absorbing two low energy photons simultaneously to reach a final state was first theorized by Maria Goppert-Mayer in 1931 (48), but was not confirmed experimentally until 1962 (49), after the advent of lasers. The principle of two photon absorption (TPA) is much the same as that for one photon absorption (OPA) except instead of a molecule absorbing one photon of ultraviolet light, for instance, it will absorb two photons of

visible light to reach the same final state. Absorption of the first photon is into a virtual state which has a lifetime on the order of 10^{-15} s, so absorption of the second photon must occur within this time span. To have a reasonable probability of this occuring requires a very high density of photons, one which can only be provided by laser excitation. The selection rules for TPA are complementary to those for OPA. This property allows one to observe transitions in TPA which are normally weak (formally forbidden) or hidden in OPA. In addition, TPA using linear and circular polarized light can reveal information concerning the symmetry, vibrational modes and transition moments of molecules that is impossible to obtain through OPA.

This technique has already yielded a wealth of new information about the electronic states of benzene (50) and numerous other molecules and atoms (for reviews see references 46,47). Callis, Scott and Albrecht (51) have recently reported the TPA of pyrimidine, a molecule of great interest to us. They have found the L_b transition in this molecule is made allowed only through vibronic coupling and that a second $n \rightarrow \pi^*$ transition peaking at ca. 480 nm (240 nm in UV) is present.

In addition, these same authors have developed new methods to interpret the perturbations that substitutions and vibrational coupling have on the electronic spectra of aromatic hydrocarbons (52,53).

As ground work is being laid in our group to obtain the TPA spectra of molecules related to thymine and cytosine, e.g. molecules which are more highly perturbed than pyrimidine but less distorted than the bases, we have begun a new modeling scheme for the spectra of the purine bases. Figure 2 shows pictorially how we are proceeding in obtaining theoretical and experimental information on these nine membered ring systems. You will note, following the arrows, that each molecule possesses a slightly more complex π electron system than the molecule preceding it. CNDO/S calculations, transition densities (52,53) and calculations of two photon absorptivities of each of these molecules has already been performed.

In chapter 5 of the text, the two photon absorptivities and circular/linear polarization ratios are presented for benzimidazole. Spectral features of this spectrum are discussed in light of CNDOS-CI calculations and results of benzene. In addition, data is presented that, for the first time, reveals the L_a 0 - 0 in the one photon spectrum of this molecule.

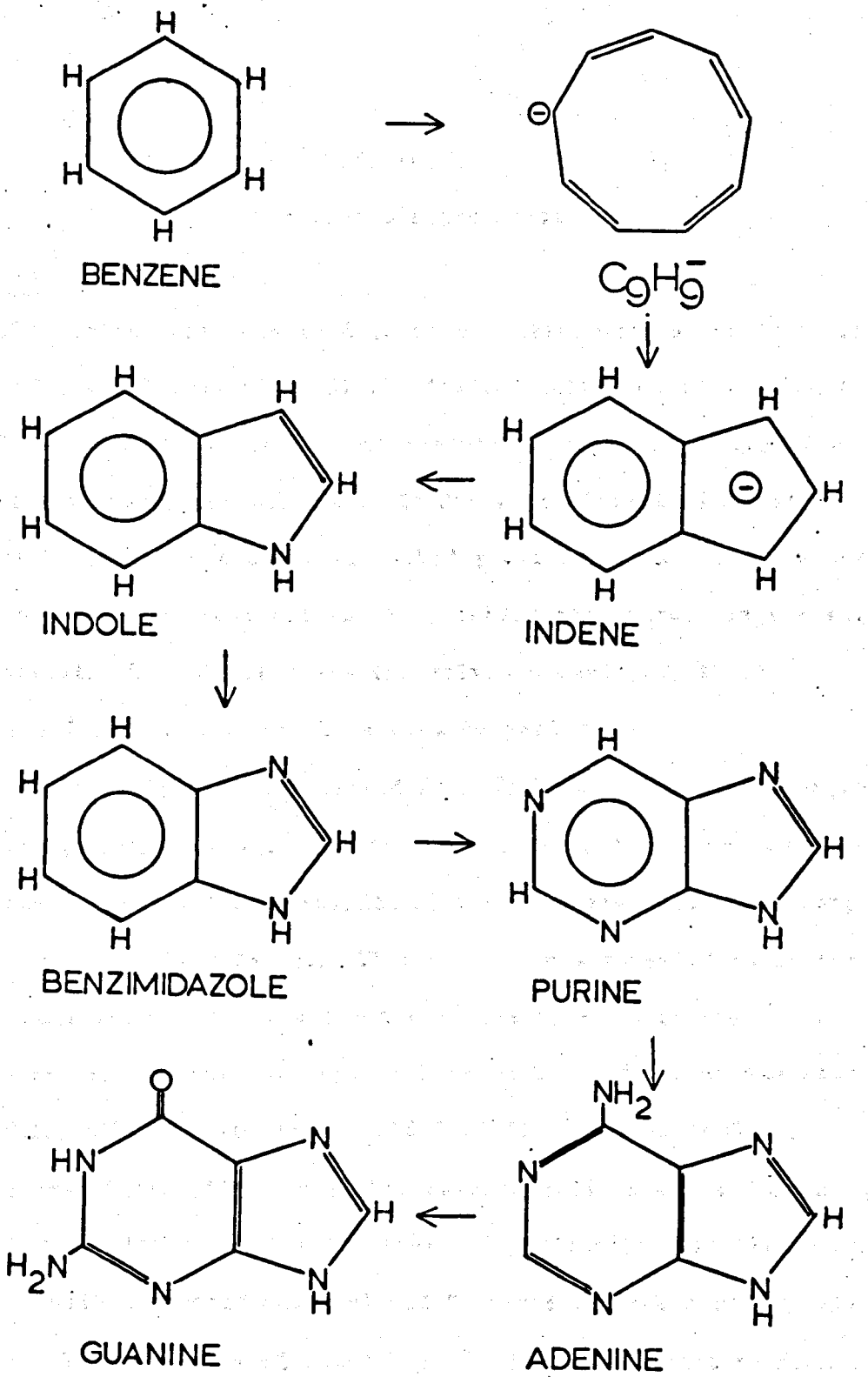

Figure 2. **Structures of benzene and various nine-membered ring systems.**

EXPERIMENTAL

One Photon Experiments

Solvents

The various solvents used to form glasses were selected on the basis of several criteria: 1) The desired solute molecules had to be soluble enough in the solvent to produce an optical density of ca. 0.30 at the absorption maximum, 2) Due to equipment limitations, the solvent had to form a clear uncracked glass at a temperature above 77K, and 3) The solvent had to be optically transparent in the region of interest. Listed below are the solvents employed, their commercial vendor and the means used to purify them.

Ethylene glycol was obtained from J. T. Baker Chemical Company (reagent grade). One liter portions were stirred 24 hours with flame activated charcoal (5.0 grams/liter) then gravity filtered through a medium fritted glass filter. This process was repeated until the emission spectrum of the solvent was less than 10% of the Raman height and the maximum absorption between 240 and 310 nm was less than 0.1. Ethanol was either Gold Seal (food grade, 100%) or undenatured bulk (95%). In either case, one liter was refluxed with 10 grams calcium oxide for two hours, fractionally distilled, stirred with activated charcoal and filtered through a medium glass filter. When the ethanol was to be mixed with methanol to form a glass, activated charcoal was not used since it was found to affect the neutrality of this solvent.

Methanol was obtained from J. T. Baker (Phototrex grade) and usually required no purification. If impurities were present, the solvent was stirred with activated charcoal and filtered.

Isopropanol was Baker reagent grade or Baker "phototrex" high purity. In the latter case, no purification was required. However, the standard reagent grade required distillation with CaO and filtration with activated charcoal.

Isopentane was obtained from J. T. Baker Chemicals as a bulk reagent. A one liter portion was stirred with ca. 200 ml of concentrated sulfuric acid for 24 hours, washed with two 100 ml aliquots of sodium carbonate, then fractionally distilled. The middle fraction was collected, stirred with flame activated charcoal and filtered through fritted glass. Cyclohexane and hexane were prepared in the same manner.

Buffers

Phosphate buffers were employed in all aqueous solutions unless the effect of the buffer was being scrutinized. To obtain a .01 M phosphate buffer, 25 ml of .04M phosphoric acid was pipetted into a 250 ml beaker and stirred with a stirring bar. A Corning model 12 or a Sargent-Welch model NX pH meter and a microelectrode was used to monitor the pH of the solution as potassium hydroxide was added dropwise. When the desired pH was obtained, the solution was diluted to 100 ml with distilled or, toward the end of this work, deionized water, the pH was rechecked and spectroscopic (fluorescence and absorption) measurements were taken to determine the purity.

Buffers not containing phosphate were obtained in a similar manner, i.e. starting from parent acids. When high or low pH's were desired, solutions were made of unbuffered acids or bases.

Instruments

Room Temperature Fluorescence Apparatus. Fluorescence measurements were obtained on the configuration of instruments shown in Figure 3. The important features of this fluorimeter are listed below.

A. Source Power Supply: A variable current (8-9 amps) and voltage (18-19 volts) supply obtained from Oriel Optics (model C-72-20).

B. Source Light: Osram 150 watt high pressure xenon lamp which provides a continuum of light throughout the UV and visible spectrum.

C. Excitation Monochromator: Bausch and Lomb grating monochromator with micrometer controlled slits and a calibrated drum wheel that provides wavelength selection with a readout accuracy of 0.5 nm. A quartz lens mounted on the entrance slits focuses the source light onto the grating and quartz wedge depolarizers at the exit slits remove any polarization introduced by the grating.

D. Polarizer: A single Polacoat PL-40 polarizer was mounted on a rotatable mount with a threaded seat which screwed into the face of the excitation monochromator. Two screw stops

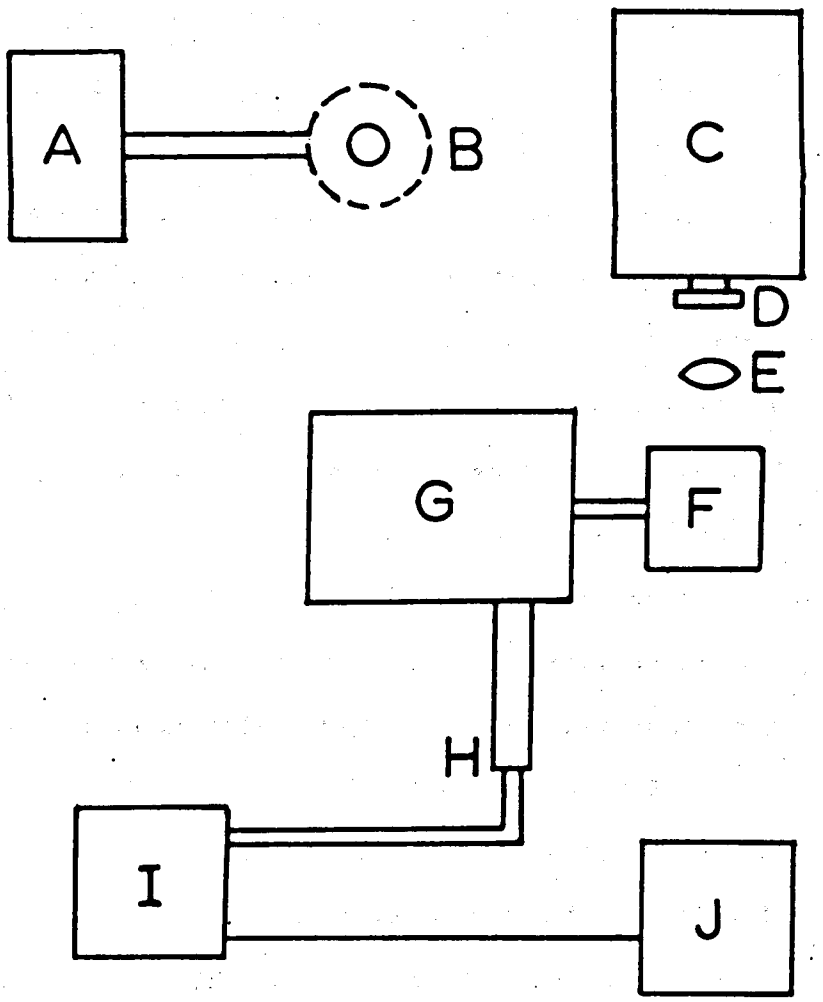

Figure 3. Optical and electronic components of the fluorimeter used in gathering fluorescence and excitation spectra.

were present at 90° and 180° so that the polarizer could be rapidly changed from vertical to horizontal.

E. Focusing Lens: A quartz, plane-convex lens with a 60 mm focal length. The lens is mounted on an X translatable stage and has a calibrated iris shutter that is used to control the amount of excitating light reaching the sample.

F. Sample Mount: A translatable stage with a 1.0 cm cell holder mounted a fixed distance from the focusing lens on the entrance slits of the fluorescence monochromator. The stage can be translated on an axis perpendicular to the fluorescence monochromator so that the excited region can be brought into the full field of view of the fluorescence monochromator. Room temperature measurements were performed on samples contained in 12mm X 12mm X 48mm (10mm X 10mm X 47mm inside) fused silica fluorescence cells.

G. Fluorescence Monochromator: This monochromator is identical to the excitation monochromator and is positioned at a 90 degree angle from the source with a quartz lens mounted on the entrance slits to focus the sample emission on the grating. The wavelength selector is driven by a potentiostat-controlled synchronous motor that can be removed and cranked by hand.

H. Photomultiplier Tube (PMT): An EMI 9558 QB, 13 stage quartz envelope PMT mounted face on at the exit slit of the fluorescence monochromator. This tube is sensitive to 200-850 nm light and has a gain of about 10^8 when operated at -

1150 V. Calibration curves for this PMT were determined empirically and will be discussed later.

I. Photometer: A Pacific Photometric model 11 amplifier with a 0 - 2000 volt variable power supply used to provide high voltage to the PMT. The amplifier has a zero offset for dark current subtraction and a variable gain setting which offers a range of 5 orders of magnitude.

J. X-Y Recorder: A Hewlett Packard model 7030 X-Y recorder potentiostatically linked to either the excitation or fluorescence monochromator via a selector switch. The Y axis length could be adjusted either by the gain selector on the photometer or by the Y axis magnifier on the recorder. Spectra were recorded on standard 8" by 11" graph paper.

Low Temperature Fluorescence Apparatus. When experiments were performed at less than 293K, the sample holder was replaced by either a custom built Sulfrian dewar or a Janis model 8DT liquid He/nitrogen dewar. When the Sulfrian dewar was employed, a Sargent-Welch Duo-Seal vacuum pump continuously evacuated the outer jacket and air was blown across the windows of the dewar to prevent fogging. Cooling of the sample was achieved by boiling liquid nitrogen contained in a 10 liter storage dewar and passing the exhaust gas directly over the sample. Temperatures down to 110K could be reached in this manner.

In experiments requiring temperatures less than 110K, the Janis dewar was used. Previous to use, this dewar was evacuated with a roughing pump and an oil diffusion pump to ca. 10^{-5} torr. The dewar,

mounted on a X-Y translatable stage, was then positioned in the fluorimeter and filled with liquid nitrogen. A microvalve was used to adjust the flow of coolant between the inner jacket and the sample compartment. Room temperature air was passed through a drier and then blown across the sample cell to reach temperatures above 77K when desired.

A digital thermometer (designed by Dr. Richard Geer) was used to monitor temperatures below ambient. Experimentally, the diode sensor was placed in direct contact with the sample cell and had a response time of less than 5 seconds when affected with a drastic temperature change.

A solvent tends to contract at temperatures nearing its glass point, thus exerting inward pressure on the container to which it adheres. For this reason, custom built thick walled fluorescence cells were used in all low temperature experiments. Two particular cells were employed in most experiments, both having outside dimensions of 12 mm X 12 mm X 23 mm, with one having inside dimensions of 6 mm X 6 mm X 20 mm and the other 3 mm X 3 mm X 20 mm. These cells were utilized in both absorption and fluorescence measurements and were found to introduce little or no added scattering to the fluorescence spectra.

Absorption Measurements

Absorption spectra were taken on either a Cary 14 UV/VIS/IR instrument or a Varian Associates Series 634 UV/VIS instrument and were referenced against air. When low temperature spectra were

required, the Sulfrian dewar was inserted into either instruments' sample compartment and cooling was affected as was previously described.

Experimental Procedure

Room Temperature Fluorescence of 5-methylcytosine (5MC). A 1 cm cell was filled with ca. 1.5 ml of aqueous solvent. The cell was placed in the fluorimeter sample holder and the stage was translated to maximize the Raman emission. The fluorescence of the blank was recorded at several wavelengths of excitation. If a flat fluorescence background was observed (i.e. the solvent was clean), 5MC was added directly to the cell and the solution was repeatedly drawn into a pasteur pipette until complete dissolution was obtained. Fluorescence spectra, including excitation with polarized and unpolarized light, were recorded with the sample mount carefully positioned so that the fluorescence monochromator viewed the maximum fluorescence intensity. An unpolarized fluorescence excitation spectrum of a Rhodamine B (Rh B) (3 grams/liter) quantum counter solution was recorded in conjunction with the above to monitor the daily variance in source lamp intensity.

When fluorescence measurements were completed, the sample, still contained in the 1.0 cm cell, was transported down the hall where its UV absorption was determined. If an optical density of greater than 2.0 was obtained, successive dilutions were made until the maximum absorption did not exceed 2.0. The spectrum was then carefully recorded on the Cary 14 UV/VIS/IR spectrometer, scanning slowly from

330 nm to ca. 240 nm with stops every 10 nm to mark the wavelength and absorption.

The above procedure was repeated on 18 different buffers, though occasionally more than one sample was processed per experiment and, in most cases, more than one experiment was performed on each buffer.

Low Temperature Experiments. Ethylene glycol-water (EGW) 60:40 by weight (w/w), ethanol-methanol 3:1 w/w (EM), methanol-water 12:1 w/w (MW) and isopropanol-isopentane 1:1 w/w (IIp) were weighed on a triple beam balance and mixed in 100 ml glass stoppered volumetric flasks. Fluorescence and absorption spectra were recorded for each of these glass forming solvents prior to use. Ten ml of the desired solvent was transferred to a clean, glass stoppered 10 ml erlenmeyer flask to which a small amount of solute was added. A UV absorption spectrum was recorded and the solution was diluted until a maximum optical density of 2.0 was obtained. This qualification yielded solutions which were 0.1 to 0.5 millimolar. A small portion of this solution was then transferred to a thick walled fluorescence cell. The diode thermometer probe was affixed to the sample cell holder (having been previously calibrated in liquid nitrogen (77K) and ice water (273K)), the sample cell was mounted and the entire assembly was inserted into the dewar contained in the fluorimeter apparatus. The signal was maximized by translating the stage relative to the viewing monochromator. A variac controlling a heating coil in the 10 liter storage dewar was adjusted until the proper temperature was obtained. Air was blown across the dewar windows to prevent fogging

and the glass quality was monitored by viewing the Rayleigh scattering of blue light from the solution.

Once the desired temperature had been reached and maintained for ca. 5 minutes, the sample was translated on an axis perpendicular to the viewing monochromator to maximize the photocurrent. Fluorescence spectra at a minimum of two different excitation wavelengths and fluorescence excitation spectra at two different viewing wavelengths were recorded. When phosphorescence was observed, an attempt was made to obtain an excitation spectrum of this also. An excitation spectrum of Rh B was taken in conjunction with each experiment.

Absorption. The Sulfrian dewar was mounted in either the Cary 14 or the Varian 634 UV/VIS spectrophotometer. Samples were poured into the thick walled cell, the diode probe was attached to the cell holder and the holder was inserted into the dewar. Cooling was affected in the same manner as for fluorescence spectra. The absorption of the solution was continually monitored in order to detect fogging of the windows or deterioration of the solvent glass. When the desired temperature was reached, the instrument was zeroed at a wavelength just to the red of the onset of absorption and the absorption spectrum was recorded scanning from low to high energy. Since the background absorption was not negligible, a blank spectrum, i.e. the absorption of solvent, cell and dewar windows, was also recorded in conjunction with each sample spectrum and subtracted from the total absorption.

Calibration. The two absorption instruments (Cary 14 and Varian 634) were calibrated versus the spectrum of benzene in hexane. Spectra recorded on the Cary 14 were always accurate to within .5 nm while those on the Varian 634 varied by up to 2 nm. If a large deviation appeared in either instrument, corrections were made by loosening the wavelength drive and readjusting the tilt of the grating.

Calibration of the fluorescence monochromator was performed by shining a low pressure Hg lamp directly into the viewing monochromator with the slits at about .15 mm width. Wavelength readings were recorded at each spectral peak in the entire mercury (Hg) spectrum. Deviations of the spectral peaks relative to those in the published Hg spectrum were averaged and the grating drive was adjusted by that amount. A MgO coated cell was then positioned in the excitation light path in order to reflect the source light from the excitation monochromator into the viewing monochromator and thus cross reference the two wavelength drives. Periodic checks were made of the synchronization of the two monochromators by viewing the 3600 cm^{-1} Raman line of distilled water. An agreement to within 1 nm was generally accepted.

Corrections and Calculations. Day to day variations of the xenon source lamp intensity were monitored by either recording the excitation spectrum from 230 to 300 nm of a Rh B quantum counter solution viewed at 640 nm (55) or by measurement of the Raman spectrum of distilled water. The former method is preferred. The Rh

B solution is assumed to absorb all the incident light within the first few millimeters of the cell and, since its quantum yield is near unity, the fluorescence intensity is no longer a reflection of the solution's quantum yield but only of the lamp intensity. The second and less effective method of measuring lamp fluctuations was by scaling the height of the Raman spectrum. This method is very sensitive to contamination and cell positioning. However, it has the attraction of availability since the fluorescence of each solvent was recorded prior to the addition of solute. Though variations in lamp intensity were assumed to be negligible during the course of the experiment, the relative heights of the Raman spectra were used to verify that fact.

Background emission from solvents and fluorescence cells usually was less than 1% of the total fluorescence. However, when corrections were required the background was multiplied by the ratio of the sample solution Raman peak height to the solvent Raman peak height and subtracted from the emission spectrum (5). In all cases, this correction amounted to less than 5%. Variations in sensitivity and efficiency of the viewing monochromator and photomultiplier as a function of wavelength were determined by the method of Parker (55). This entailed placing a MgO screen at a 45 degree angle in the optical intersection of the two monochromators and reflecting light from the excitation monochromator into the emission monochromator. Emission spectra were then recorded at 5 nm intervals from 280 nm to 550 nm. The peak heights obtained in this manner were divided by the excitation spectrum of Rh B to correct for the variation in intensity

of the excitation source and the resulting vector reflects the response of the detection apparatus. All fluorescence spectra presented in this work were divided by the vector obtained by Mr. Berk Knighton (18).

The bandwidth and thus the resolution of any fluorescence instrument is dependent on the slit width of light allowed to reach the grating. In our instrument, a slit width of 2 mm in the viewing monochromator yields a bandwidth of 13.2 nm. Therefore, if resolution in the fluorescence spectra is to be achieved, one must view a small portion of the sample cell. This is not a problem when dilute samples are used. However, if solutions of greater than .05 optical density are used, which was more often the case than not in this work, the intensity of the source light cannot be assumed to be constant throughout the cell. This can be compensated for in one of two manners. A standard solution of a compound with a known quantum yield can be made with a matching optical density. By recording the fluorescence of both the sample and standard simultaneously, the sample fluorescence intensity can be found relative to that of the standard. An alternate method and the one presently used in our lab, is correction of the absorption spectrum using an empirical equation that takes into account the beam absorption along the excitation path and the geometry of the detection system. This equation was derived by P. R. Callis and a more extensive explanation can be found in references (18,56). The equation is

$$G = 1 - \left(\frac{1 - e^{-2.303Aa}}{2.303Aa}\right) \qquad [5]$$

where G is the corrected absorption value, A is the solution absorption per centimeter and a is the effective path length of the cell. The a value used in this work was obtained by Mr. Tim Aoki (56) by taking the ratio of the fluorescence intensities of two tryptophan solutions having different concentrations and finding a unique value which makes the ratio of G values calculated for the two solutions equal to the ratio of their fluorescence intensities. A value of .21 cm was used throughout this work.

Interpretation. Raw uncorrected excitation spectra were obtained by setting the viewing monochromator to a wavelength within the fluorescence band of a compound and measuring the fluorescence intensity as a function of excitation wavelength. This essentially gives the quantum yield as a function of wavelength and, if this value is constant throughout the absorption band, the excitation spectrum will merely reflect the light absorption of the solution. Experimentally obtained fluorescence excitation spectra are corrected by application of the following formula,

$$E(corr) = \frac{E^{\lambda}_{raw} \cdot Abs^{B}}{G^{\lambda} \cdot E_{RS}} \qquad [6]$$

where G^{λ} is the factor discussed above, E^{λ}_{raw} is the uncorrected excitation spectrum, Abs^{λ} is the absorption spectrum of the solution

and E^{λ}_{RB} is the excitation spectrum of the quantum counter. These spectra were usually normalized and plotted along with the normalized absorption spectra.

Quantum yields were calculated relative to a standard solution of L-tryptophan, which has a generally accepted quantum yield of .15 (57), by use of the following formula,

$$\frac{\phi^{\lambda}_s}{\phi^{\lambda}_t} = \frac{F_s \cdot A_s \cdot G^{\lambda}_t \cdot I^{\lambda}_t}{G^{\lambda}_s \cdot I^{\lambda}_s \cdot F_t \cdot A_t} \qquad [7]$$

where F is the product of peak height and meter gain, A is the area under the fluorescence curve (normalized to unity), I is the intensity of the quantum counter signal and G is the factor discussed above. The subscripts s and t denote sample and L-tryptophan quantities, respectively. Rearrangement of this expression yields:

$$\phi^{\lambda}_s = \frac{F_s \cdot A_s}{G^{\lambda}_s \cdot I^{\lambda}_s} \times \frac{\phi_t \cdot G^{\lambda}_t \cdot I^{\lambda}_t}{F_t \cdot A_t} \qquad [8]$$

and it is readily seen that the second term on the right-hand side is constant, the value of which was determined to be 5650. It should be noted however, that previous students have found a variation of 10% in this constant (18,56).

In some of the work done at room temperature, quantum yields were calculated from fluorescence spectra excited by polarized light. Since the DNA bases emit very rapidly with fluorescence lifetimes on the order of 10^{-12} s, corrections had to be made for the directional emission of these compounds. The following equation was developed by

Callis (58) and it simply relates the polarized emission to what the emission would be in a randomly fluorescing solution.

$$\phi_f = \phi_f^{POL} \left[\frac{3S - 1}{3S + 1} \right] \qquad [9]$$

where $S = \langle \cos^2 \theta \rangle$ and θ is the angle between the absorbing and emitting moments. Quantum yields corrected in this fashion were found to be invariant to those found using unpolarized light.

Two Photon Experiments

Lasers

The nitrogen laser is an NRG-0.5-5-150/B and was obtained from National Research Group in Madison, Wisconsin. The specifications for this instrument are:

Lasing Wavelength: 337.1 nm

Peak Power: 500 kw at 60 pulses per second

Pulse Duration: 5 nanoseconds full width at half maximum

Average Power: 150 mW at a repetition rate of 60 Hz

Power Requirements: 550 watts at 115 volts, 60 Hz.

Nitrogen gas was provided to the laser from a 100 liter liquid nitrogen dewar with regulators attached to the gas release valve. Under normal operating conditions, one dewar of liquid nitrogen supplied enough gas to run the laser ca. two weeks.

Reduced pressure in the nitrogen discharge cavity was obtained from a Kinney Vacuum pump, model # KC-8, capable of 8 cubic feet per

minute through-put. Discharge from the pump is vented into the building drain system.

Experimentally, the laser was run at 10-20 Hz with a spark gap pressure of 30 psi and a cavity pressure of 120 millibars. Operation at these pressures are reported to give maximum peak power with a minimum pulse width.

The dye laser was also obtained from National Research Group and is model NRG-DL-0.03. The beam from the nitrogen pump laser is passed through a 1.5 inch cyclindrical lense and focused onto the front surface of a quartz walled cell. Dye solution is continually flowing through this cell to prevent photochemistry or "burnout" of the dye. The sidewalls are also slanted to prevent lasing from the cell surfaces.

The feedback mirror, a partially-reflecting glass plate, is positioned to reflect a portion of the fluorescence to pass back through the cell, thus obtaining a small degree of gain. This beam is gathered by a telescope and expanded onto a 316 lines/mm grating which is mounted on a rotatable platform. Adjustment of the platform is made using a micrometer to feed the selected wavelength of light back through the telescope and through the excited region of the dye cell. Wavelength scanning of the dye laser is accomplished by adjusting the tilt angle of the grating relative to the base with a micrometer. To facilitate quick reproducible scanning, a stepping motor and belt gearing were attached to the tilt micrometer. Light pulses from the dye laser are passed through an iris to block unwanted stray light.

Laser dyes were obtained from commercial vendors and were reagent grade, where possible, and laser grade when the dye was unavailable as any other grade. Each dye was used without further purification. Table 1 gives the lasing range, vendor, molecular weight and concentration in grams per unit volume of solution for the dyes used in our experiments. Solvents used to make dye solutions were reagent grade, all from J. T. Baker Company with the exception of EtOH, which was absolute (food grade) from U.S. Industrial Chemical. Dye solutions were mixed and stored in 500 ml containers at room temperature. Dioxane or toluene based solutions were isolated within a glass fronted hood.

Electronics and Fluorescence Detection

Components for the two photon excitation apparatus were purchased and built in the period from February through July of 1982. Below is a description of each element shown in Figure 4.

A. Pulse generator: This device was built by the author and Figure 5 shows a circuit diagram of it along with a graph of voltage going to the nangate versus time after laser pulse. The diode, enclosed in the dashed box, is positioned within the dye laser. When the laser fires, the resistance of the diode drops from ca. 2 meg Ω to around 200 Ω. This results in 99.9% of the 5 V being dropped across the 2K resistor. The pulse is then shaped by a nandgate (CMOS 4093) and output to the pulse delay circuit.

B. Pulse delay circuit: This device was built by the author and was patterned after the control circuiting for the constant

Table 1. Specifications of laser dyes.

Dye	λ(lasing) nm	Vendor	Solvent	Mol. Wt.	Conc. g/ 500 ml
p-quaterphenyl	360-390	Sigma	toluene	306	1.07
α-NPO	393-423	Sigma	toluene	271	0.33
PPO	359-391	Baker	toluene	221	0.66
DPS	396-416	Sigma	p-dioxane	332	0.20
BBO	400-440	Aldrich	toluene	675	0.84
Stibene 420	421-442	Exciton	EtOH	—	0.50
DMPOPOP	424-441	Sigma	toluene	382	0.65
Bis-MSB	411-430	Chemalog	p-dioxane	310	0.19
POPOP	425-451	Sigma	p-dioxane	364	0.18
Coumarin 120	420-460	Sigma	EtOH	246	0.92
Coumarin 1	440-478	Aldrich	EtOH	231	1.15
7-dimethylamino, 4-methylcoumarin	440-460	Sigma	EtOH	203	1.00
7-hydroxy,4-methyl coumarin	480-505	Aldrich	EtOH+ 1 M $HClO_4$	176	0.176
7-hydroxycoumarin	480-505	Aldrich	EtOH+ 1 M $HClO_4$	167	0.167
7-diethylamino, 4-methylcoumarin	420-450	Aldrich	EtOH	231	0.50
Coumarin 102	460-480	Eastman	EtOH	255	0.50
Coumarin 307	495-527	Eastman	EtOH	271	0.50
Coumarin 152	515-545	Eastman	EtOH	257	0.50
Coumarin 480	520-545	Exciton	EtOH	—	0.50
Coumarin 153	535-555	Eastman	EtOH	309	1.00
Rhodamine 110	550-575	Exciton	EtOH	367	0.30
Rhodamine 6G	570-605	Sigma	EtOH	479	1.20
Rhodamine B	595-630	Sigma	EtOH	479	1.20
Cresyl Violet	641-687	Sigma	EtOH	362	0.60
Nile Blue A	682-715	Sigma	EtOH	733	0.80

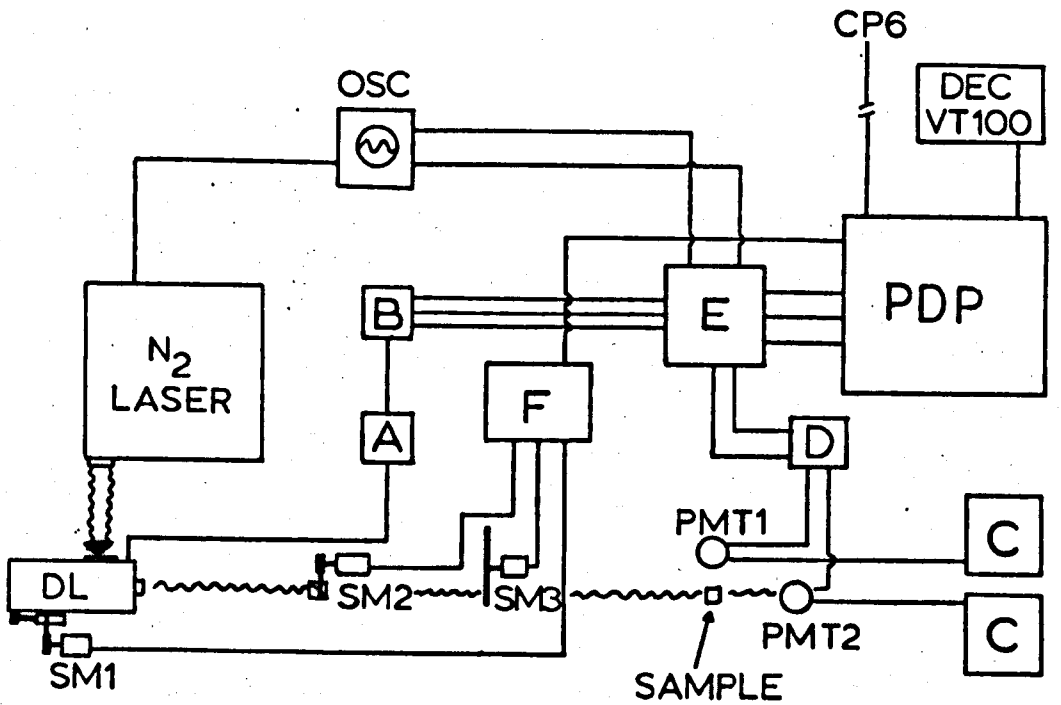

Figure 4. Electronic components of the two photon fluorescence excitation apparatus.

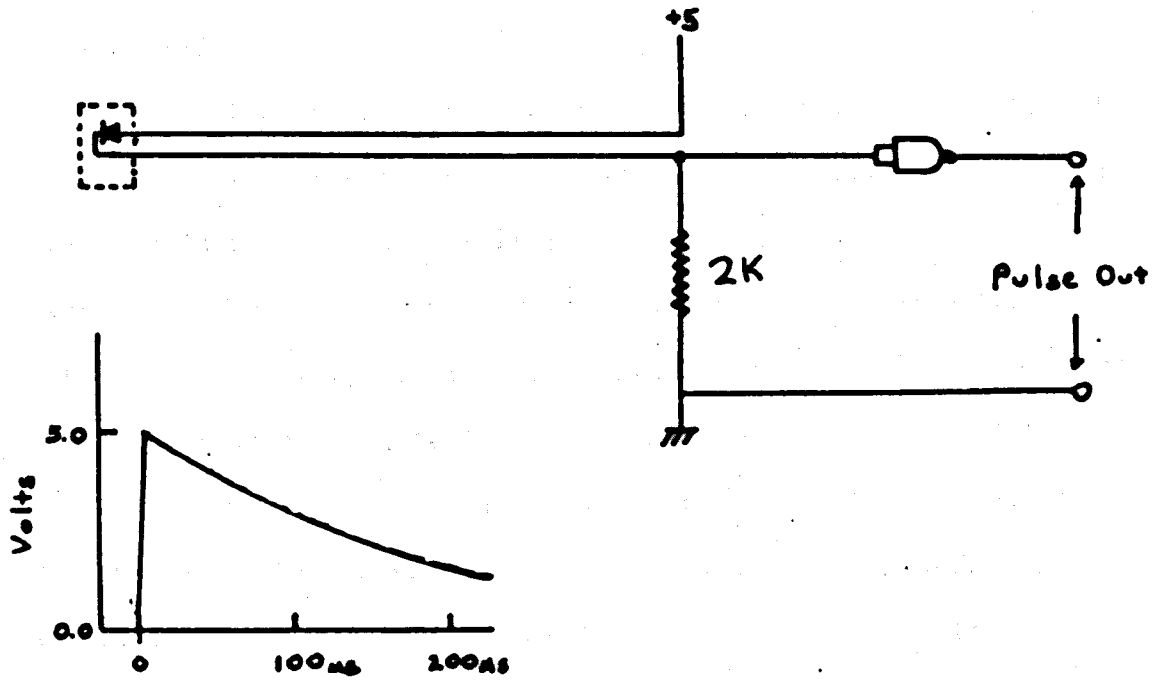

Figure 5. Circuit diagram of the device used to generate electronic pulses coinciding with the firing of the dye laser. Nangate is a cmos4093.

current Electron Capture detector for gas chromatography used in Dr. Eric Grimsrud's lab. The author wishes to thank Berk Knighton for supplying information and discussions leading to the final design of this circuit.

Figure 6 shows a diagram of the pulse delay circuit. Input is from the pulse generator discussed above. The circuit is essentially composed fo four monostable flip flops comprised of pairs of nandgates. This pulse is shortened, but remains variable from 2 μsec-200 msec through resistors R_1 and R_2. The output (pin 4 of IC1) from the first monostable is shaped and buffered in IC4 (a TTL buffer) and then output to the integrator module (D in Figure 4). This pulse is also inverted and fed into a second monostable which generates a pulse (#1) rising at the end of the first pulse and falling 2 μsec to 200 msec later as set by R_3 and R_4. Output from this, the second monostable, is directed into the third set of gates, on IC3, to provide a pulse (#3) which is delayed by the duration of pulse #2. The width of pulse #3 is controlled by R_7. Pulse #3 is buffered and goes to the A/D converter to alert it that data is available.

The reset pulse (#4) for the integrator circuit is triggered by the trailing edge of pulse #3. All pulses are TTL compatible, e.g. the logic states are +5 and 0.

The quartz enveloped photomultiplier tubes (PMT1 and PMT2) are used to measure the fluorescence of the sample (PMT1) and the intensity of fluorescence from a Rhodamine B solution (3g/l) indirectly illuminated by the dye laser beam. Two different types of

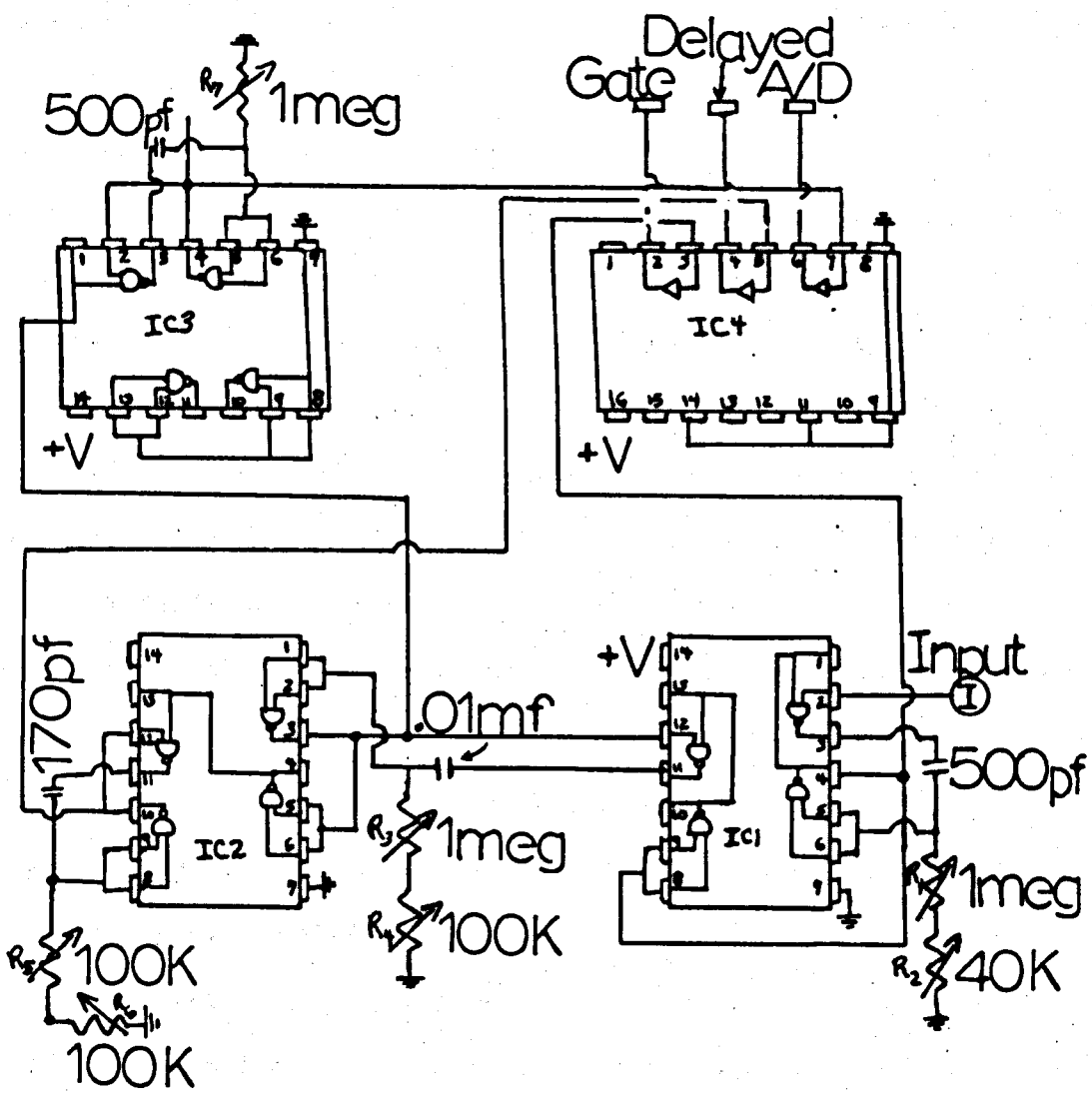

Figure 6. Pulse shaping and delay circuitry. IC1 = IC2 = IC3 = CMOS4093, IC4 = CMOS4050.

tubes were used in the experiment. PMT2 was always an RCA IP28Q operated from -300 to -600 volts. Gain in the photocurrent operated at this voltage is $10^3 - 10^4$, an adequate amount considering the large number of photons impinging on the photocathode. The tube used to measure two photon excited fluorescence of the sample was either 1P28Q, an EMI 9558QB, or Hamamatsu R955. The EMI's gain is two orders of magnitude greater than that of the 1P28QB and its signal to noise ratio is much greater.

Figure 7 shows the plug configuration and output circuiting for a 1P28B photomultiplier tube. You will note that the negative high voltage is dropped evenly over the eight dynodes of the PMT, which accelerates electrons toward the anode. From there current flows through a 1 meg Ω resistor (whose purpose is to spread out the rise time of the pulse) then into an RC circuit. The resistance and capacitance shown yield a time constant of 10^{-5}s. Output signals are passed onto an amplifier.

C. High voltage power supplies: These are used to provide high voltage to PMT1 and PMT2. These supplies were very generously loaned to us by the late Dr. Ray Woodriff and are matching Fluke model 412B 0-2000 volt variable with selectable polarity, High voltage coaxial cables and BNC connectors were used to connect the power supplies with the PMT's.

D. Amplifier: A dual polarity, linear op-amp based amplifier constructed by the author. Figure 8 shows a circuit diagram of this device. Signals from the phototube are fed directly into the inputs. By use of the variable resistor inputs can be matched so that dark

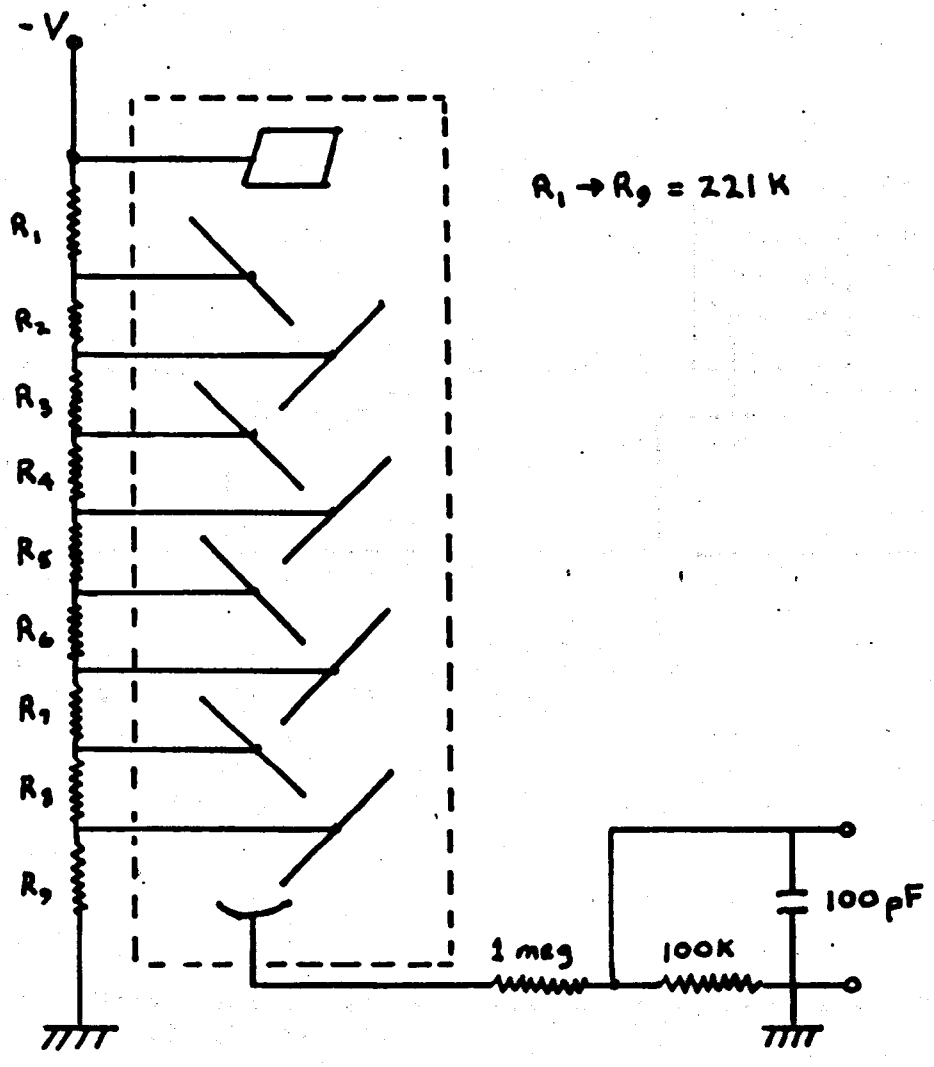

Figure 7. Base plug and current to voltage convertin circuitry for a 1P28 photomultiplier tube.

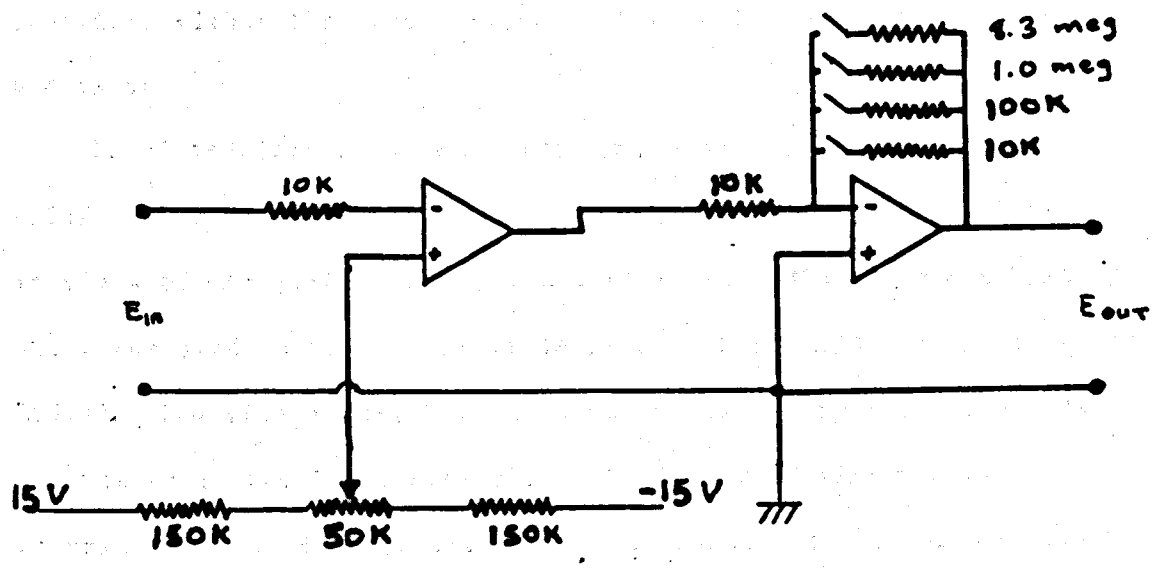

Figure 8. Circuit diagram of the amplifiers used to collect and magnify PMT signals.

current from the phototubes are effectively subtracted. Resistors R(5)-R(8) are selective via an external switch so that a gain of 1 - 830 can be obtained. All resistors are precise to 1 % and the op-amps are CMOS 3140s or 307. Two identical amplifier circuits are contained within the same box, so that signals from both PMT's can be processed.

E. Gated integrator modules: Evans Associates of Berkeley, California supplied us with two model 4130 devices which perform the services of integrating amplified signals from the PMT's and holding the integrated voltage until it is read into the A/D converter on the LSI 11. The time interval of integration is set by the pulse delay circuit as is the integrated signal hold time. Under normal experimental conditions, signals are integrated for ca. 200 μs and held for 5-10 msec before being reset to await the next incoming pulse. Specifications and circiut diagrams are available in the lab of P. R. Callis.

PDP11/03: A high speed, 16 bit computer from Digital Equipment Company (DEC). The processor is an PDP11/03 with 32K of RAM. The processor was a ift from Dr. Michael Schaer of Computers Unlimited, Billings, Montana, and supports the RT11FB operating system. The power supply, housing (with 32 slot backplane), 16 bit bus and dual 8-inch floppy disk drives are from Charles Rivers Data Corporation. The parallel interface board (64 bidirectional ports with handshaking) is a DEC model DRV11-J and the serial interface is a DEC model DLV11-J with 4 send/receive RS232 compatible ports and variable baud rates (150 - 9600) for each port. Data from the experiments is

read into the computer through an analog-to-digital (A/D) converter (Data Translation model 762) and is used in our experiments to alert the computer that data is being held on the gated integrator module. Each channel is individually addressable, however only one channel can be read on a single conversion.

Control of the PDP11/03 is from a DEC model VT100 terminal operated at 9600 baud and interfaced through port 3 of the DLV11-J. Hard copies of data can be obtained either by connecting a line printer to port 2 of the DLV11-J or by passing the data through port 0 onto a hard wire connection to CP6, the campus computer system. Details of the computer dump hardware are available in the lab of P. R. Callis.

SM1,SM2,SM3 stepping motors: These three stepping motors are used to scan the dye laser, turn a glan prism polarizer and rotate a shutter. SM1 is rated at 4.3 volts, 1.8 amps/phase, 40 oz. inch torque and 200 step per rotation. SM2 and SM3 are identical and require 8 volts at 0.85 amps per phase and provides 200 steps per revolution at 50 oz. in. torque. Connections between the motors and the physical devices named above were constructed by Richard Jones and/or myself. The shutter is controlled by direct drive, whereas the prism is connected through gears and the dye laser by a belt.

F. Stepping motor drivers: Four separate boards were constructed to provide sequenced pulses to the stepping motors (the fourth motor is connected to a small monochromator). These boards were designed by Timothy Aoki and the author and were built by

Timothy Aoki, Richard Jones, Andrew Valkenburg and/or myself. Circuit diagrams are available from P. R. Callis. Control of the stepping motor drivers is switch selectable to manual or computer. Under computer control, the desired number of steps (sequences of pulses), the direction of stepping (forward/reverse) and the stepper motor number are sent to a multiplexer, which was designed and built by the author, through the parallel interface. The multiplexer then switches all control signals to the desired motor's driving circuit. Manual control is through a remote circuit attached directly to the motor's driving circuit.

All detection and control circuits are isolated from the ground of the N_2 laser. Signals and control pulses are relayed between devices with coaxial cables and BNC connectors. Power supplies for all the electronic devices were built in our lab by Richard Jones or myself.

Software

Several programs were written to provide control over instrumentation data collection and data processing. A program called SPEC was written in fortran and performs the following functions:

1. Reads in data collected on the A/D converter.
2. Sends pulses to the appropriate stepping motors and keeps track of the position or state of these devices.
3. Averages the signals from PMTs and subtracts dark current from same.

4. Writes gathered data to disk files.

Documentation and copies of this program are available in the lab of P. R. Callis.

A terminal control program was obtained from Paula Fischer (MSU Physics Department) which dumps files from the PDP11 to the campus Honeywell computer through the DLV11-J interface. This program was used extensively to transfer data so that manipulations and graphs could be made. It is written in Macro and can be obtained in the lab of P. R. Callis.

In order to fit the separate two photon excitation curves segments together, a program was written in fortran called CURVE. This program can be executed on any graphics terminal and allows for hard copies to be made on the campus Calcomp plotter. Again, details and copies are available in the lab of P. R. Callis.

Optics

The optical arrangement used a majority of the time experimentally is presented in Figure 9. Described below are each component comprising the apparatus.

A. Double-convex lens: A 12.6 cm focal length double-convex lens with antireflective coating mounted on an x translatable stage. This lens is used to gather the dye laser light and focus it to a point.

B. Focal length lens: A 2.5 cm focal length lens coated and mounted in the same manner as A. The x translatable stage is used to

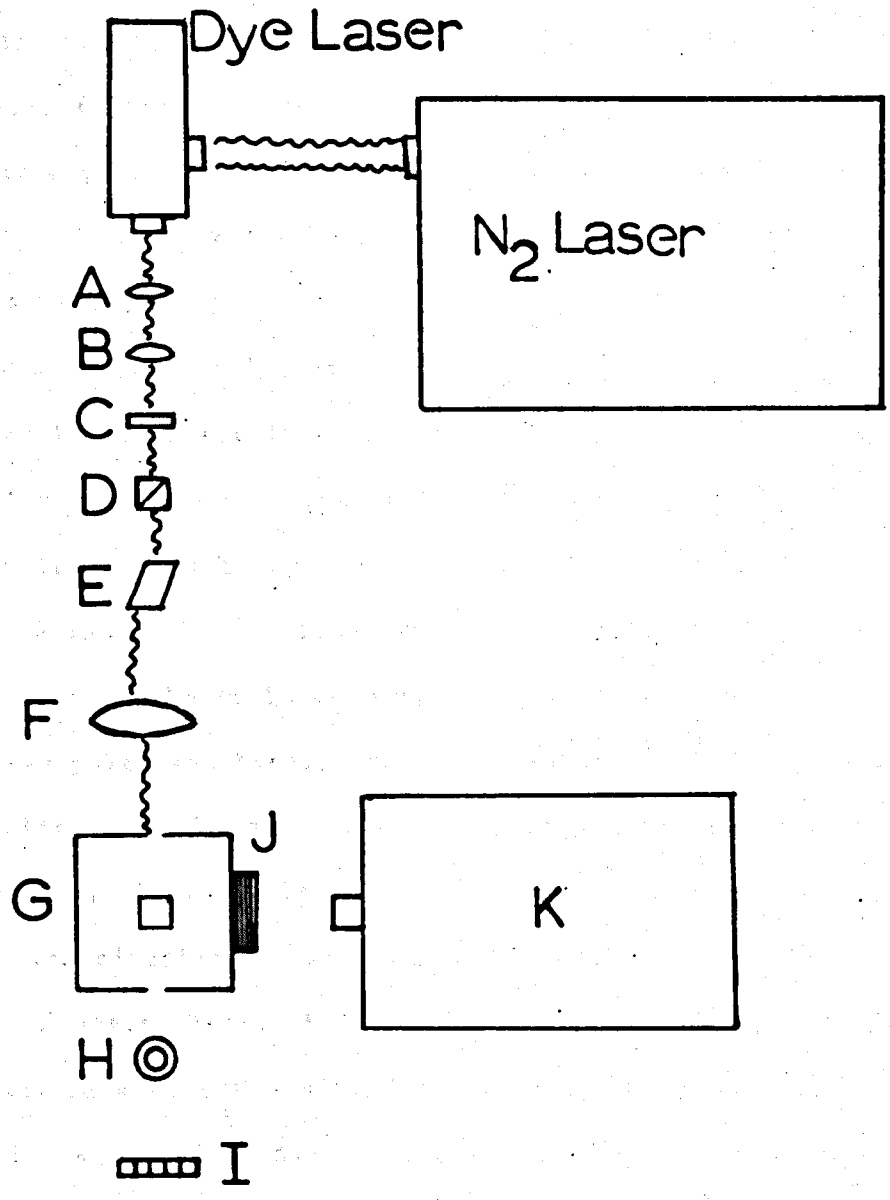

Figure 9. Arrangement of optics used in the two photon fluorescence excitation apparatus.

position this lens one focal distance away from the focal point of lens A resulting in a columated output beam.

C. Neutral density filter: Four 2" by 2" filters were purchased from Rolyn Optics and had transmissions ranging from 9% - 50%. These filters were moved into the light beam to check the quadratic dependence of the sample two photon absorption on light intensity. When data was being taken, the the filter was removed from the beam path.

D. Glan-laser polarizer: This polarizer was used to convert the laser light to all linearly polarized photons. It was mounted on a stepping motor so that its orientation could be varied from 90°, relative to the bench top, to 45° in a quick, reproducible fashion.

E. Fresnel Rhomb: This device was mounted on a goniometer head so that it could be positioned very precisely and was used to produce circularly polarized light. When the incident beam is polarized 90° to any side of the Rhomb, the outgoing beam retains the same polarization. However, if the incoming beam is polarized 45° to the Rhomb base, circularly polarized light results.

F. Focusing lens: A 18 cm focal distance double convex lens, 2.5 inches in diameter was used to focus the columated laser light onto the sample. In order to test whether sample emission resulted from two photon absorption, the focal point of the lens was moved in and out of the solution.

G. Sample cell and compartment: Teflon stoppered 48 mm height by 12.5 mm length by 12.5 mm width fused silica fluorescence cells were used to contain samples. The cell holder was mounted within a

box which also contained a 1P28B photomultiplier. The top of the box was hinged to allow easy replacement of samples and to black out reflected light.

H. Beam diffuser: The purpose of this element was to diffuse the beam in order to measure its intensity. A 34/45 to 25/40 ground glass bushing adapter placed directly in the beam was selected to serve this purpose.

I. Reference cells: Four plastic disposable absorption cells were filled with Rhodamine B solution (3 g/l) and taped onto the light entrance of the reference PMT housing. The diffused laser light was absorbed by the Rhodamine B solution and emitted at a constant wavelenght which, in turn, struck the PMT photocathode.

J. Light filters: Quartz plate filters were purchased from Rolyn Optics and were CS-7-54-9863 UV transmitting. To further filter the light reaching PMT2, a 1 cm X 4 cm X 4.6 cm quartz cell was filled with $NiSO_4$ solution and placed in the emission path.

K. Fluorescence monochromator: In order to measure two photon excited fluorescence spectra, the fluorescence monochromator of the analog instrument described earlier was placed in the configuration shown in Figure 9. The 9558QB PMT was attached to the exit slits to measure sample fluorescence.

The mounts for the optics and devices described above were built by either the personnel of the Physics machine shop, Richard Jones or myself. A 3/8" X 48" X 144" sheet of aluminum was placed on top of the bench in our lab and was drilled and tapped to provide a

surface on which to mount the optics. No specific care was taken to reduce building vibrations at the optical surface.

Experimental Procedure

Samples were mixed in 50 ml ground glass stoppered volumetric flasks. Benzimidazole solutions were 0.2 molar in a 1:1 mixture of cyclohexane and isopropanol. Absorption and fluorescence measurements were taken of dilute samples of these mixtures to check their purity.

Approximately 5 ml of each sample was transferred to 13 X 13 X 48 ml fused silica cells and sealed with teflon stoppers. The samples were then excited, in turn, by dye laser light in the wavelength range from 400-600 nm at .5 nm increments and the fluorescence intensity divided by the square of the laser intensity was recorded.

The emission was checked several times over the tuning range of each dye to insure that it varied as the square of the laser intensity. Since the range of the laser dyes were limited to ca. 30 nm, overlaps of 5 nm between dyes were measured where possible. Special care was taken to make sure that scattered light surrounding the beam was eliminated and that the light reaching the sample was of high quality. The data gathered from each dye was written to the PDP11 disk, then transferred via a hard wire couple to the campus Honeywell 66 computer.

When the desired wavelength range had been covered, the curve segments were fit together by use of the program CURVE (described

above) which requires visual inspection (on a Tektronics 4010 CRT) and user issued commands to scale the curve segments relative to each other. When the spectrum was completely assembled, a hard copy was produced on the Calcomp plotter.

To check whether our equipment and methods provide a true TPA spectrum, excitation of benzene's L_b band was determined using the above equipment and procedures. Figure 10 displays the results of this first attempt. These results are identical in wavelength and intensity to those kindly sent to us by Thomas Scott, a former graduate student of A. Albrecht at Cornell University.

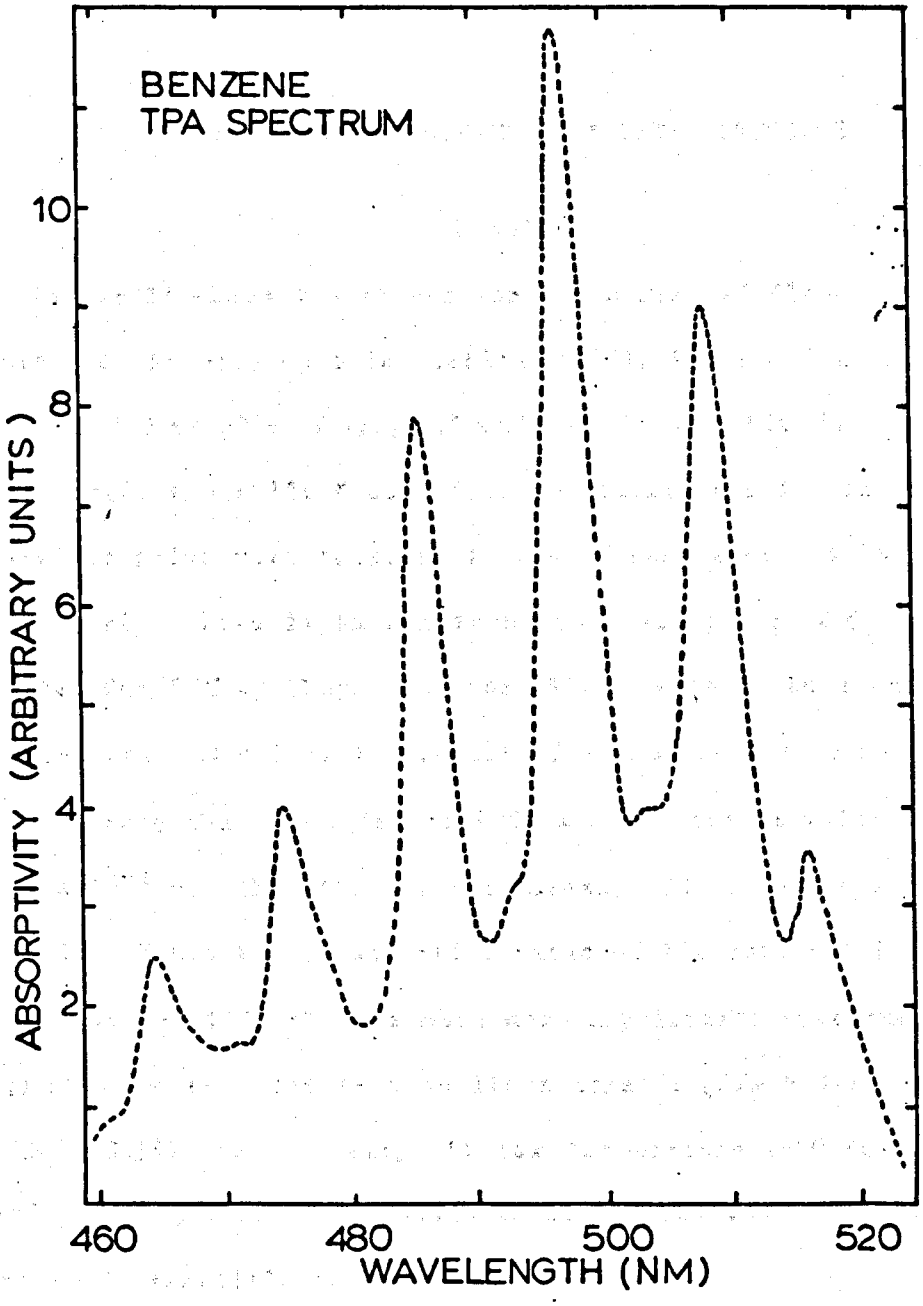

Figure 10. TPE of benzene's L_b band.

POLARIZED FLUORESCENCE OF 5-METHYLCYTOSINE

Results

Figure 11 shows the absorption and corrected fluorescence spectra for 5-methylcytosine cation ($5MC^+$), 5MC and 5-methylcytosine anion ($5MC^-$) at pH's of 1.8, 7.5 and 14.0, respectively. In related experiments, the shift from cation to neutral speciation and that of neutral to anion were observed in the pH ranges of 4-6 and 11-13, respectively. This is in agreement with the pK_a of 4.6 and 12.4 reported for 5MC by Shugar and Fox (52). Table 2 shows our experimental and calculated results for the three species of 5MC. You will note that the ϕ_f's for $5MC^-$ and 5MC are very low at 3×10^{-4} and 5×10^{-4} but that the anion fluoresces 30 to 50 times more strongly. Since the polarization ratio of fluorescence is inversely related to ϕ_f, $5MC^-$ shows a much more depolarized spectrum (I_V/I_H = 1.04) at room temperature than its neutral (I_V/I_H = 1.4) and cation (I_V/I_H = 1.69) counterparts. At low temperature (-100°C), all three display high polarization ratios in accordance with strongly allowed electronic transitions.

Lifetimes, either calculated or experimental, are also shown in Table 2. Radiative lifetimes were calculated by the Stickler-Berg method (3), e.g. by integrating the area under the first absorption band, and were found to be about 10 ns for each species.

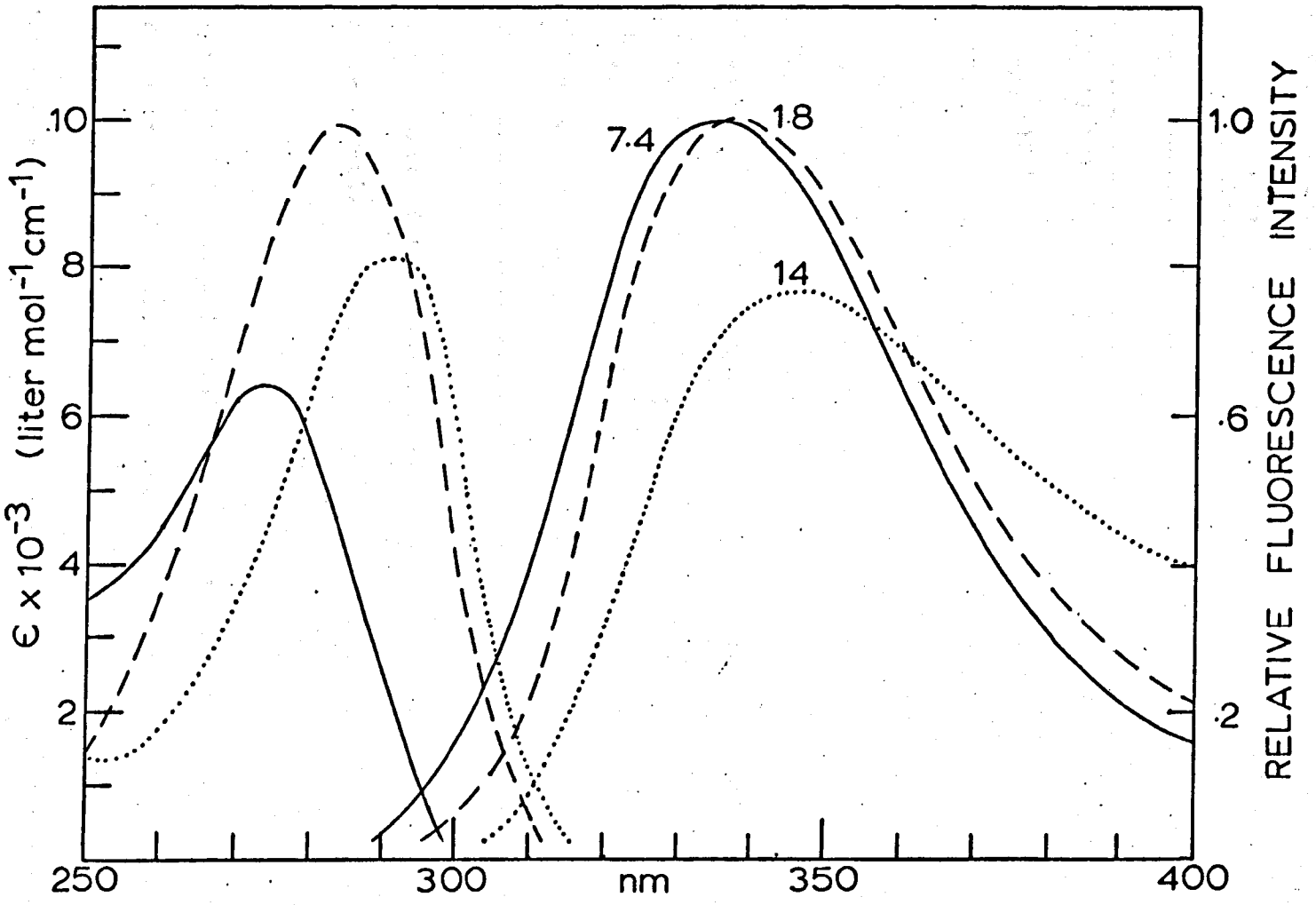

Figure 11. Absorption and fluorescence of $5MC^{+}$ (——), 5MC (——) and $5MC^{-}$ (···) in room temperature aqueous solution.

Table 2. Polarizations at room temperature and in low temperature glasses, fluorescence yields, computed radiative lifetimes and calculated rotational correlation times for 5-methylcytosine species.

	$5MC^+$	5MC	$5MC^-$
I_V/I_H (293K)	1.69 ± .001	1.40 ± .01	1.04 ± .01
I_{Vo}/I_{Ho} (180K)	1.79 ± .01	1.75 ± .01	1.70 ± .01
P (293K)	.256 ± .003	.167 ± .003	.020 ± .005
P_o (180K)	.283 ± .003	.273 ± .003	.260 ± .003
τ_f/τ_c	0.1 ± .02	0.58 ± .06	12 ± 4
ϕ_f X 10^4 (293K)	3 ± .5	5 ± 1	140 ± 10
τ_o^{SB} ns	7 ± .7	10 ± 1	11 ± 1
τ_c^{SB} ps	22 ± 10	9 ± 4	11.5 ± 3
τ_f^{SB} ps	2 ± 0.5	5 ± 1	140 ± 10
τ_c^{stick} ps	40	40	40

Fluorescence lifetimes (τ_f) are also shown and were calculated by use of the formula

$$\tau_f = \tau_o \phi_f \qquad [10]$$

From this data, experimental polarizations and the Perrin equation (60) (see equation 1), τ_c^{SB} were determined and found to be about 2-4 times faster than those calculated by sticking hydrodynamics. Values for the ratios τ_f/τ_c were obtained from the measured polarizations and the Perrin equation.

Figure 12 shows a plot of log quantum yield and polarization ratio versus pH for 5MC. Curvature is seen in both sets of data near the reported pK_a's of 4.6 and 12.4, indicative that two different fluorescing species existing in equilibrium are present in those regions. The solid curves seen in this plot were calculated from the reported pK_a's and molar extinction coefficients and the data in Table 2. Quantum yields and polarization data presented here are in good agreement with those reported previously (6,67).

Conventions and Theory

Polarization ratios (N) can be obtained in several different manners. The two most popular methods are to position a polarizer between the light source and sample and either measure the resultant fluorescence intensity with or without a polarizer in front of the analyzing monochromator. These two methods are roughly equilvalents in that polarization ratios ($N = I_V/I_H$) and polarizations {$P = (I_V - I_H)/(I_V + I_H)$} found by use of a single polarizer can easily be translated to those values expected from use of two polarizers by the expression $P_2 = (N_1 - 1)/(N_1)$. One polarizer was used in all the experiments reported here.

Rotational correlation times for a sphere with solvent sticking to its surface can be calculated by use of the Stokes-Einstein equation

$$\tau_c^{stick} = \eta V/kT \qquad [11]$$

where η is the viscosity and V is the molecular volume of a sphere.

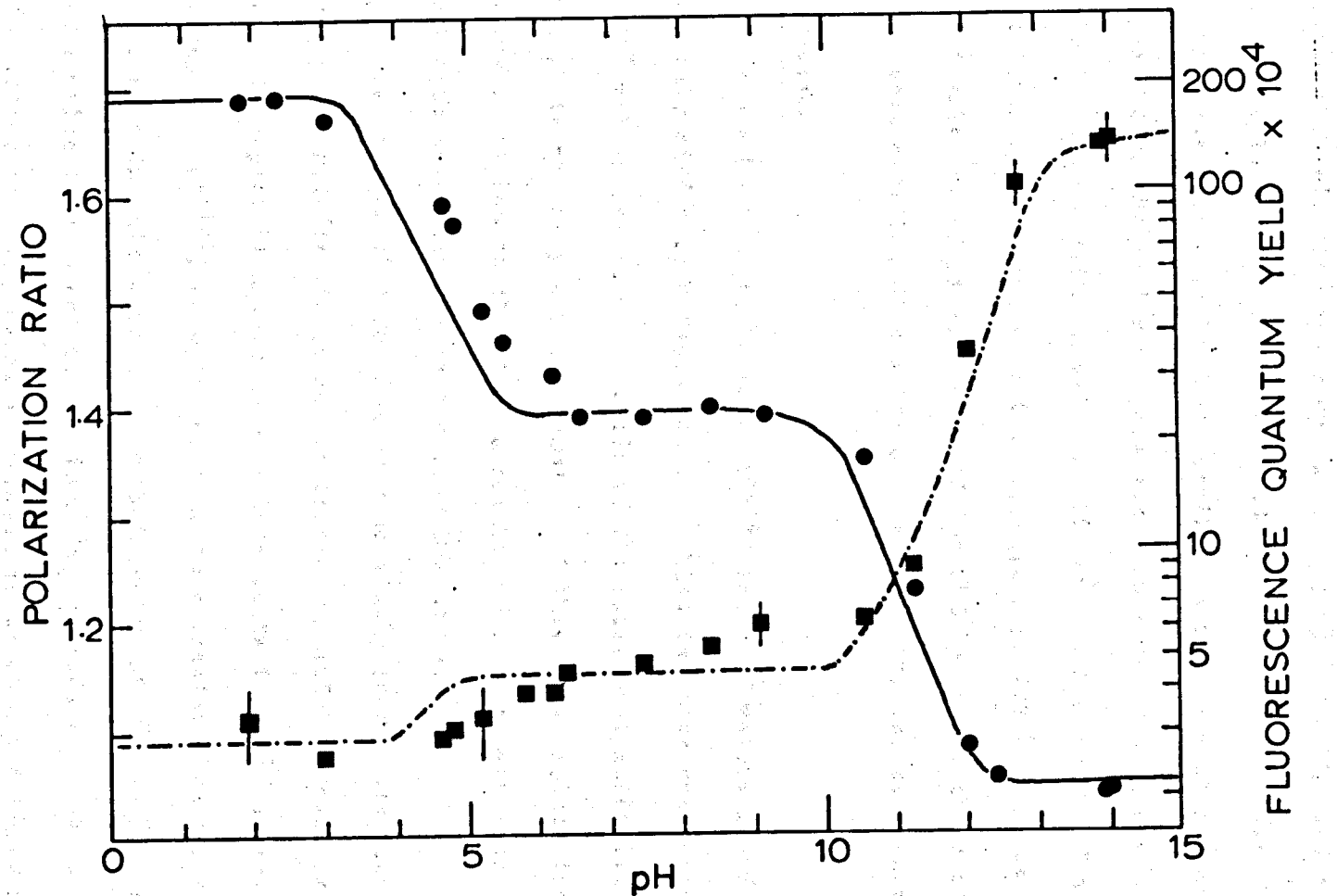

Figure 12. Experimentally obtained ϕ_f's (●) polarization ratios (■) of 5MC as functions of pH in room temperature aqueous solution.

We used a slightly different form of this equation which takes into account the molecular geometry in finding τ_c^{stick} (62). 5MC was assumed to be an oblate elipsoid with axial lengths of 3.4 and 8.1 for the axes perpendicular and parallel to the molecular plane, respectively. Molecular volumes were found by summing the Van der Waals increments (63). A value of 118 $Å^3$ was found for 5MC while that found by assuming an oblate ellipsoid is 117 $Å^3$. An average τ_c^{stick} value of 40 ps was obtained for 5MC by use of these methods. For a more detailed discussion on these points, see reference 28.

Discussion

As can be seen in Table 2, τ_c^{stick} and τ_c^{SB} values found in this work only differ by a factor of 2-4. This is quite reasonable since τ_c^{stick} values are an upper limit of the rotational diffusion times and τ_c^{SB} is probably a lower limit (5). This also implies that τ_f^{stick} is 2-4 times longer than τ_f^{SB}, a result which is in agreement with the work done by Callis (5) on the four DNA bases.

That our results for 5MC vary so widely from those found by Morgan and Daniels (6) is due to different, and incorrect on their part, interpretation procedures. They state that τ_c^{SB} is ca. 50 times faster than τ_c^{stick}, an order of magnitude greater than the difference calculated in this work. Using their value of $\tau_c^{SB} = \tau_c^{stick}/50 = 0.85$ and a value of 0.58 for the ratio τ_f/τ_c, yields $\tau_f = .45$ ps, a factor of 9 faster than τ_f^{SB} which is assumed to be an upper limit for 5MC.

Morgan and Daniels (6) found their values for τ_c from the slope of 1/P vs. ϕ for 5MC where pH conditions were changed under the

assumptions that τ_f for 5MC was changing with pH and that τ_c is given by

$$\tau_c = \tau_o^{SB} \left(\frac{\text{slope}}{\frac{1}{P_o} + \frac{1}{3}} \right)^{-1} \qquad [12]$$

This equation is only valid for a single emitting species. In the experiments performed in our lab, the results of which are seen in Figure 12, we were only able to change the ϕ_f of 5MC solutions by introducing cation or anion fluorescence. Since obviously the ϕ_f and τ_f of neutral 5MC do not change, Morgan and Daniels interpretation is inappropriate.

In 1952, Weber (64) derived an equation for finding the polarization of fluorescence from a solution containing more than one fluorescing species when excited by unpolarized light. It is given by

$$\frac{1}{P} + \frac{1}{3} = \frac{\left(\frac{1}{P_{oi}} + \frac{1}{3}\right)}{\sum_i (f_i)} \qquad [13]$$

where

$$f_i = \frac{I_i}{\sum_i I_i} \qquad [14]$$

and I_i is the total fluorescence intensity emitted by the ith species at the exciting wavelength chosen.

If there is a wavelength of excitation where the I_i's are in the same proportion as the integrated fluorescence intensities, then the following equation is valid,

$$f_i = \frac{X_i\phi_i}{\sum_i X_i\phi_i} = \frac{X_i\phi_i}{\phi_{TOT}} \qquad [15]$$

where X_i is the fraction of light absorbed by the ith species, ϕ_i is the quantum yield of the ith species and ϕ_{TOT} is the apparent quantum yield of the solution.

The exciting wavelength meeting the above criteria for 5MC and $5MC^-$ is 355 nm. We deduced this after all our experiments were complete, however, so all the polarization work was done at 345 nm. This has only a negligible effect on our results.

We can rewrite the Perrin equation by introducing equations 12 and 13 to get

$$\frac{1}{P} + \frac{1}{3} = \frac{\phi_{TOT}}{\sum_i \frac{X_i\phi_i}{(\frac{1}{P_{oi}} + \frac{1}{3})(1 + \frac{\tau_{fi}}{\tau_{ci}})}} \qquad [16]$$

where P_{oi} is the limiting polarization of the ith species, τ_{fi} is the fluorescence lifetime of the ith species and τ_{ci} is the rotational correlation time of the ith species. Rewriting equation 16 for 5MC and $5MC^-$ and letting $\tau_{fa}/\tau_{ca} = Ra$, $\tau_{fn}/\tau_{cn} = Rn$, where the

subscripts denote the anion and neutral, respectively, we obtain,

$$\frac{1}{P} + \frac{1}{3} = \frac{X_a\phi_a + X_n\phi_n}{\dfrac{X_a\phi_a}{(\frac{1}{P_{oa}} + \frac{1}{3})(1 + Ra)} + \dfrac{X_n\phi_n}{(\frac{1}{P_{on}} + \frac{1}{3})(1 + Rn)}} \qquad [17]$$

If we substitute $X_n = 1 - X_a$ and take the derivative of equation 9 with respect to ϕ, we find that the slope in the limit of small X_a of a 1/P vs. ϕ_f plot is given by

$$\text{slope} = (\frac{1}{P_o} + \frac{1}{3})(\phi_n^{-1} + \frac{\tau_{cn}}{\tau_c})\left[1 - \frac{(1 + Rn)\left(\dfrac{\phi_a}{1 + Ra} - \dfrac{\phi_n}{1 + Rn}\right)}{\phi_a - \phi_n}\right] \qquad [18]$$

where Po and τ_o are the same for both species. If we let Z be equal to the terms enclosed in brackets and solve for τ_c we obtain

$$\tau_c = \tau_o^{SB}\frac{\text{slope}}{Z(\frac{1}{P_o} + \frac{1}{3})} - \frac{1}{\phi_f^{OBS}} \qquad [19]$$

where the Z value was found to vary slowly from 0.9 to 0.95 at small anion concentrations. From equation 19 we can see that the linear variation Morgan and Daniels found for ϕ_f of 5MC was merely an unfortunate coincidence.

Figure 13 shows a plot of 1/P vs. ϕ_f^{OBS}. The boxed in area in the lower left hand side of the graph indicates the region studied by

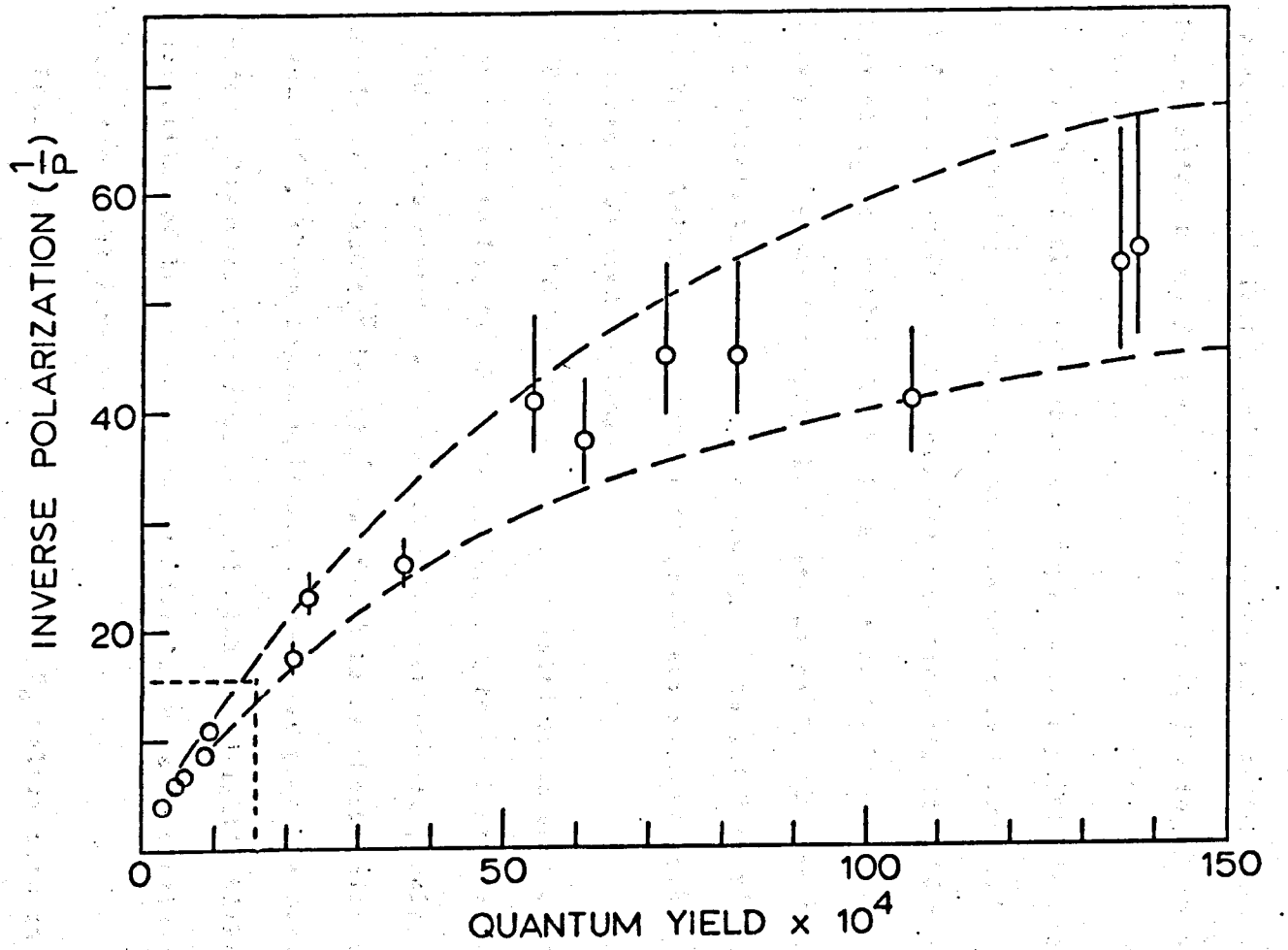

Figure 13. Experimental values of 1/P plotted versus ϕ_f^{OBS} for 5MC. The dashed lines above and below the points were obtained semi-empirically.

Morgan and Daniels (6). The slope in this area is ca. 10^4 which is in agreement with that found by the above authors (6). However, using equation 19 we find τ_c = 13 ps, as compared to 1.7 ps obtained by use of equation 12.

You should also note that the experimental points in Figure 13 become increasingly non-linear as more anion is introduced. The dashed curves in Figure 13 were produced from equation 16 using the values of τ_f reported in Table 1 and τ_o = 10 ns for both the anion and cation. Values for τ_c of 11 ps and 14 ps for 5MC and $5MC^-$ were used to obtain the lower curve while τ_c = 7 ps and 9 ps yielded the upper line. Values taken from this graph are in very good agreement with those presented in Table 1.

Comment should be made on the accidental appearance of the cation point in Figure 13. That it appears to fall on the line created by the neutral and neutral-anion mixtures is purely coincidental. The τ_c^{SB} for $5MC^+$ was found to be about twice that for 5MC and $5MC^-$, which is not unlikely since it is probably more highly solvated. However, this fact coupled with the slightly higher polarization and lower ϕ_f places it directly on a line passing through the first five points.

Lastly, it should be pointed out that P_o values used in obtaining τ_c values above were from low temperature-viscous glass experiments. These are somewhat below the theoretical maximum of 0.333. However, experiments in our lab have never obtained this high value. Albrecht (65) pointed out that there is some intrinsic depolarization in molecular fluorescence even at very short times

after excitation, so we felt it appropriate to use the experimental P_o values. If 0.333 had been used, τ_c would be 5.5 ± 1 and 7.7 ± 1 ps for 5MC and $5MC^+$, respectively.

Conclusion

It was shown that the fluorescence lifetime of 5MC does not vary with pH as previously reported (6) and that changes in ϕ_f of 5MC can only be affected by introducing small amounts of its cation or neutral form. Using Weber's (64) equation and the Strickler-Berg method (3), we have found that τ_c^{SB} values for 5MC and $5MC^-$ differ by a factor of ca. 4 from those predicted by sticking hydrodynamics.

In addition, it was found that $5MC^+$ appears to rotationally diffuse twice as slowly as the neutral and anion species. This is thought to be a consequence of this charged molecules more tightly bound hydration sphere.

WAVELENGTH DEPENDENT QUANTUM YIELDS OF 5MC, CYTIDINE AND THYMINE

Results and Discussion

Tautomers

Unlike in the case of adenine and guanine, no single tautomer exists which can readily be blamed for causing the excitation energy dependent ϕ_f of cytosine. Although more than ten tautomers and conformers can be written for cytosine, only a few have actually been characterized in experiments. Six of these tautomers are pictured in Figure 14. We see that two of the structures shown in this figure are in the amino - keto form (I and II), one is shown as an imino - keto (III), two are pictured as imino - enol tautomers (IV and V) and the last is seen to be an amino - enol (VI). Structures I and II and molecules IV and V only differ by the placement of the ring hydrogen (from N(1)H ——> N(3)H). Early research (66) has shown that cytosine exists as structure I a majority of the time in aqueous solutions while it has been asserted that structure VI is most stable in the gas phase (67). Only a small number of studies, both experimental and theoretical, have been performed with the aim of elucidating the equilibrium between tautomeric forms of cytosine. A survey of the current literature will be presented here along with a further discussion of the consequences of cytosine tautomerism.

In one of the earliest papers appearing on this subject, Goddard, et. al. (67), have used an ab-initio LCAO-MO-SCF

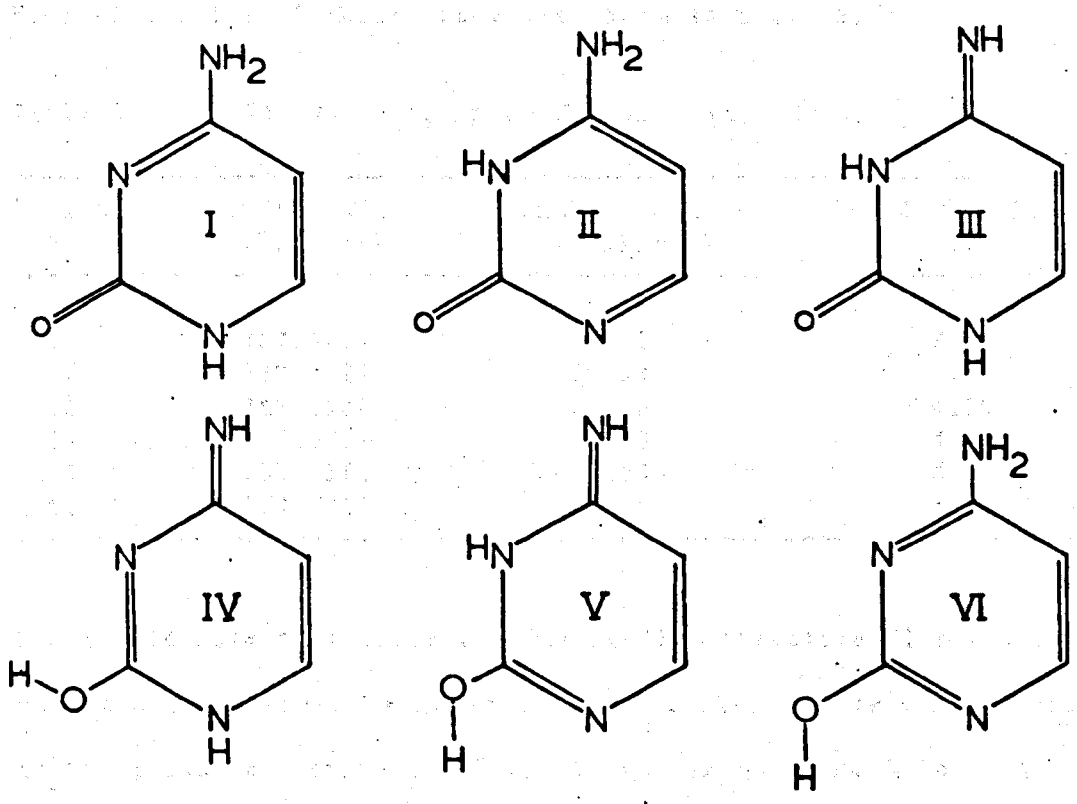

Figure 14. Structures of six of the possible cytosine tautomers.

Hartree-Fock-Roothan calculation with a contracted Gaussian basis set to investigate the six cytosine tautomers shown in Figure 14. Partial results of their study are shown in Table 3.

Table 3. Results from study by Goddard, et.al.(67).

TAUTOMER	TOTAL ENERGY (Hartree)	RELATIVE ENERGY (kcal/mol)	IONIZATION POTENTIAL (eV)
IV	-387.4784	41.42	5.45
V	-387.4977	29.29	5.47
III	-387.4984	28.48	6.26
II	-387.5066	23.70	5.42
I	-387.5161	17.73	5.80
VI	-387.5400	00.00	6.80

One should note that these results predict structure VI to be the most stable tautomer as an isolated molecule, i.e. in the gas phase at low pressure. Tautomers I and II appear to be much less favorable, with a ΔH of 17.73 and 23.70, respectively, with the energies of structures III, V and VI lying even higher in energy. These results are more or less those expected for low pressure gas phase experiments. Possibly, the aromatic character of structure VI could provide added stability in the absence of any solute-solute or solute-solvent interaction. In aqueous solution, this tautomer might likewise be expected to be the least favorable due to its lack of solvation energy. The relative ordering of the remaining five tautomers energies would be expected to remain intact in moving from the isolated molecule to that of the solvated molecule case judging from the similarity of their solvation sites.

In a more recent study by Czcinirski, Lesyng and Pohorille (68) using the semi-empirical MNDO/3 method, structure I was found to be lowest in energy, followed by tautomers II (ΔH = 3.7 kcal/mol), III (ΔH = 4.7 kcal/mol), VI (ΔH = 8.9 kcal/mol), V (ΔH = 19.2 kcal/mol) and IV (ΔH = 20.0 kcal/mol). These authors employed complete geometry optimization which could account for some of the differences found between this work and that of Goddard, et. al. (67). Assuming no large changes in entropy, tautomers IV - VI would possess K_T's on the order of 10^{-6} to 10^{-15}, assuring that their occurrence in aqueous solution would be rare indeed.

Yu, Peng, Akiyana, Lin and Lebreton (69) performed a UV photoelectron spectroscopic investigation of cytosine and various methyl substituted cytosines in which CNDO/S calculations were employed in correlating spectroscopic data. These authors found that the CNDO/S generated molecular orbitals of tautomer I were in excellent agreement with the photoelectron spectrum of cytosine. CNDO/S calculations of the amino-oxo forms of 1-methylcytosine, N^4,1-dimethylcytosine, N^4-N^4-dimethylcytosine, 1,5- dimethylcytosine, 1,6-methylcytosine, 5-methylcytosine and 6-methylcytosine were found to give the best fit to experimentally obtained UV photoelectron spectra of these molecules.

Only scant direct experimental information has been gathered on the tautomerism of cytosine. Barber and Marsh (70) have observed that 1(H)cytosine is predominant in the crystal form. A study by Bensaude, Dreyfus, Podin and Dubois (71) provides the only other available tautomeric information on cytosine. These authors have

utilized temperature jump kinetic experiments in order to characterize the thermodynamic (ΔH) and kinetic (K_T) behavior of cytosine tautomers. They estimate by use of temperature jump experiments along with UV and IR spectroscopy on methylated cytosines that the equilibrium constants for the reactions

$$\text{1(H)cytosine} \xrightarrow{K_T} \text{3(H)cytosine} \qquad [20]$$

$$\text{1(H)cytosine} \xrightarrow{K_T} \text{1,3(H)-immocytosine} \qquad [21]$$

are 1.3×10^{-3} and 2×10^{-15}, respectively, that the ΔH for reaction 20 is $3.2 \pm .6$ kcal/mol and further conclude that the lifetime of imino-cytosine is 3×10^{-6} seconds.

Several authors have circumvented the inherent difficulties of investigating cytosine tautomerism by, instead, researching the possible tautomeric forms of cytidine. This molecule has only three possible structures (excluding movement or addition of protons on C(5) and C(6)) which are illustrated below.

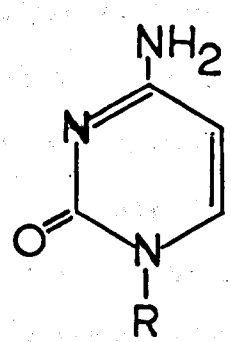

I

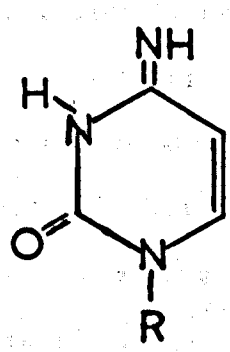

II

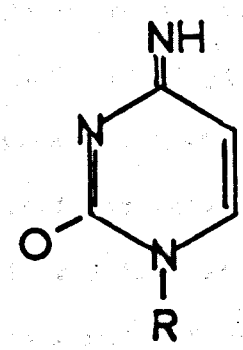

III

[22]

Structure I, which is generally conceded to be predominant in aqueous solutions, is merely cytosine with a ribose ring substituted for the N1 proton. As has been discussed above, this replacement should only introduce a small change in the properties of cytosine. Indeed cytidine's ABS is very similar to that of cytosine and the pK values of the two (4.6 and 12.4 for cytosine, 4.1 and 12.4 for cytidine) correspond very closely. From this point onward, the present author will consider trends in cytosine's and cytidine's physical and photophysical properties to be interchangeable.

One of the most thorough experimental investigations of the cytidine tautomer and also the most applicable to the fluorescence spectroscopy of cytidine tautomers, was performed by Vipond, et. al. (72). In order to establish the major tautomeric form of cytidine found in neutral aqueous solution, UV absorption spectra of cytidine, N^4,N^4-dimethylcytidine (representative of structure I), and 3-methylcytidine (II) were taken. An attempt to obtain spectral information for structure III (mimicked by 1-methyl-2-methoxy-4-imino-pyrimidine) failed due to this molecule's tendency to rapidly hydrolyze to form 1-methylcytosine in basic aqueous solution. Thus eliminating structure III, the authors find that 3-methylcytidine's (3MCD) absorption curve does not in the least resemble that of cytidine while that of N,N-dimethylcytidine correlates very closely with that of the nucleotide. From this and the fact that structures II and III have pKa's in excess of 9.0, cytidine's amino form (I) is

assumed to be the major tautomeric structure found in aqueous solution.

Tautomerism was first investigated as a source for thymine's wavelength of excitation dependent ϕ_f (2). Figure 15 shows the six tautomers that can be drawn from thymine's general structure. Gerdic (73) established that structure I is predominant in the crystal form from x-ray crystallographic data.

In later work (7), absorption and luminescence data was collected for thymine and some closely related pyrimidine derivatives in EGW at 77K. Uracil and thymine were reported to display no emissive character at room temperature in aqueous solution in contrast to EGW at 77K where both were seen to fluoresce only. When comparisons were made with 1,3-dimethyluracil (DMU), 2,4-dimethoxypyrimidine (DMP) and 4-ethoxy-2-pyrimidine (EP), thymine and uracil were concluded to behave most nearly like DMU since DMP and EP were found to exhibit measureable quantum yields of fluorescence at room temperature along with both strong fluorescence and phoshorescence at 77K in neutral EGW. DMU (structure I, lactam only) did not luminesce at 298K and only a weak fluorescence was seen in low temperature glass indicating that uracil (and thymine) must exist in tautomeric form I with the implication that tautomers III, IV and VI are unlikely challengers for the minor species responsible for thymine's fluorescence.

In slight disagreement with the above results is a more recent report on the room temperature luminescence and tautomerism of thymine in aqueous solution. Two tautomers are contended to be

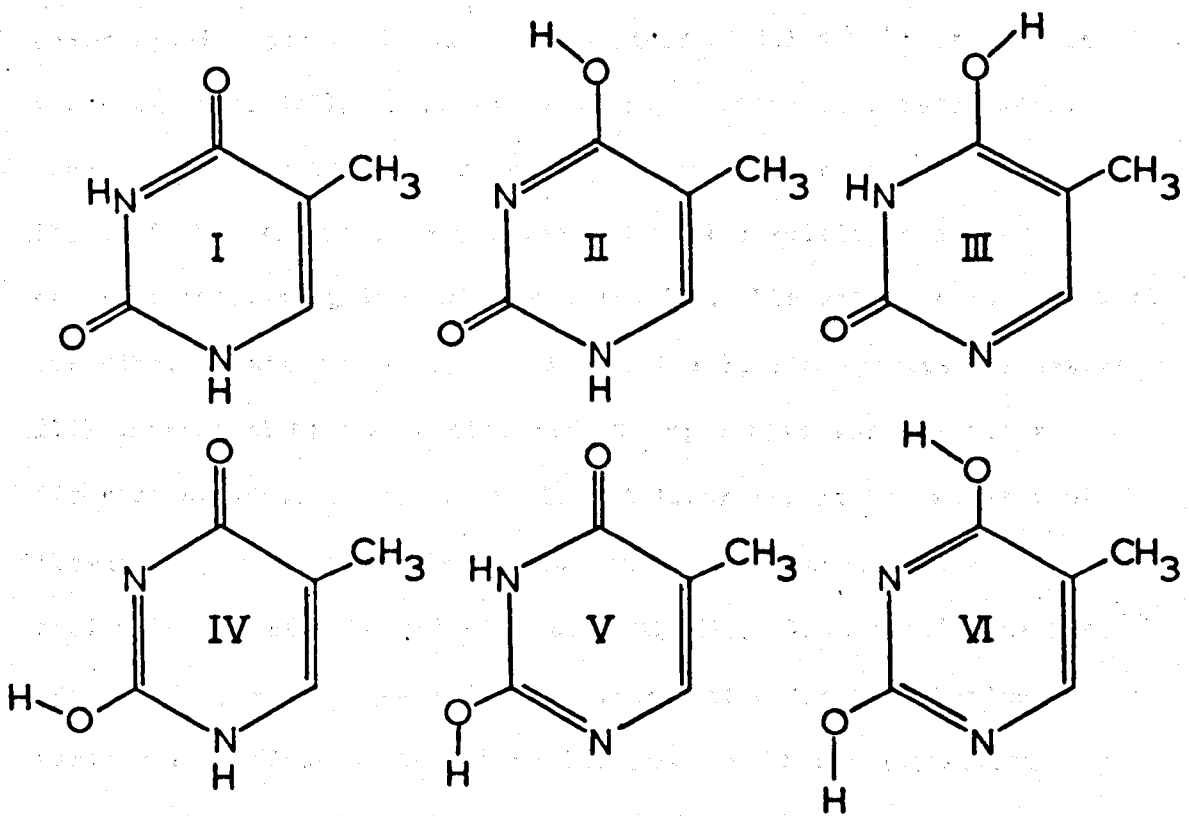

Figure 15. Structures of six of the possible thymine tautomers.

responsible for the molecule's apparent luminescence, one nonfluorescent species with a measurable triplet yield and another minor species possessing a quantum yield of 2.5 X 10^{-4} at 298K in neutral buffer (17). A curve resolving routine is excercised in order to fit two bands representing those required above into thymine's ABS spectrum, a process not unlike solving a single equation containing two unknown variables. The author concludes that the diketo tautomer (structure I) and the lactim species (structure III) correspond to the nonfluorescent major form and the minor fluorescent species, respectively. A later report has shown that thymine's quantum yield is independent of the wavelength of excitation in aqueous solution at 298K (19). This result has been confirmed by a subsequent investigator (18) and thus, thymine tautomeric studies at 300K have lost most of their attraction.

The fact remained, however, that thymine's FES and ABS do not coincide in low temperature neutral EGW glasses. The phenomena was once again addressed in 1980 by Kogan and Becker (39) as they examined the ABS, FES and fluorescence properties of thymine, uracil, thymidine, dimethylthymidine and dimethyluracil in ethanol-methanol (3:1 by weight) and in 2-methyl-tetrahydrofuran (MTHF) at 77K. They concluded that all observed luminescence is intrinsic to the major tautomeric form (diketo,structure I) for each of the five pyrimidine derivatives under consideration.

Competitive Deactivational Pathways

A third possible explanation for the wavelength of excitation dependent quantum yields has been proposed by Weber and Teal (74) and involves competition between nonradiative deactivational pathways either within the singlet manifold or between the singlet and triplet states with vibrational relaxation, which would be violations of Varilov's law (75). This law states that all rates of molecular relaxation are slow compared to vibrational cascade. Coincidence of fluorescence excitation and absorption curves rely heavily upon this law, since if the rate constants for fluorescence (k_f), internal conversion (k_{ic}), intersystem crossing (k_{isc}) and vibrational relaxation (k_{vr}) were competitive, one could just as easily talk of quantum yield curves instead of values.

Given below is a kinetic representation of the reaction

$$M^* \xrightarrow{k_o} M + E \qquad [23]$$

where M* is the excited molecule, M is the ground state molecule and E is energy. This equation can be expanded to contain all the rate constants discussed above.

$$M^*(Sv) \xrightarrow{k_{vr}} M^*(S1) + E' \qquad [24]$$

$$M^*(S1) \xrightarrow{k_{isc}} M^*(T1) \begin{cases} \xrightarrow{k_{ic}} M(So) + E'' \\ \xrightarrow{k_p} M(So) + h\nu_p \end{cases} \qquad [25]$$

$$M^*(S1) \xrightarrow{k_f} M(So) + h\upsilon_f \qquad [26]$$

$$M^*(S1) \xrightarrow{k_{ic}} M(So) + E \qquad [27]$$

Equation 24 is vibrational relaxation from upper vibrational states to the ground vibrational level of the first excited state, equation 25 is intersystem crossing followed by internal conversion or phosphorescence, equation 26 represents fluorescence and equation 27 is internal conversion from S1 to So. Under constant illumination assuming Valilov's law is valid, e.g. $k_{vr} \gg k_f$, k_{ic} and k_{isc}, the rate determining steps are 25, 26 and 27 and the quantum yield for any process is a constant given by equation 28.

$$\phi_i = \frac{k_i}{\sum_i k_i} \qquad [28]$$

where i is for ic, isc and f and the following equation can readily be written

$$\sum_i \phi_i = 1 \qquad [29]$$

Equations 28 and 29 are always true for any given wavelength of excitation. It can readily be seen from these equations that the only way energy dependent quantum yields can be obtained is if one or more of the rate constants vary with energy above the 0-0 transition.

Therefore, the constants must not only be on the same order as k_{vr} in magnitude, but also must increase at vibration modes above the zeroeth. Under these circumstances, equation 28 could be rewritten as

$$\phi_i^\lambda = \frac{k_i^\lambda}{\sum_i k_i^\lambda} \qquad [30]$$

Bonifide violations of Vavilov's law are quite common in gas phase, isolated molecule experiments (36) and in fact, pyrimidine, the parent compound of uracil, thymine and cytosine exhibit wavelength of excitation dependent quantum yields when viewed under these circumstances (37).

Values of ϕ_{isc} have been reported for thymine (76) in aqueous solution and it seems that its value is also dependent on wavelength of excitation, increasing by a factor of four as excitation energy is increased above the 0 - 0 into the first absorption band. These authors have invoked an argument which suggests that a violation of Vavilov's law is responsible for this phenomena. Brown and Johns (77) have also noted that the yield of uracil photodimer is dependent on wavelength.

Vibrational relaxation rates have been estimated to be on the order of 10^{-12} seconds and values for k_f have been calculated by use of the Stickler-Berg equation (3) to be 1.4×10^8 sec^{-1} and ca. 1.0×10^8 sec^{-1} for 5MC and thymine, respectively. Here it is assumed that τ_o is constant in going from room temperature aqueous solution to low temperature EGW glass. Quantum yields of 5MC and thymine are found

to be ca. .05 and .002 in low temperature glass when exciting at the absorption maximum. From this information, and from estimating ϕ_{isc} for the molecules to be near 10^{-3}, we can use equation 28 to derive values of k_{ic} and k_{isc} which are on the order of 10^{11} sec^{-1} and 10^{8} sec^{-1}, respectively for both molecules.

One would expect to find smaller values of kic in low temperature glass versus room temperature aqueous solution due to the large dependency shown in the quantum yields of thymine and 5MC on the temperature of solution.

On comparison, k_{isc} is seen to be approximately 10^4 smaller than k_{vr}, an observation which tends to exclude competition between these two rate constants as being the source of noncoincidence in the action and absorption spectrum of thymine or 5MC.

Turning to k_{ic}, we see that this rate constant is only one order of magnitude less than 10^{12}, an approximate value for k_{vr} and, given that the values seen here are probably no better than ± 50% accurate, it is quite likely that the two are nearly equal.

Assuming that the above is true, e.g. $k_{ic} \simeq$ kvr and that k_{ic} increases with excitation energy, the following luminescence properties could be expected from 5MC or thymine solutions: 1) Quantum yields of fluorescence and phosphorescence which decrease with increasing excitation wavelength, 2) An increase in the energy dependence of quantum yields as temperature increases, 3) Slight increases in the polarization ratios as the excitation is varied across the band.

Figure 16 shows the absorption and phosphorescence excitation spectrum of 5MC at pH 9.0 in EGW at 140K. The phosphorescence excitation can be seen to perfectly fit the absorption to within experimental error. Thymine is not known to exhibit phosphorescence in neutral solution, but it seems abundantly clear that 5MC's ϕ_f and ϕ_p are not both functions of excitation wavelength.

As to hypothesis 2, that the quantum yield will show even greater energy dependence at higher temperatures, recent results have shown that the only way red-shifted FES's can be obtained for the bases at 300K is through tautomerism (18,19,20). And, finally, the polarization ratios of 5MC and thymine are high and constant throughout both their excitation and fluorescence curves.

Local Heating

5MC's fluorescence intensity in neutral EGW glass as a function of temperature in the region 100K - 203K is graphed in Figure 17. An increase of only a factor of 15 is apparent in going from 293K to 152K, however, as the temperature is lowered an additional 40K, 5MC's fluorescence intensity becomes 2 orders of magnitude greater than that viewed at room temperature. In additional experiments, the luminescence was found to increase steadily to around 105K at which point, it flattened out and remained nearly constant to 77K. It should be noted that similar behavior was exhibited by 5MC in EM glass.

The series of absorption and excitation curves shown in Figure 18 are from neutral EGW glass at various temperatures. At 203K, the

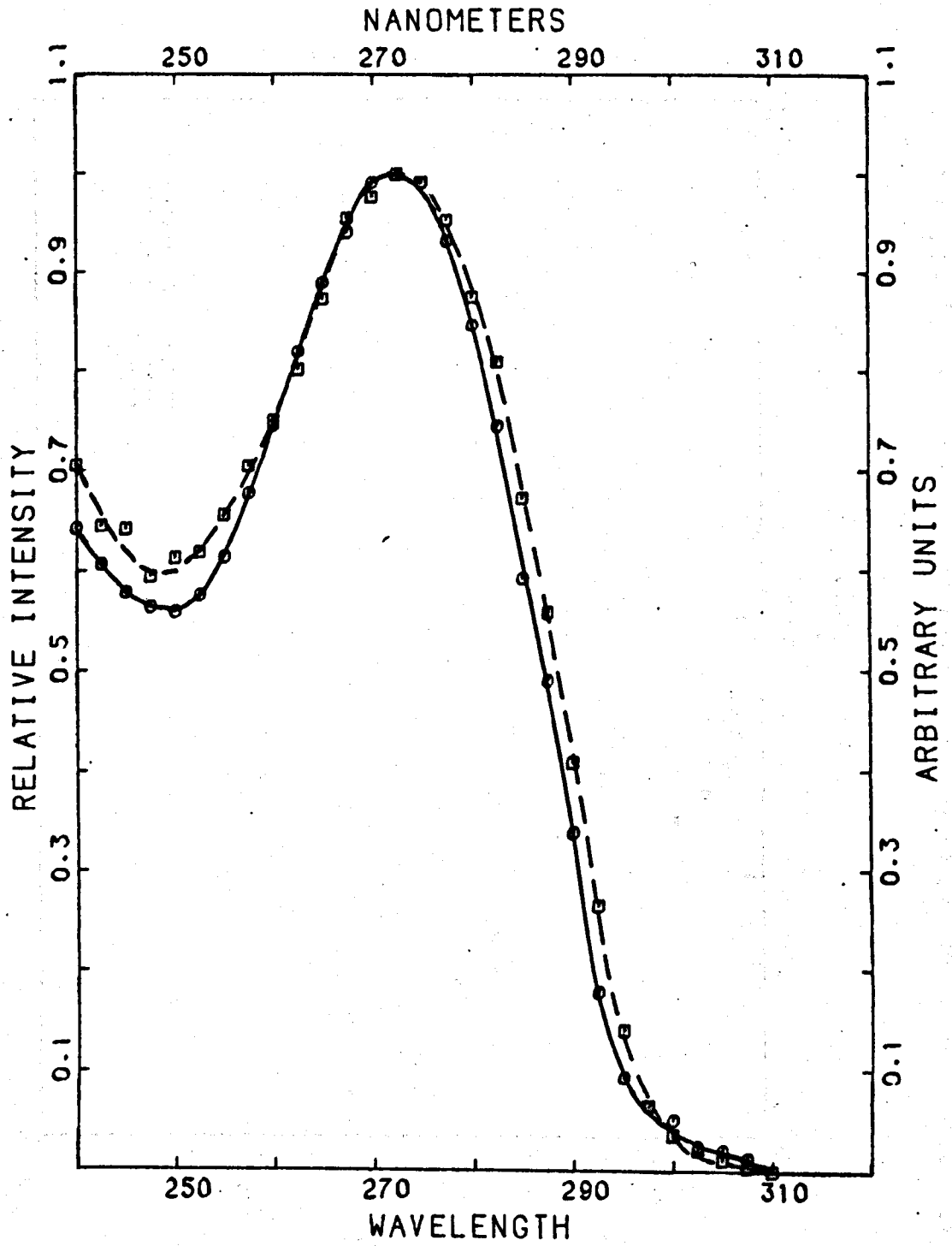

Figure 16. Absorption (——) and phosphorescence excitation (——) of 5MC in neutral EGW at -130°C. λ_p = 425 nm.

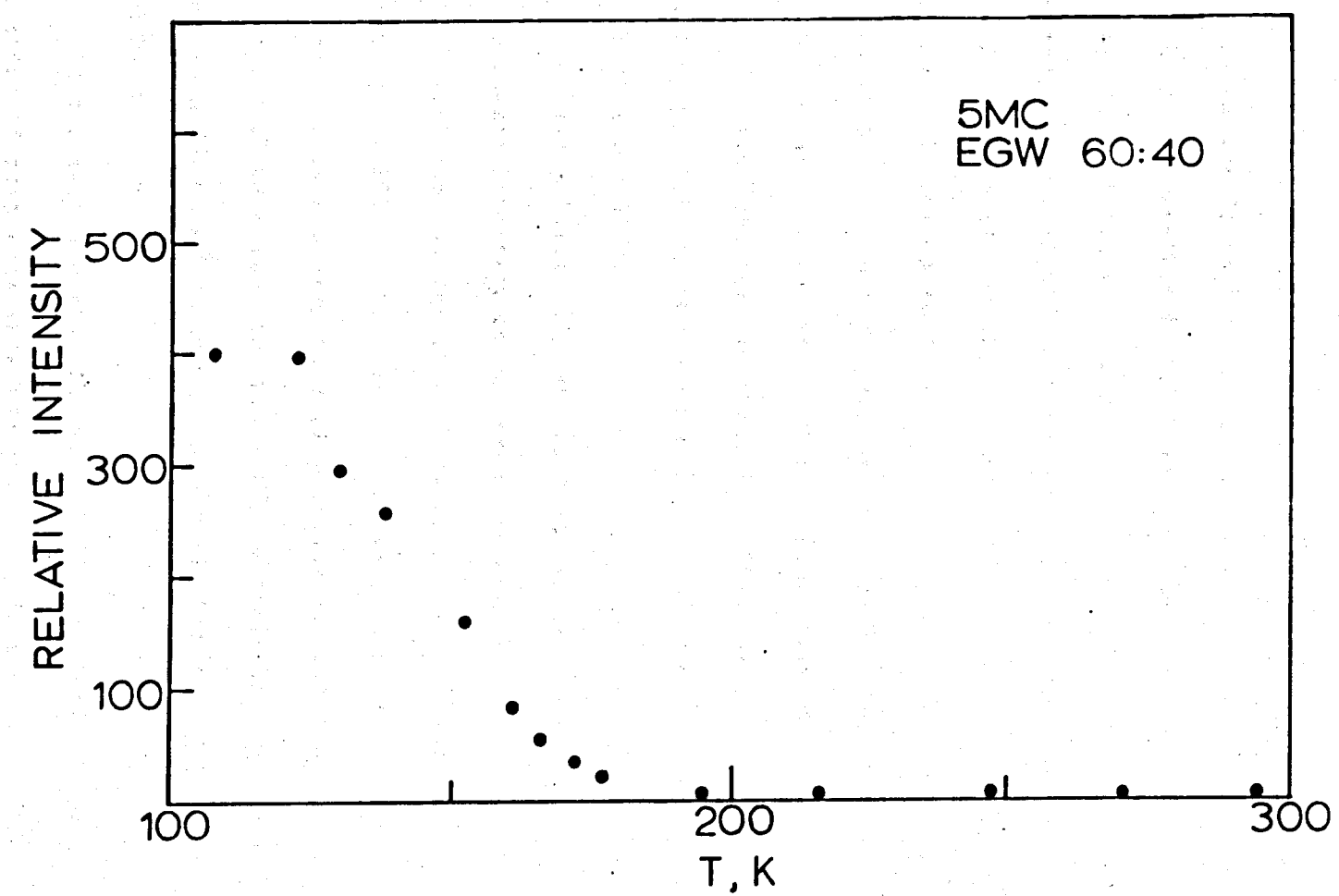

Figure 17. Quantum yield of 5MC versus temperature of EGW solutions. λ_x = 270 nm.

excitation of 5MC is seen to nearly coincide with its corresponding absorption. Any error is probably experimentally induced due to the low signal to noise ratio at this low signal intensity. No difference was found between the excitation at 293K and that at 178K, though the temperature is 95° lower and the quantum yield is an order of magnitude stronger. The spectrum from 5MC in EGW at 178K, however, shows a significant amount of red-shifting on the leading edge from those at the higher temperatures. Also, it's minimum has deepened and moved 3 to 5 nm to higher energy. In comparison, the FES at 163K shows an even greater shift on the red edge and it's minimum is seen to be further deepened and blue shifted. Results from 148K are identical to those from 163K, indicating that the shifting process has been completely affected within the temperature range of 198 - 163K.

Reviewing Figure 17, we see that the greatest change in fluorescence intensity occurs over the temperature interval of 152 - 110K. That the wavelength dependence in 5MC's ϕ_f is introduced in the range of 198 - 163K would not be surprising considering the present theory and experimental parameters. All the intensity values in Figure 17 were measured under 270 nm excitation which provides more than 3500 cm^{-1} energy in excess of that required to excite the 0 - 0 band.

In the last section, the formula for quantum yields as a function of rate constants was presented (see equation 28). If we assume that $k_{ic} \gg k_{isc}, k_{pc}$ then we can rewrite this equation as

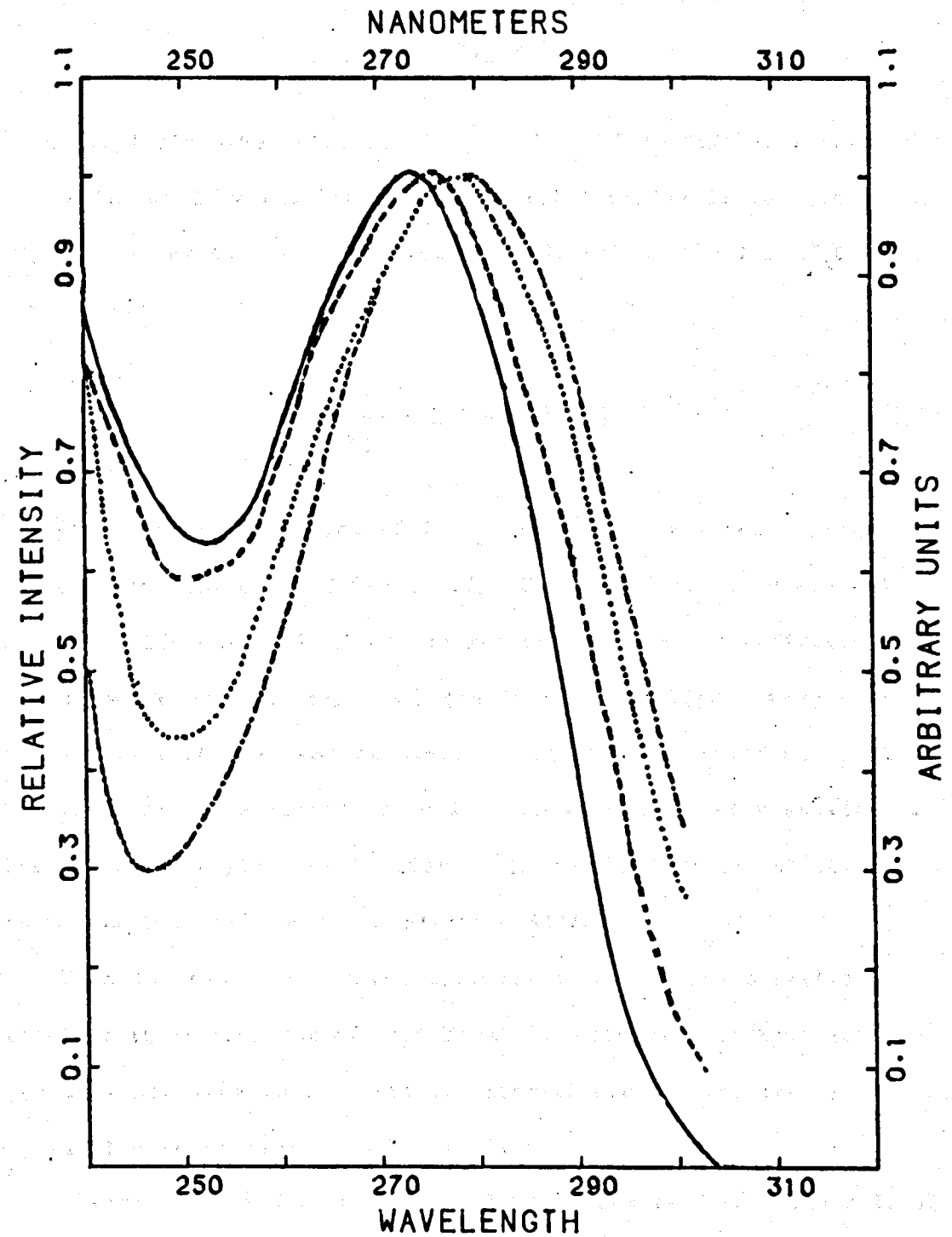

Figure 18. FES spectra of 5MC in EGW at 293K (——), 178K (——), 163K (···) and 148 K(·—·). λ_f = 330 nm.

$$\phi_f = \frac{k_f}{k_{ic} + k_f} \qquad [31]$$

which simplifies the relationship greatly. If we further assume that kf as calculated by the Strickler-Berg relationship is constant with temperature, we can rearrange equation 31, taking the log of both sides to yield

$$\ln \left(\frac{k_f}{\phi_f} - k_f\right) = \ln(k_{ic}) \qquad [32]$$

Figure 19 shows a plot of ln k_{ic} versus inverse temperature produced from the data of Figure 17. These results could suggest that two different mechanisms are responsible for the variation of 5MC's ϕ_f with temperature, one being dominant at higher temperatures and the other at low temperatures. It should be pointed out that this graph is not expected to be linear, since solvent viscosity is also reported to play an important role in the increase of the DNA base's quantum yield with temperature (24).

From the above graphs and discussion, it can quite easily be seen that if dissipation of heat from the molecular environment is slow in comparison to the rate of internal conversion, energy dependent quantum yields could result.

Observations and experimental facts which tend to exclude local heating as being the source of wavelength dependent ϕ_f's are: 1) Thymine and 5MC show wavelength dependent ϕ_f at 77K, a temperature at which the quantum yield is almost independent of temperature change,

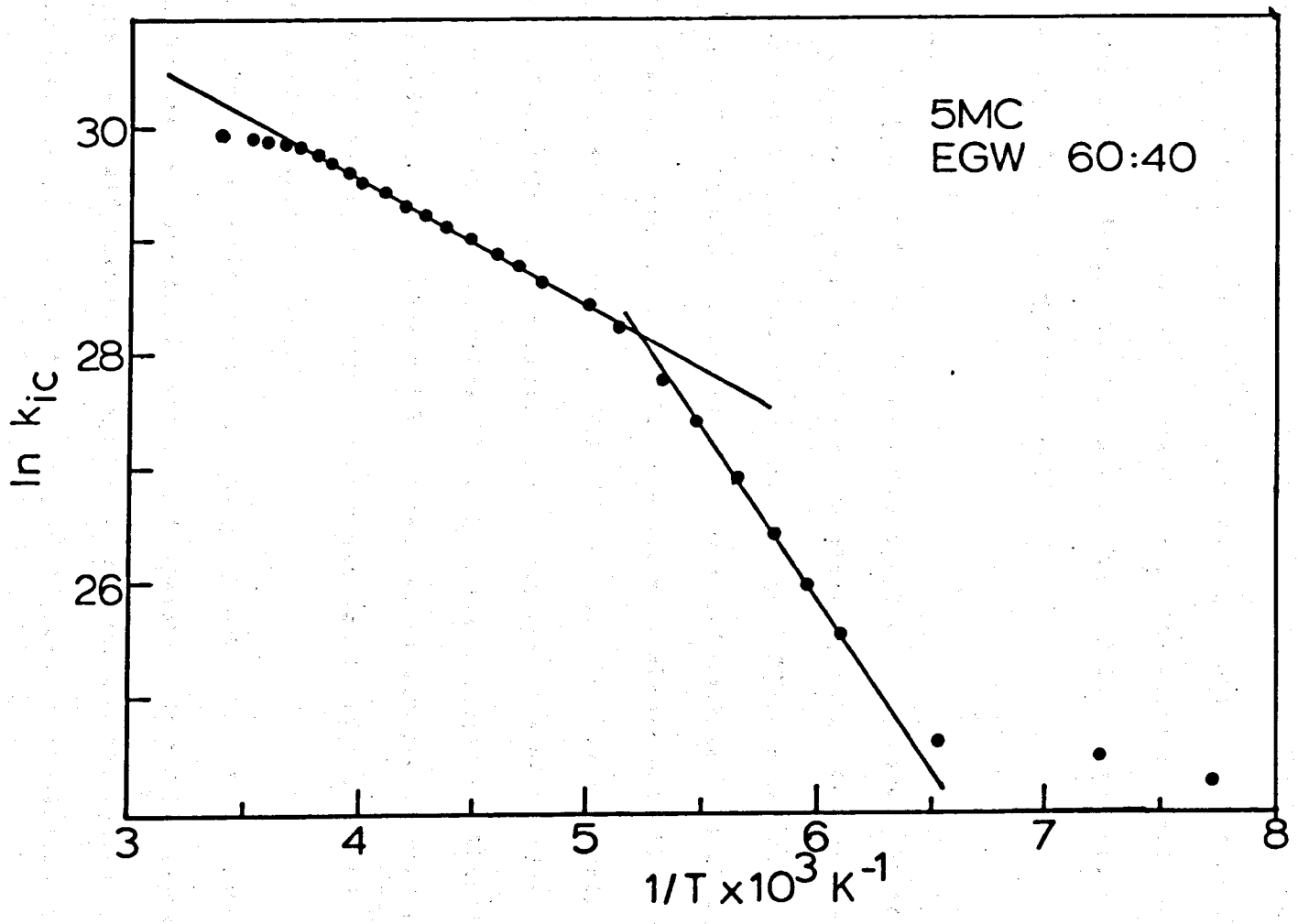

Figure 19. In k_{ic} of 5MC in neutral EGW solution versus T^{-1}.

2) Kogan and Becker found that thymine, though highly sensitive to temperature in its fluorescence intensity, did not display a red shifted excitation spectrum in EM, 3) 5MC's cation, which exhibits an even greater temperature dependence in its quantum yield and has constants very similar to the neutral form, does not possess a wavelength dependent quantum yield.

Solvent Effects

Thymine. In Figure 20 is shown the fluorescence excitation and absorption spectrum of thymine in EM glass at 123K. Comparison of these results with those displayed in Figure 21 reveals that the ABS maximum for thymine occurs at the same wavelength in both glasses, but that the peak of the excitation curve is almost coincident with absorption in EM whereas in EGW, it is not. We also see that, in the case of EM solvent, the entire excitation spectrum of thymine is only a couple of nanometers red-shifted from the absorption. This sort of weak shift has been observed by us many times for weakly emitting molecules which are reported to have wavelength of excitation independent quantum yields.

Further experiments by us have produced much the same results. On further reducing the EM solution temperature to -100K, thymine showed only slightly better agreement between the absorption and fluorescence excitation, which is probably due to the increase in signal to noise ratio. This agreement seemed to be insensitive to the method of sample preparation, contrary to the findings for 5MC

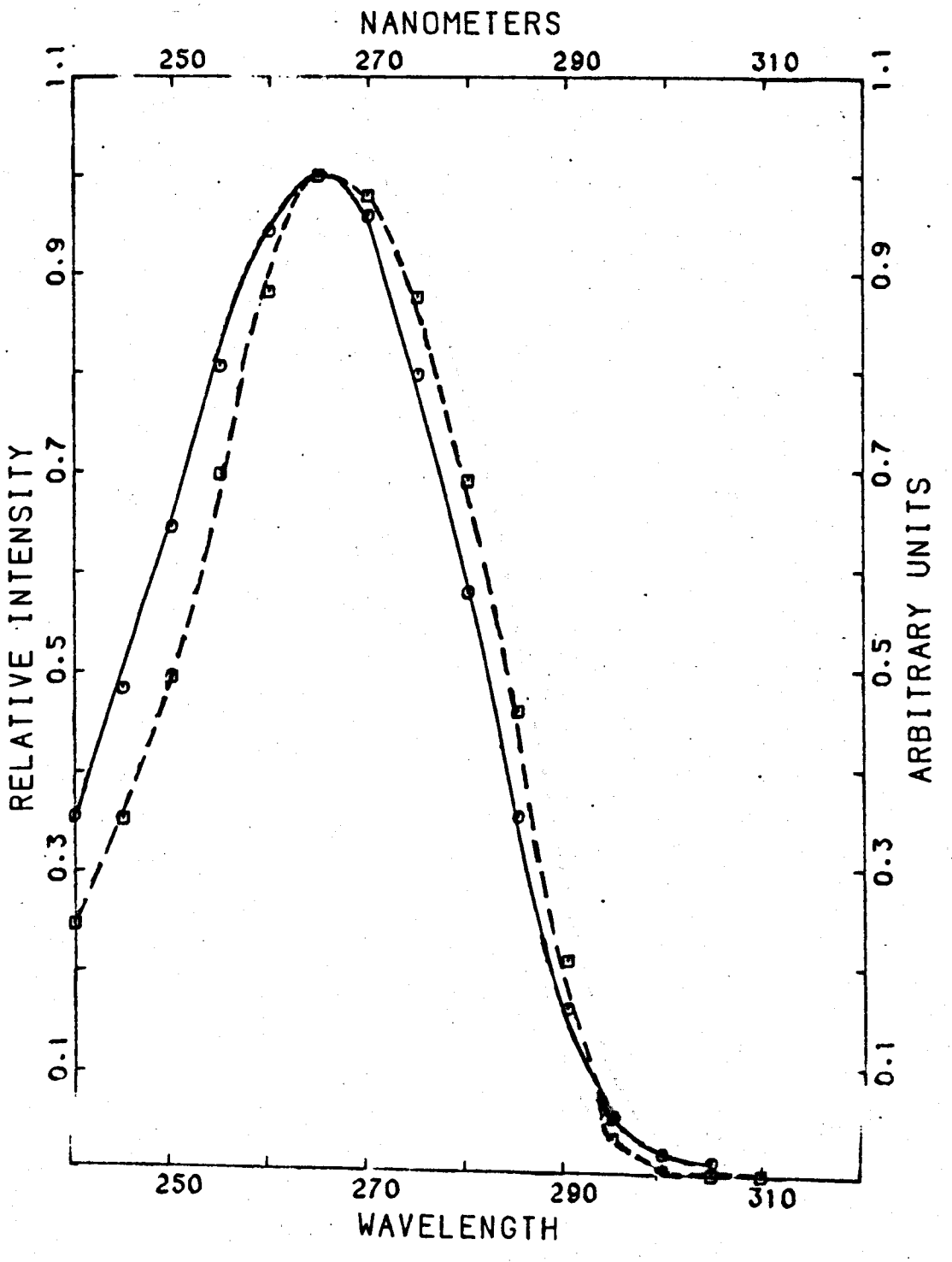

Figure 20. ABS (——) and FES (---) of thymine in EM glass at 123K. λ_f = 320 nm.

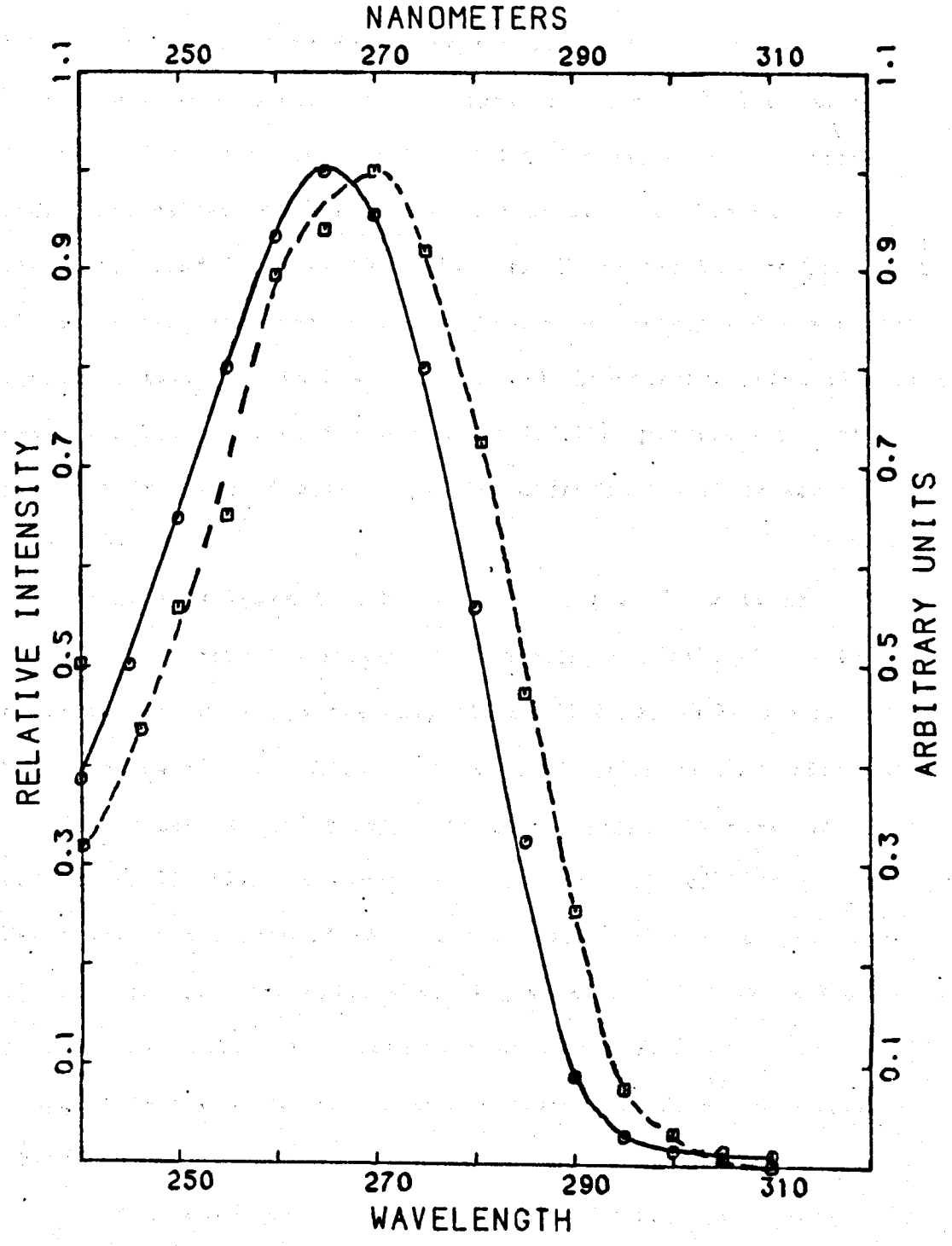

Figure 21. ABS (——) and FES (– – –) of thymine in EGW glass at 143K. λ_f = 320 nm.

which will be discussed later. The slight mismatch in the FES and ABS of thymine could be due to experimental error.

As was pointed out earlier, Kogan and Becker (39) found no dependence in the quantum yields of thymine and some methylated uracil derivatives on the energy of excitation within the first absorption band in EM or MTHF glasses. These results, coupled with the supporting evidence uncovered in our laboratory and the recent agreement that thymine has well-behaved fluorescence properties in aqueous solution at room temperature (18,19), provide a powerful argument in favor of solvent participation in the fluorescence of this molecule.

It is well known that hydrogen bonding and/or solvent interaction lowers the energy of nonbonding orbitals of a molecule a considerable amount, while only slight differences have been seen in the energies of the π M.O.'s. In fact, the absorption maximum of thymine is seen to shift only 4 nm in going from EM glass to 2-MTHF solvent at 77K (39). However, the quantum yield of fluorescence decreases by a factor of 10 in the nonpolar solvent as opposed to the alcohol mixture. The major absorbing species in EGW shows a maximum near 264 nm while the excitation peak is at ca. 270 nm. It is quite conceivable that thymine, being heavily solvated, could display an absorption shift of 6 nm.

Another point to consider is that in EM all the solvent molecules are of nearly the same hydrogen bonding strength, while in EGW, at least two distinct sites of widely different strengths exist, on the water molecules and degenerate positions on ethylene glycol.

No thermodynamic or kinetic data has been collected for the non-hydrogen bonded - hydrogen bonded equilibrium of thymine. A similar case exists though in the fluorescence of retinals. Becker and coworkers (78) found nonagreement between the FES and ABS spectra of this molecule and the same hydrogen bonding equilibrium was invoked as an explanation.

It seems likely that the noncoincidence in the absorption and excitation spectra of thymine in EGW is due to a variance in solvation. The absorption of the major species is at 264 nm and results in very little emission, while a minor hydrogen bond form absorbs near 270 nm and provides considerable emission.

5-methylcytosine. The picture in Figure 22 is the ABS and FES of 5MC in EM glass near 123K (a) and 100K (b). Graph (a) displays two curves which are closely matched, with only small differences apparent through the entire band. The slight umbrella effect seen in the excitation relative to the absorption spectrum is most likely caused by experimental error. Even less disparity is seen between the two curves, in b.

Figure 23 presents the ABS and FES of 5MC in various nonaqueous solvents at or near each's individual glass point temperature, e.g. the temperature at which the solvents form a clear uncracked rigid solid. Quite clearly, the results from EGE (EG-ethanol 60:40 by weight) and MeOH-t-butyl mirror those seen above for 5MC in EM. Only slight discrepancies are apparent in the ratio of FES to ABS and again, probably arise from experimental error. In contrast, the

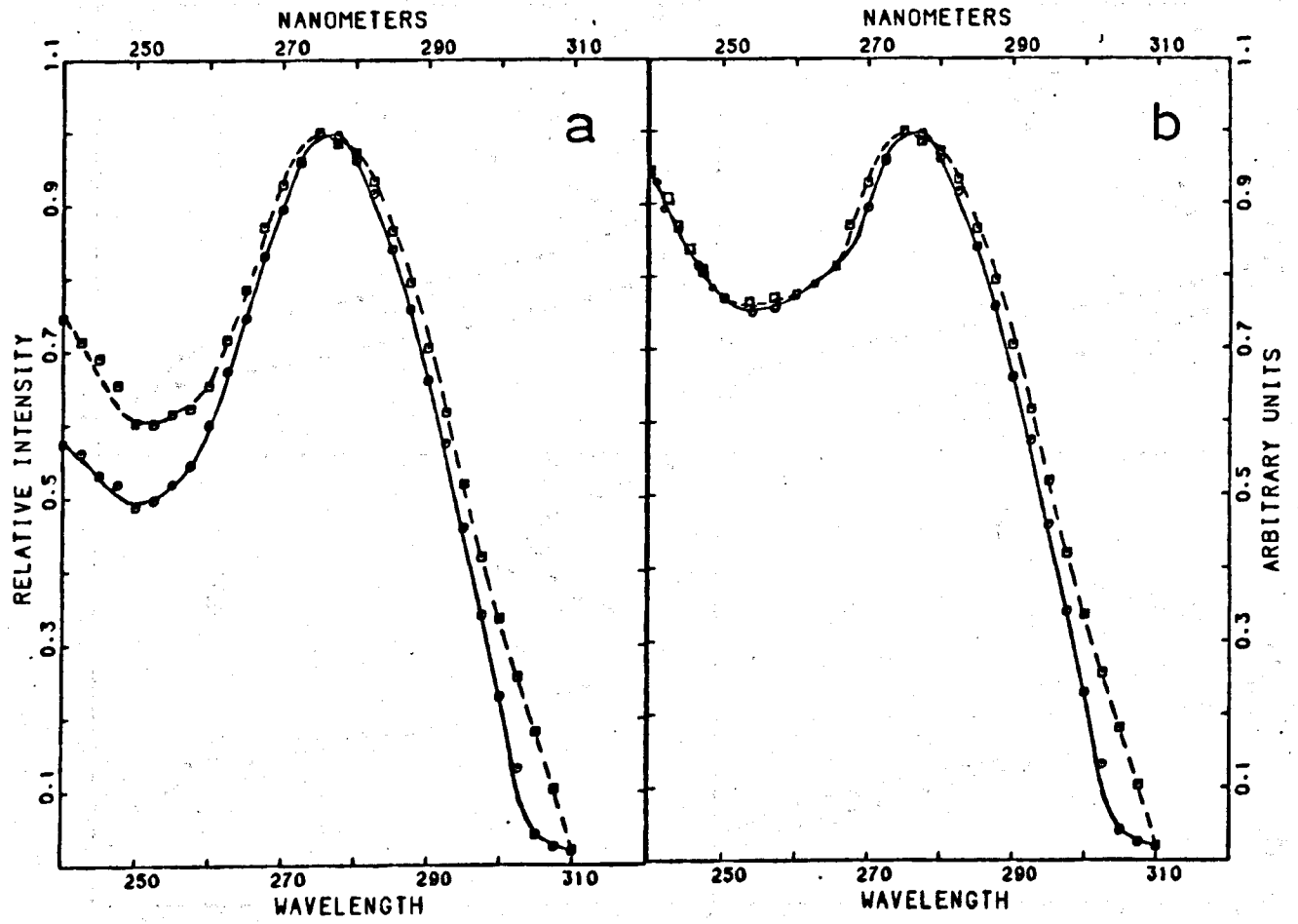

Figure 22. ABS (——) and FES (---) of 5MC in EM glass at (a) 123K and (b) 100K. λ_f = 330 nm.

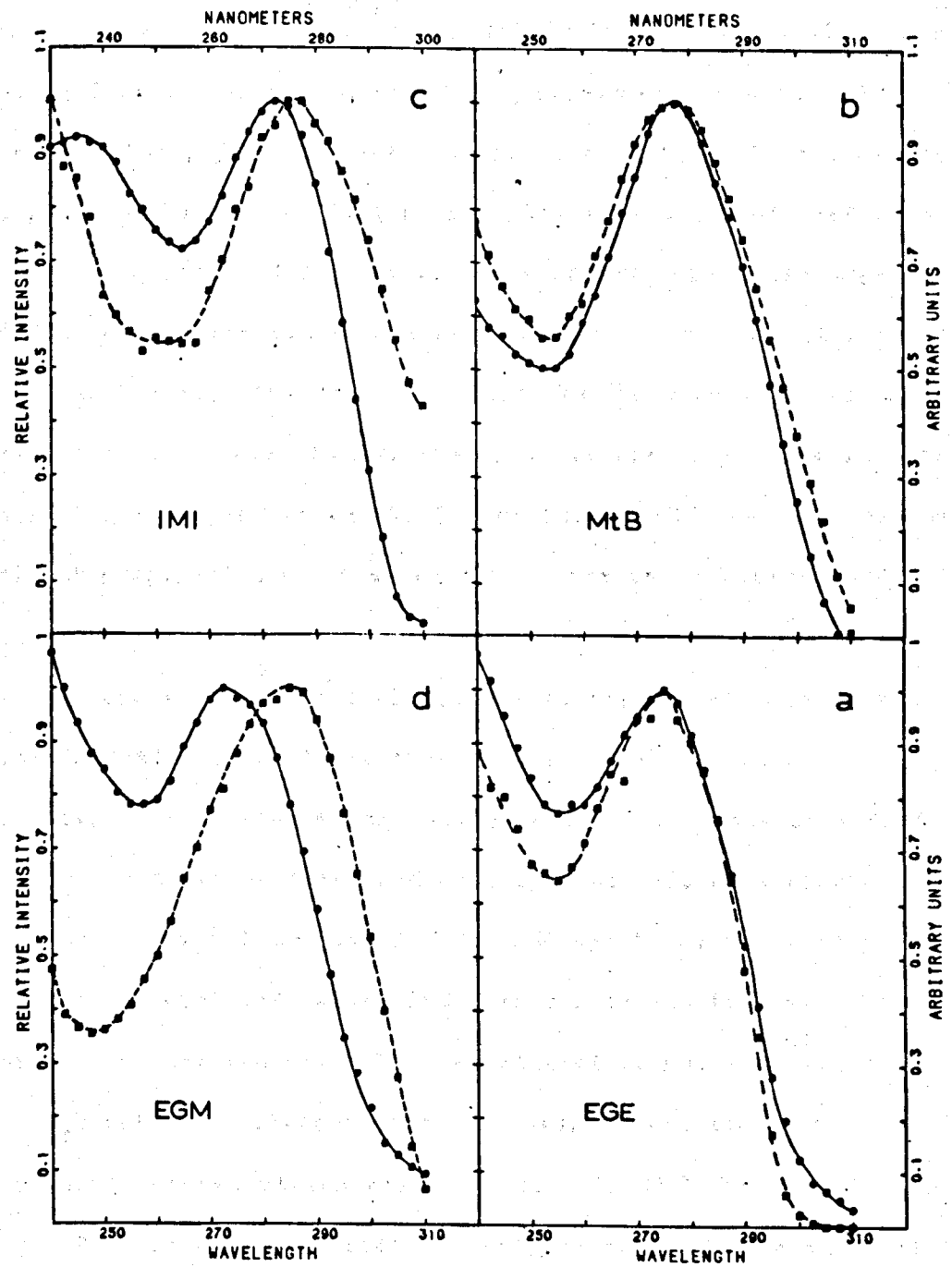

Figure 23. ABS (——) and FES(---) of 5MC in isopropanol-methanol-isopentane (IMI), methanol-t-butanol (MtB), ethylene glycol-methanol (EGM) and ethylene glycol-ethanol (EGE) near 143K. τ_f = 330 nm.

graphs produced in EGM (EG-methanol 60:40 by weight) and IMI (isopentane-methanol-isopropanol 4:2.5:1.25 by weight) glasses are more reflective of the corresponding curves observed for 5MC in EGW glasses. Here, gross mismatches are seen in the FES spectra with respect to the ABS, telling of a highly wavelength of excitation dependent quantum yield. In the case of IMI, one would expect to view a coincidence in the ABS and FES which exceeds that found in EM.

Further experiments proved that the above results were quite irreproducible. Even in EM, the fluorescence properties were found to be highly dependent on the lot number of 5MC used, the vendor, the solvent preparation and the length of time taken between ABS and FES measurements.

In order to sort out the intrinsic solvent effects from those experimentally induced, we began a methodical series of investigations during which the following facts were uncovered: 1) 5-methylcytosine precipitated from hydrochloric acid always displayed noncoincidence between its ABS and FES spectrum, regardless of which solvent was employed, while 5MC monohydrate was inconsistent with respect to this property, 2) When ethanol or methanol was filtered through activated charcoal prior to use, almost invariably wavelength dependent quantum yields resulted for 5MC, 3) If the samples were exposed to room air for extended lengths of time, the probability of viewing anomolous fluorescence properties was heightened, 4) Addition of one drop of neutral water buffer to any of the nonaqueous solutions employed produced spectra which were consistently similar to those found in EGW. Introduction of pure doubly distilled water

did not always yield this effect, and 5) Degassing of the alcoholic solvent provided no improvement in the reproducibility of spectral data collected from the resulting solutions.

From the above experimental evidence, it became clear that two solvent parameters could very well be causing the noncoincidence in 5MC's ABS and FES spectrum. The first to be discussed here will be the presence and/or concentration of buffering ions. In Figure 24 we see the results of 5MC where doubly distilled water only was used. We observe that the two curves in this plot are quite dissimilar, with a separation of ca. 8 nm in the peaks and 8 - 10 nm on the leading edges. Plot 24 represents the data collected for 5MC in .01 mol phosphate (π) buffer, pH 7.95 at 143K. This set of spectra is a bit more well behaved in that the red-shift displayed in the FES is only 5 - 6 nm at the peak and leading edge relative to the absorption spectrum. In graph 24 appears the same spectral data for 5MC in .1 mol pH 7.88 phosphate buffer at 143K. Here we note that both the absorption and excitation spectra are red shifted relative to those seen in a and b. The minima of both curves are lower and the absorption maximum has shifted 3 - 4 nm to the red. This progression to the red is even more pronounced in plot 24, a graph of the FES and ABS of 5MC in 1.0 mol pH 7.88 phosphate buffer. A fairly large absorption shift has occurred in going from .01 (b) to 1.0 mol phosphate (d) with the maxima positioned at 272 nm in the former and 278 nm in the latter. We should also note that the minima in both

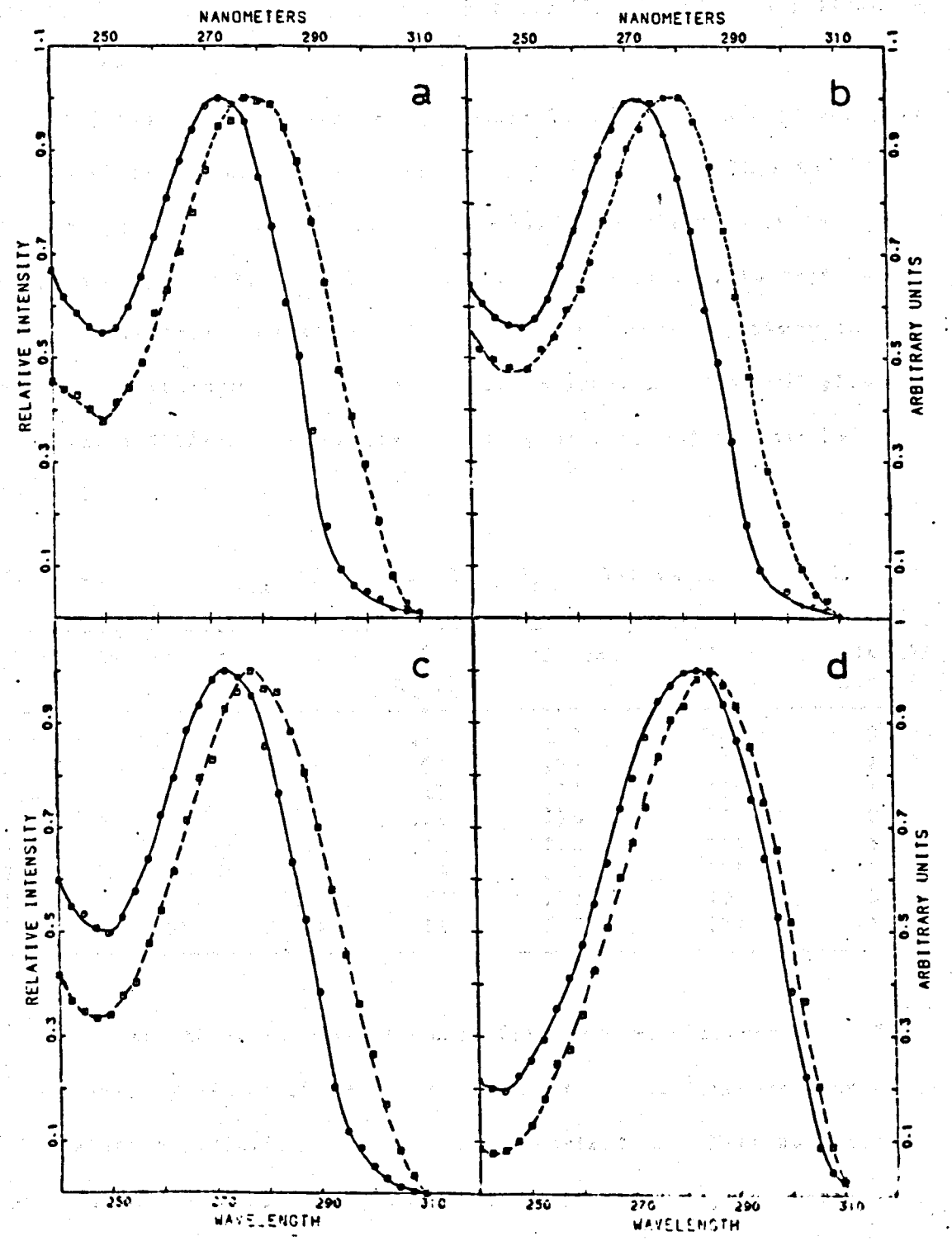

Figure 24. ABS (——) and FES (—-) of 5MC in EGW glass at 143K where the water portions are (a) distilled water, (b) .01 mol, (c) 0.1 mol and (d) 1.0 mol phosphate buffers. λ_f = 330 nm.

the FES and ABS are quite low and that the FES maximum has shifted to ca. 285 nm.

All the spectra presented in Figure 24 are from, except for part a, phosphate buffers prepared from phosphoric acid (H_3PO_4) and KOH. We also performed experiments using π buffers containing sodium cations only. In Table 4 is shown the quantum yields, absorption maxima, excitation maxima and the ratio of absorption maximum to absorption minimum for a number of single experiments on EGW glasses containing different concentrations of phosphate buffer with Na^+ and K^+ cations.

Table 4. ϕ_f, ABS_{max}, FES_{max} and A_{max}/A_{min} 5MC in EGW at 143K.

pH	buffer con	cation	ϕ_f λ_x=270	ABS max	FES max	A(max)/ A(min)
7.8	1.0	K+	.28	278	285	3.56
dd H_2O	—	—	.09	272	278	1.82
7.5	.001	K+	.17	272	281	1.83
6.7	.1	K+	.22	278	285	3.57
7.4	1.0	K+	.41	282	285	5.10
7.6	1.0	Na+	.19	276	285	2.3
8.0	.1	K+	.07	272.5	277.5	2.0
7.95	.01	K+	.11	272	277.5	1.79

Viewing these results, we can offer several observations: 1) The quantum yield of 5MC tends to increase as the concentration of the cation in solution increases at a constant pH. This was noted when either K+ or Na+ was present, 2) Increases in ϕ_f are accompanied by a red shift both in the FES and ABS curves, 3) As red shifts appear in the absorption, the ratio of the maximum to the minimum absorption increases, 4) The effect of ions in solution does not

appear to be independent of pH. We note that the quantum yield of 5MC increases from .28 to .41 in going from a 1.0 mol phosphate buffer at pH 7.8 to a -1.0 mol phosphate buffer at pH 7.4. Similarly, in the low concentration buffers, ϕ_f increase from .07 to 0.11 to .22 in going from pH 8.0 to 7.95 to 6.7, respectively, 5) In general, it is seen that high concentrations of cations are not neccessary to produce high quantum yields, i.e., 5MC's quantum yield in .1 mol phosphate at pH 6.7 is nearly as high as that in 1.0 mol phosphate at pH 7.8, 6) In none of the cases shown here was the quantum yield seen to be independent of excitation energy.

From the data presented above it is quite apparent that buffer concentrations do effect the quantum yield of fluorescence of 5MC, however, this cannot be blamed for the total phenomenon of wavelength dependency. Indeed we have seen that slight changes in pH probably contribute more to the outcome as does ion concentration.

pH Dependence

5MC. The results seen in the previous section alerted us to the possibility that the pH 7.0 EGW glasses commonly used in our low temperature investigations were not "neutral" in the same sense as would be expected at room temperature. In this regard, we collected spectral data for 5MC in numerous EGW solutions of pH values ranging from near 0 to ca. 14. Partial results of these experiments are seen in Figures 25 and 26. At pH 2 we see that the two curves match very closely and are quite different than the absorption of 5MC in neutral

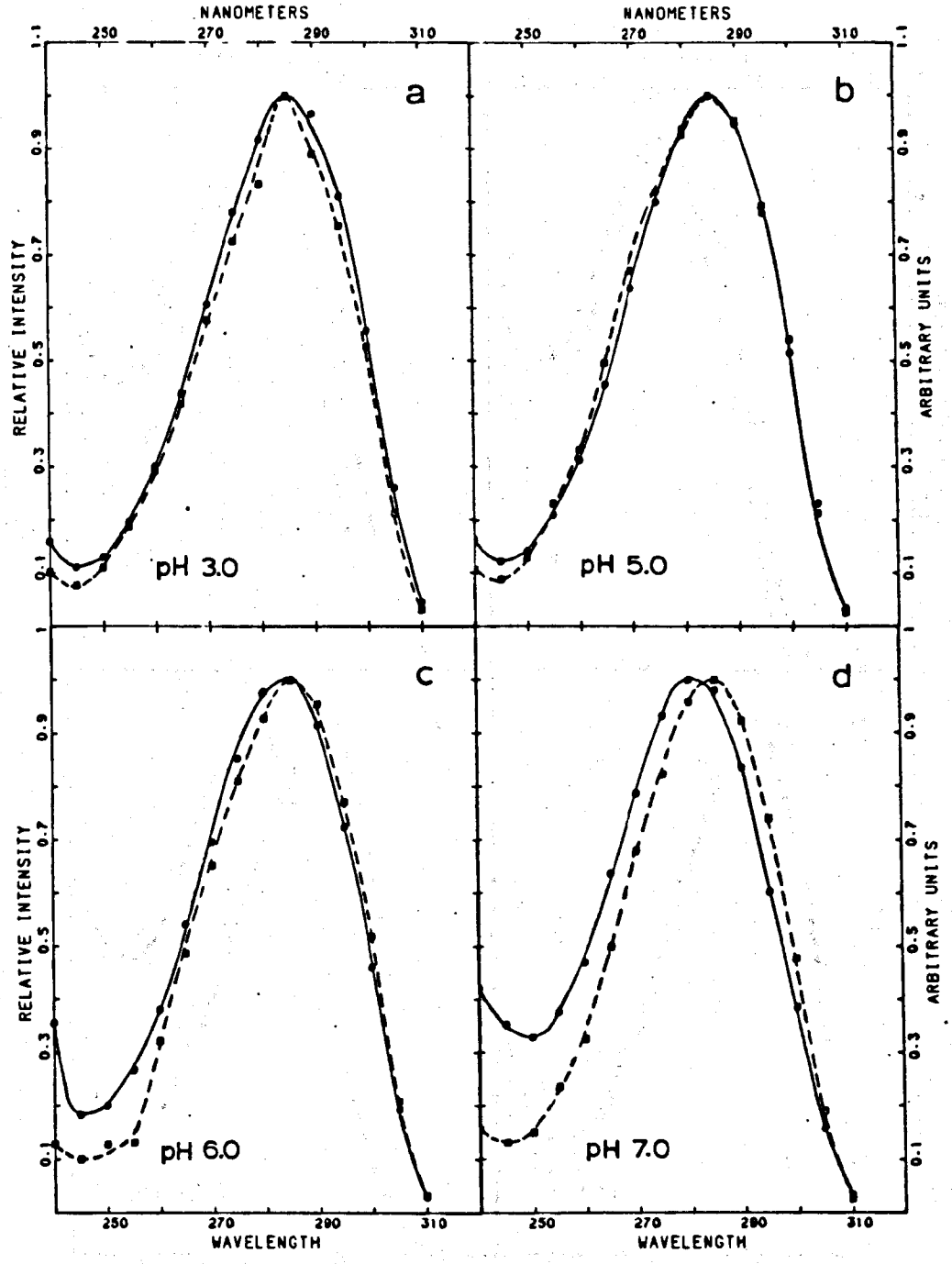

Figure 25. ABS (——) and FES (---) of 5MC in EGW glasses at pH (a) 3.0, (b) 5.0, (c) 6.0 and (d) 7.0 near 143 K. λ_f = 330 nm.

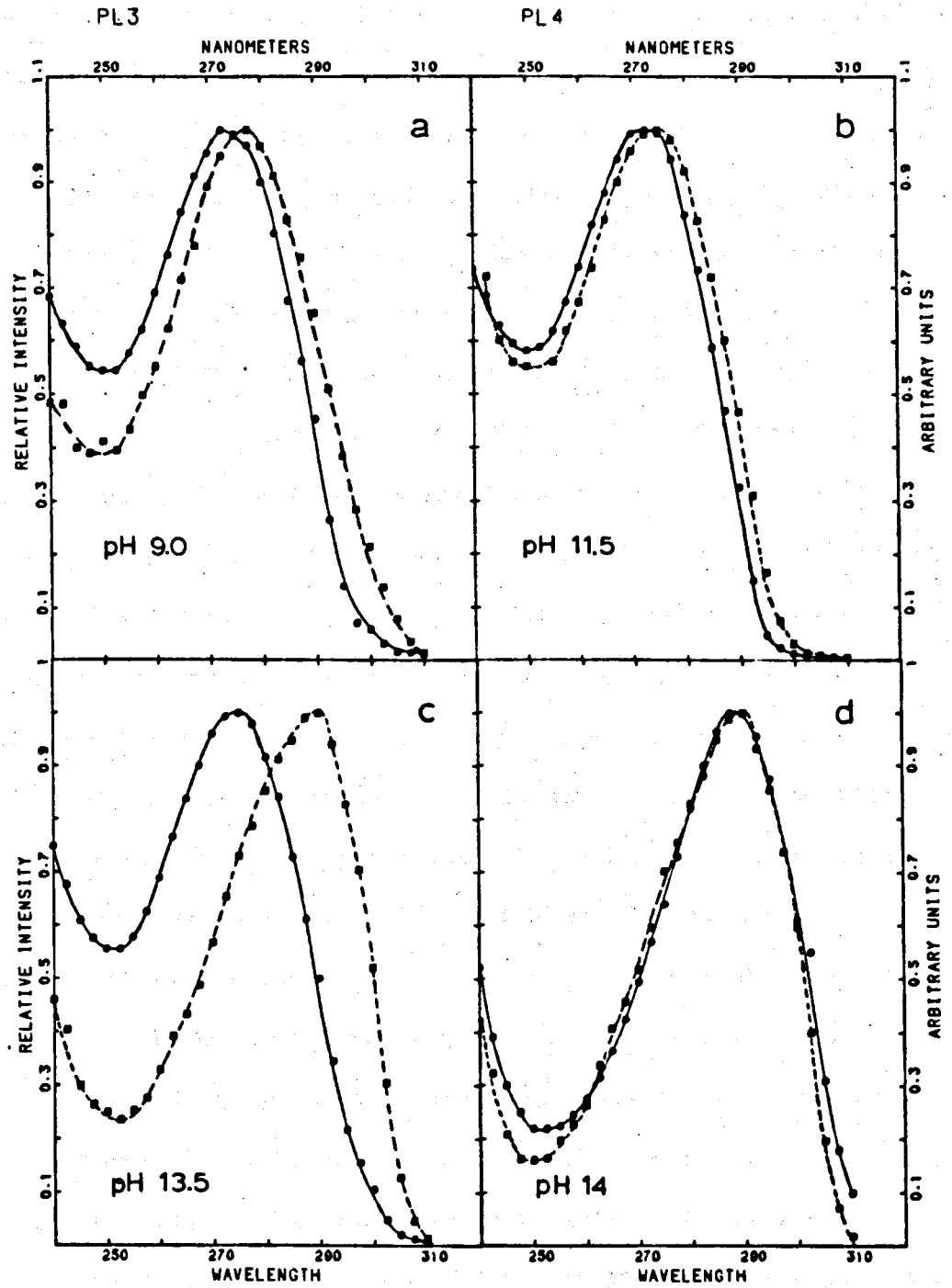

Figure 26. ABS (——) and FES (---) of 5MC in EGW glasses at pH (a) 9.0, (b) 11.5, (c) 13.5 and (d) 14.0.

EGW glasses. Reported pK_a values of 5MC are 4.6 and 12.4 (59) in room temperature aqueous solution, so the spectral data seen here is assumed to be intrinsic to the cation of this molecule. As the pH is increased to 5.0, little change is apparent in either of the curves. This would seem somewhat surprising, considering the pK_a values cited above. Further, at pH 6.0, only a slight increase in the absorption at the minimum and a ca. 2nm blue-shift differentiates this plot from those seen at pH 12 and 5. A more familiar plot appears in Figure 25, a graph of the FES and ABS of 5MC in pH 7.0 EGW. You will note that the absorption has blue-shifted and the ratio of A(max):A(min) has decreased. This spectrum is typical of the neutral 5MC molecule in neutral hydroxylic solvents. Turning to the corresponding excitation spectrum, it is clear that much of the cationic character has been retained, sharing great similarity with those seen at pH's 2 and 5. Only a small increase in height is seen near the minimum, with all other qualities preserved. In pH 9.0 EGW glass (Figure 26) the excitation and absorption of 5MC are almost coincident, with only a minor discrepancy apparent throughout the band. When the pH is raised to 11.5, almost all anomaly vanishes and a "well-behaved" relationship exists. The slight variation remaining is either an experimental artifact or possibly due to the solvent-solute hydrogen bonding equilibrium seen to be active in thymine.

Figure 26 displays the FES and ABS of 5MC in EGW at pH 13.5 near 143K. Once again a large red-shift has been produced in the excitation, one which is seemingly much greater than that viewed near pH 7.0. You will note that the minimum has red-shifted relative to

that of the absorption and the maximum appears at ca. 290 nm. Addition of a small amount of KOH to this solution produced the spectra seen in Figure 26. Here there is a perfect match in the absorption and excitation, as one would expect from a solution possessing a quantum yield near unity.

From the above we see that the solution pH plays a very important role in determining the fluorescence properties of 5MC. In addition, the reported room temperature pK_a values are inappropriate for use at low temperature, and/or measured pH values at room temperature are not accurate in low temperature glasses.

Additional support for the contention that the gross mismatch in the FES and ABS of 5MC in "neutral" solution arises from competition between its cation and neutral forms can be seen in Figure 27. Here is presented the emission of 5MC in a pH 8.0 EGW glass at 143K excited, in turn, with 270 and 300 nm light. When excitation is at the higher energy, the resulting fluorescence spectrum has a maximum at ca. 320 nm with its onset near 288 nm. Also, a phosphorescence component with a maximum between 420 and 440 nm is apparent on the long wavelength edge of this curve. As excitation nears the red edge of the absorption band of 5MC, a red-shift in the fluorescence occurs accompanied by a loss of triplet emission. The dotted curve shown in Figure 27 represents the emission observed from 300 nm excitation. Comparison with the spectrum obtained from 270 nm excitation shows that the maximum has shifted 5 - 7 nm and no sign of phosphorescence remains.

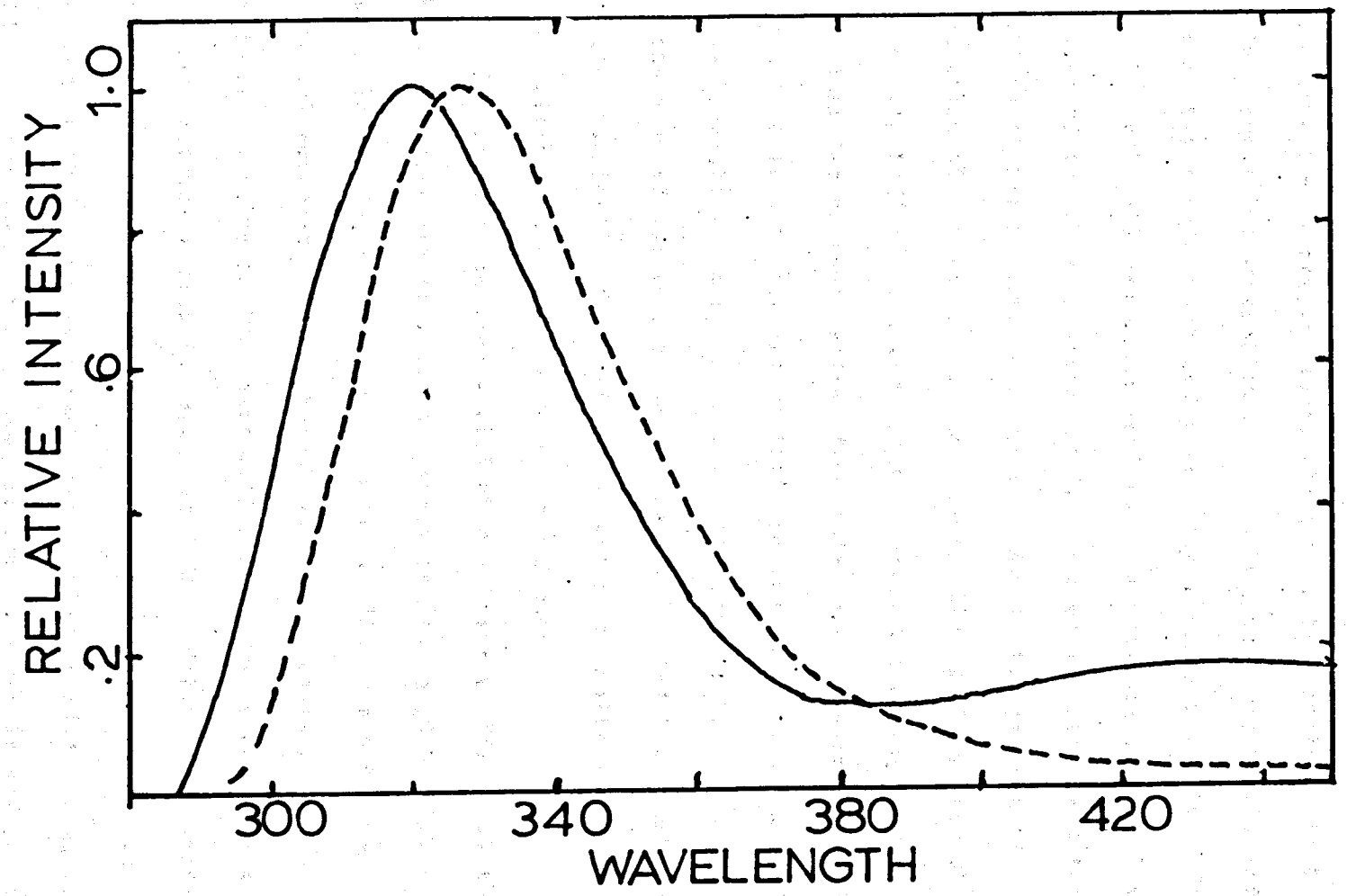

Figure 27. Fluorescence spectra of 5MC in neutral EGW solution at 143K when excited at 270 nm (——) and 300 nm (——).

It was noted earlier that the fluorescence spectrum of 5MC was not constant with respect to wavelength as the exciting light was varied across the absorption band. This effect has been noted several times in our lab and previously a process labeled "The Red Edge Effect" (79) was considered to be a probable cause. However, in view of the above results, it is quite easily seen that the shifting of the fluorescence curve is due to the preferential excitation of one species or the other. When light is absorbed near the onset, $5MC^+$ carries most of the oscillator strength so the resultant fluorescence arises from this form. Conversely, 270 nm excitation selects for the neutral species and thus the fluorescence curve blue-shifts in accordance to the ratio of $5MC:5MC^+$. Excitation in the area of the absorption minima for 5MC and $5MC^+$ yields very little contribution from the cation since its molar absorptivity coefficient is low in this wavelength region.

In Figure 28 is seen a kind of corollary to Figure 27 above. Presented here are excitation spectra of 5MC in pH 8.0 EGW at 143K when the viewing monochromator is set at 330 nm and 425 nm. Emission data collected at the long wavelength is, of course, phosphorescence and its resulting luminescence action spectrum is known as a phosphorescence excitation spectrum (PES). Coincidence between the PES and ABS is quite remarkable in this graph. This fit is as good or better than those seen for tryptophan or benzimidazole, both being highly fluorescent at room temperature. The FES is not in such good agreement however, a result which, in general, supports the above contentions. Since $5MC^+$ shows no measureable triplet emission in low

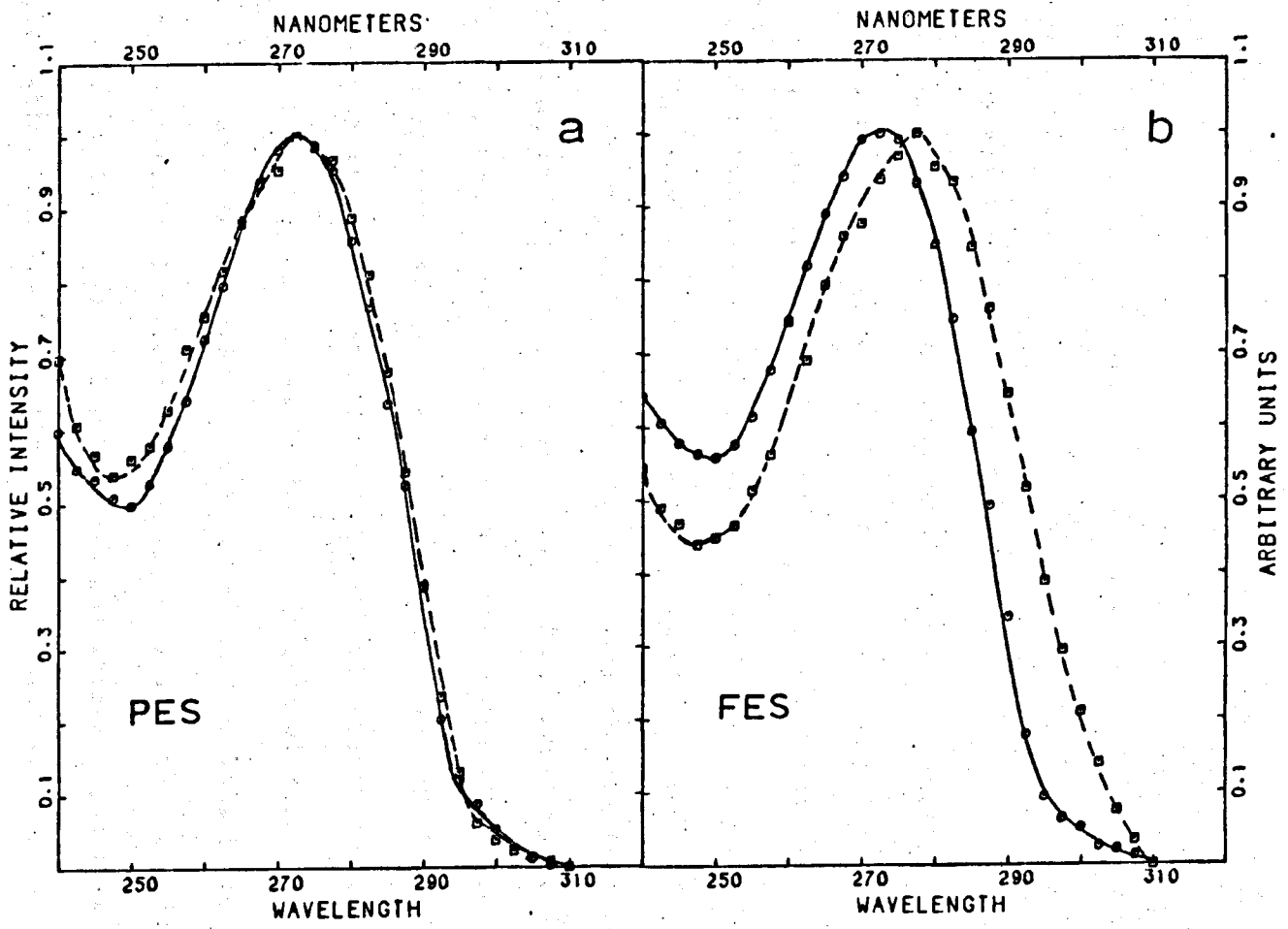

Figure 28. ABS (——), FES (a) and PES (b) of 5MC in EGW at 143K. λ_f = 330 nm, λ_p = 425 nm.

temperature glass, all the luminescence seen at 425 nm is due to the neutral species. At 330 nm, the fluorescence contains contributions from both forms with $5MC^+$ being dominant at longer wavelengths of excitation and 5MC carrying more of the responsibility at higher energies.

Figure 29 shows the results of a calculation of the apparent absorption and emission of a $5MC^+$ and 5MC mixture. A computer program was written which, when the absorption spectra, fluorescence spectra, quantum yields and relative concentration of the individual species were entered, produced the total absorption curve, the excitation curve from a specific viewing wavelength and the fluorescence curve and quantum yield as a function of excitation wavelength. Also, each components contribution to the absorption and emission were graphed. Seen in this particular plot is the results for a 10% cation - 90% neutral solution of 5MC. Quantum yield values of .35 and .05 were used for the two species, respectively and the excitation spectrum is relative to viewing at 330 nm while the fluorescence is excited at 270 nm. One should note that ca. 85% of the total absorption spectrum is due to the neutral species, yet the excitation is quite similar to that of the cation. This is to be expected since, in this case, approximately 55% of the emission is due to $5MC^+$. In addition, the fluorescence spectrum peaks near that of the cation, but its leading edge is due almost entirely to emission from the neutral form. Several additional plots were produced using this program, each of which only lent more credence to the idea that 5MC's anomolous fluorescence arises from a mixture of

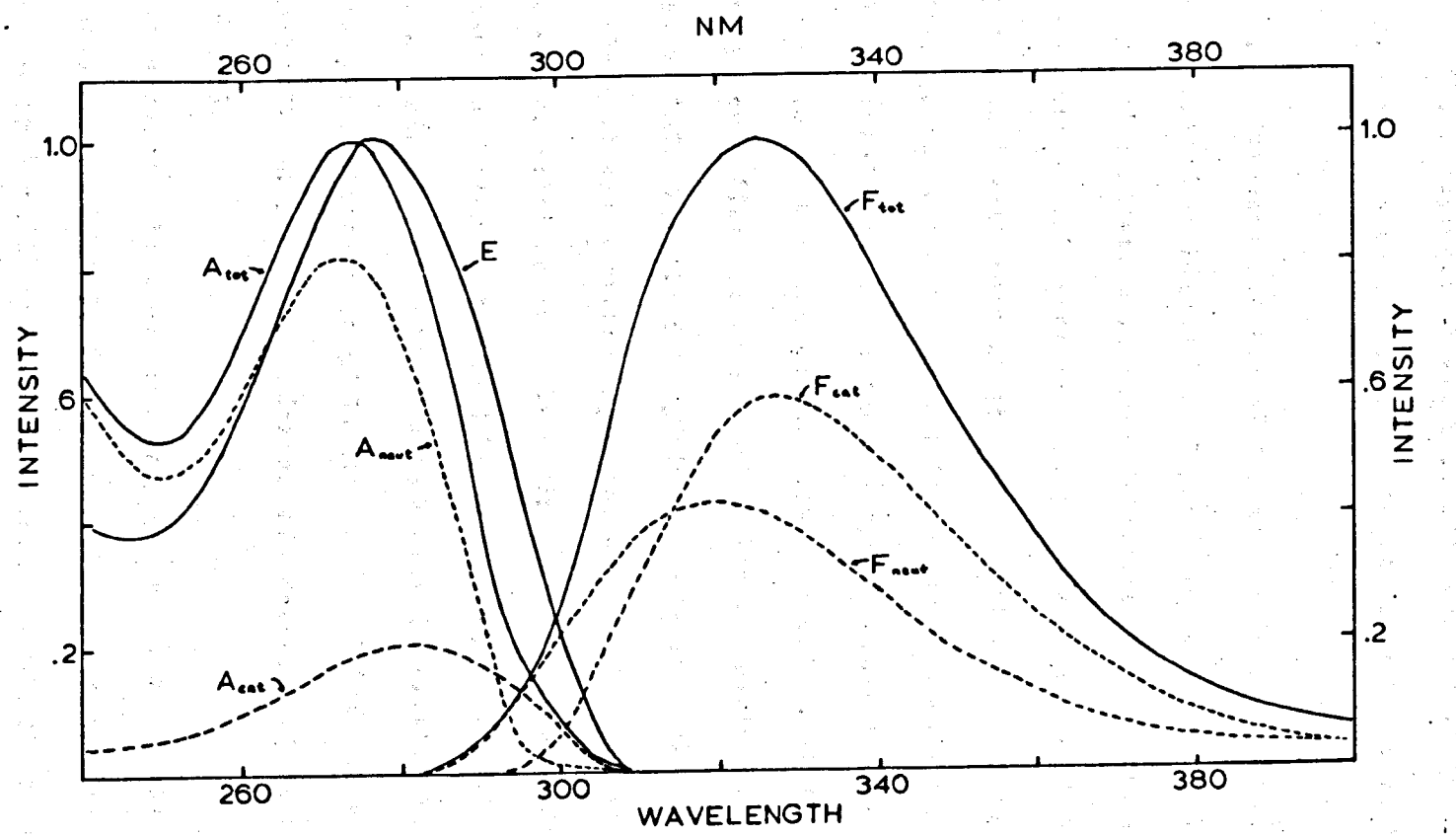

Figure 29. Calculated total ABS (A_{tot}), FES (E) and fluorescence (F_{tot}) (——) of an EGW solution containing 10% $5MC^+$ and 90% 5MC at 143K. ABS and fluorescence curves for the two species are the dashed spectra. λ_x = 270 nm, b_f = 330 nm.

species. The wavelength of excitation dependence in the position of the fluorescence spectrum is a natural consequence of this phenomenon.

Further evidence for the pH dependence in the quantum yield of 5MC can be viewed in Figure 30. A graph of quantum yield versus wavelength of excitation in three different pH EGW glasses at 143K. In acid solution, this plot is seen to be flat across the entire absorption band with only about a ± 5% variation. At pH 7.0, considerable curvature has been introduced. The quantum yield is .07 at 240 nm dropping to .05 at the absorption minimum (250 nm) then increasing to .31 near the onset. You will note that this reflects an absorption difference spectrum between the cation and neutral species of 5MC. Results from pH 10.65 are much more well behaved, with only a slight variation apparent across the band which could be due to experimental error or lingering amounts of the highly fluorescence cation. It should be pointed out that in the high pH region a similar effect occurs with a totally wavelength independent quantum yield observed at pH 14 (the anion of 5MC has a $\phi_f \simeq .6$ in EGW at 143K) and curved dependence, similar to that at pH 7.0, at pH 12.5 - 13.5.

Summarizing the above results, we see that: 1) 5MC's fluorescence at pH 7.0 is due to contributions from two species, the cation, with $\phi = .35$, and neutral form, $\phi = .05$, 2) The cation and neutral forms of 5MC have slightly different absorption curves which, when combined, yield quite anomalous spectra and give rise to the apparent dependence of 5MC's quantum yield on exciting wavelength.

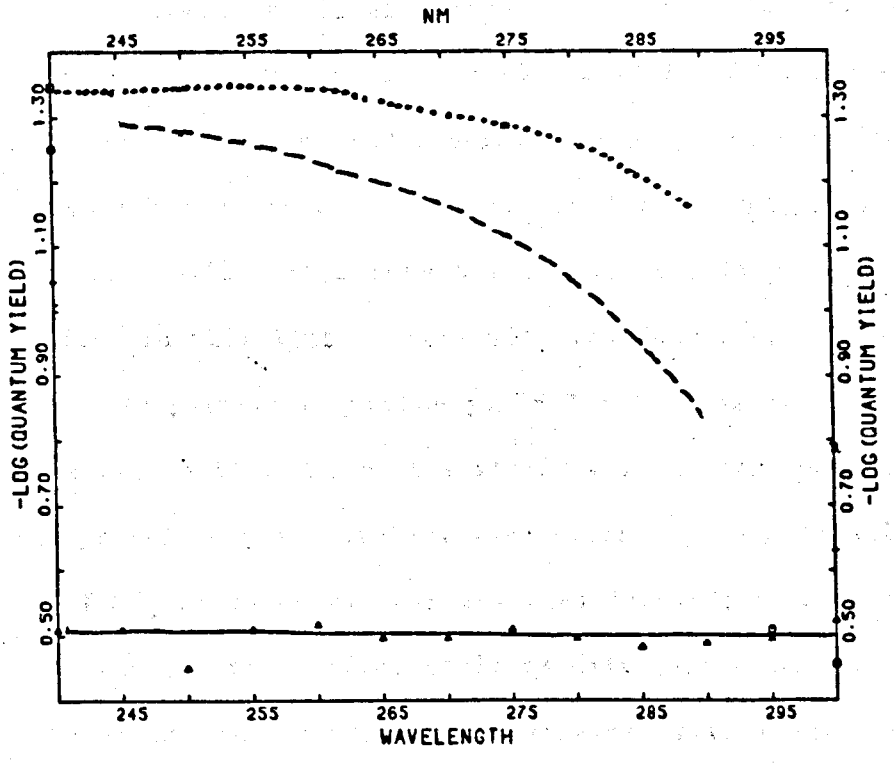

Figure 30. ϕ_f of 5MC at 143K in EGW solutions at pH's 2.0 (——), 7.0 (– – –) and 10.65 (···) versus wavelength of excitation. λ_f = 330 nm.

3) Shifts in the apparent fluorescence curve of 5MC with exciting wavelength are due to preferential excitation of one species or the other, 4) 5MC's quantum yield was found to be independent of excitation energy at pH's 2 - 5, 10 - 12 and 14 in EGW glass at 143K, 5) Changes in the absorption and fluorescence properties of 5MC in low temperature EGW glasses do not correspond to the pK_a values reported for this molecule in room temperature solution.

Point five in this list coupled with the fact that $5MC^+$ has been observed by us to possess a quantum yield 7 - 8 times that of the neutral form can be blamed for this simple effect going unnoticed through the years. Few researchers have taken any note at all of the dependence of pK_a or pH on the temperatures involved in fluorescence studies. We thought this effect could be disregarded in 5MC, since at room temperature the neutral form fluoresces with almost twice the intensity of the cation. Only after a series of experiments which revealed the greatly increased quantum yield value of $5MC^+$ were we alerted to the possible pH dependence of the apparent excitation spectrum.

In an effort to quantitate the change in the pK_a of 5MC, we set out to investigate the thermodynamic and kinetic properties of this molecule more thoroughly. Two equilibria are involved in the sample solutions composed of ethylene glycol and buffered distilled water. The first involves the solute molecule, in this case 5MC, and its protonated form:

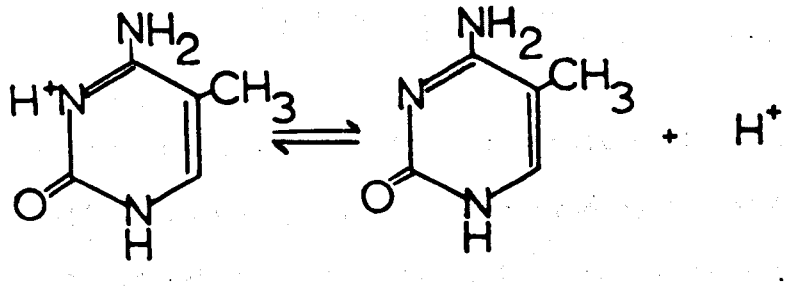

[33]

which can be written in abbreviated form as

$$5MC^+ \underset{}{\overset{K_a}{\rightleftharpoons}} 5MC + H^+ \qquad [34]$$

The equilibrium constant can be written as

$$K_a = \frac{[5MC][H^+]}{[5MC^+]} \qquad [35]$$

which has a value of 4.6 at 298K in dilute solution. Coupled with the solute equilibrium is that of the solvent buffer which was, in all cases, phosphate. This weak acid is triprotic and all the following reactions are possible.

$$H_3PO_4 \overset{k_1}{\rightleftharpoons} H_2PO_4^- + H^+ \qquad [36]$$

$$H_2PO_4^- \overset{k_2}{\rightleftharpoons} HPO_4^{2-} + H^+ \qquad [37]$$

$$HPO_4^{2-} \overset{k_3}{\rightleftharpoons} PO_4^{3-} + H^+ \qquad [38]$$

At pH 7 only one equilibrium is active and the constant for this reaction is given by

$$K_2 = \frac{[HPO_4^{2-}][H^+]}{[H_2PO_4^-]} \qquad [39]$$

where each component is assumed to have a unit activity coefficient. The concentration of hydrogen ions contributed by the 5MC molecules in solution can be assumed to be negligible since the buffer concentration was usually 100 - 1000 times larger than that of the solute. Therefore, the pH of the solution would be given by

$$-\log[H^+] = -\log \frac{[H_2PO_4^-]K_2}{[HPO_4^{2-}]} \qquad [40]$$

and the equilibrium constant for 5MC can be rewritten to give

$$[H^+] = \frac{[5MC^+]K_a}{[5MC]} \qquad [41]$$

Substituting equation 43 into the above and rearranging yields

$$K_a = K_2 \frac{[H_2PO_4^-][5MC]}{[HPO_4^{2-}][5MC^+]} \qquad [42]$$

Here we see that the equilibrium constant for reaction 33 is dependent not only on its own equilibrium constant but also on the equilibrium of the solvent buffer. Further rearrangement of equation 42 yields the following

$$\frac{[5MC^+]}{[5MC]} = \frac{K_2}{K_a} \frac{[H_2PO_4^-]}{[HPO_4^{2-}]} \qquad [43]$$

and we see that the ratio K_2/K_a is the important term governing the speciation of 5MC in solution. Substituting thermodynamic state functions for the equilibrium constants and taking the log of both sides of the equation gives

$$\ln \frac{[5MC^+]}{[5MC]} = -\frac{\Delta H_2^\circ - \Delta H_a^\circ}{RT} + \frac{\Delta S_2^\circ - \Delta S_a^\circ}{R} + \ln \frac{[H_2PO_4^-]}{[HPO_4^{2-}]} \qquad [44]$$

which shows how the ratios of the ions vary with the enthalpy and entropy of the reaction.

A thorough search of the literature failed to provide thermodynamic data (ΔH, ΔS) for the reactions described above under the experimental conditions that we employed, e.g. 143K in 60% ethylene glycol, 40% water, so the discussion from this point onward is qualitative in nature.

Table 5 lists the ΔH, ΔS and pK_a values of several different acids as a function of temperature (80). We see that phosphoric acid, along with other acids (citric, formic, boric), have very high negative ΔS values and low ΔH values. In addition the values of these two state functions seem to vary in tandem such that ΔG is almost a linear function of temperature. In contrast, the molecules with high ΔH's of ionization (imidazole, ammonia) show considerable temperature dependence in their respective pK_a's indicating that ΔG is not linear.

From Table 5 we see that the DNA components (cytosine, thymine and cytidine) possess high positive ΔH values and relatively low ΔS values at 25°C. Thus we can anticipate that the pK_a's of these

Table 5. Thermodynamic Constants for Acid Dissociations of some selected acids (ΔH and ΔS kcals).

Species	Ammonia			Acetic Acid			Boric Acid		
°C	ΔH	ΔS	pK_a	ΔH	ΔS	pK_a	ΔH	ΔS	pK_a
0	-	-	-	.714	-14.7	4.78	-	-	-
5	12.54	-.21	9.90	.552	-15.3	4.77	-	-	-
10	-	-	-	.389	-15.8	4.76	3.92	-29.1	9.38
15	12.50	-.34	9.57	.223	-16.4	4.75	3.75	-29.7	9.32
20	-	-	-	.057	-17.0	4.75	3.57	-30.3	9.28
25	12.48	-.45	9.25	-.112	-17.6	4.75	3.36	-	9.23
30	-	-	-	-.282	-18.1	4.75	3.14	-31.7	9.19
35	12.44	-.56	8.95	-.455	-18.7	4.7	2.90	-	-
40	-	-	-	-.628	-19.1	4.76	2.63	-33.4	9.13
45	12.41	-.67	8.67	-.804	-19.8	4.77	2.35	-	-
50	-	-	-	-.982	-20.4	4.78	2.04	-35.2	9.08
55	-	-	-	-1.161	-20.9	4.79	-	-	-
60	-	-	-	-1.342	-21.5	4.81	-	-	-

Species	Citric Acid			Formic Acid			Imidazole		
°C	ΔH	ΔS	pK_a	ΔH	ΔS	pK_a	ΔH	ΔS	pK_a
0	1.76	-8.3	3.22	.931	-13.9	3.78	8.66	-2.99	7.58
5	1.61	-8.8	3.20	.755	-14.5	3.77	8.70	-2.82	7.47
10	1.46	-9.4	3.17	.573	-15.2	3.76	8.74	-2.69	7.33
15	1.31	-9.9	3.16	.384	-15.8	3.76	8.77	-2.59	7.22
20	1.15	-10.4	3.14	.189	-16.5	3.75	8.79	-2.53	7.10
25	.997	-11.0	3.12	-.013	-17.2	3.75	8.79	-2.51	6.99
30	.836	-11.5	3.12	-.221	-17.9	3.75	8.79	-2.52	6.89
35	.673	-12.0	3.11	-.436	-18.5	3.76	8.77	-2.57	6.78
40	.507	-12.6	3.10	-.657	-19.3	3.77	8.75	-2.66	6.68
45	.338	-13.1	3.10	-.884	-20.0	3.77	8.70	-2.79	6.59
50	.167	-13.6	3.09	-1.18	-20.8	3.78	8.65	-2.95	6.50
55	-	-	-	-1.358	-21.5	3.79	-	-	-
60	-	-	-	-1.605	-22.2	3.81	-	-	-

(continued)

Table 5 (continued)

Species	Phosphoric Acid			Water		
°C	ΔH	ΔS	pK_a	ΔH	ΔS	pK_a
0	2.28	-25.1	7.31	14.51	-15.23	14.93
5	2.03	-26.0	7.28	14.31	-15.95	14.73
10	1.78	-26.9	7.25	14.11	-16.67	14.53
15	1.52	-27.8	7.23	13.90	-17.40	14.34
20	1.26	-28.7	7.21	13.69	-18.12	14.16
25	.99	-29.6	7.20	13.48	-18.83	13.99
30	.71	-30.5	7.19	13.27	-19.53	13.83
35	.44	-31.4	7.19	13.05	-20.24	13.68
40	.15	-32.4	7.18	12.83	-20.96	13.53
45	-.13	-33.3	7.18	12.61	-21.66	13.39
50	-.43	-34.2	7.18	12.39	-22.35	13.26
55	-.72	-35.1	7.19	12.16	-23.05	13.13
60	-1.02	-36.0	7.20	11.93	-23.74	13.02

Species	Cytosine			Cytidine			Thymine		
°C	ΔH	ΔS	pK_a	ΔH	ΔS	pK_a	ΔH	ΔS	pK_a
25	5.14	-3.7	4.58(1)	4.47	-3.9	4.08(1)	8.83	-15.7	9.90
25	11.15	-17.0	12.15(2)	10.7	-20.2	12.24(2)			

molecules might change drastically with temperature. The only way this change would be apparent, however, is if the pK_a of the solvent buffer varied less with temperature than that of the bases. Although the results discussed above are from aqueous solutions, we can assume that these trends extend to lower temperature. Therefore, the change seen in the pK_a of 5MC arises from the 5MC moiety, not from the solvent buffer (phosphate).

Figure 31 shows a plot of the log of 5MC's quantum yield of fluorescence determined from 270 nm excitation versus pH in EGW at

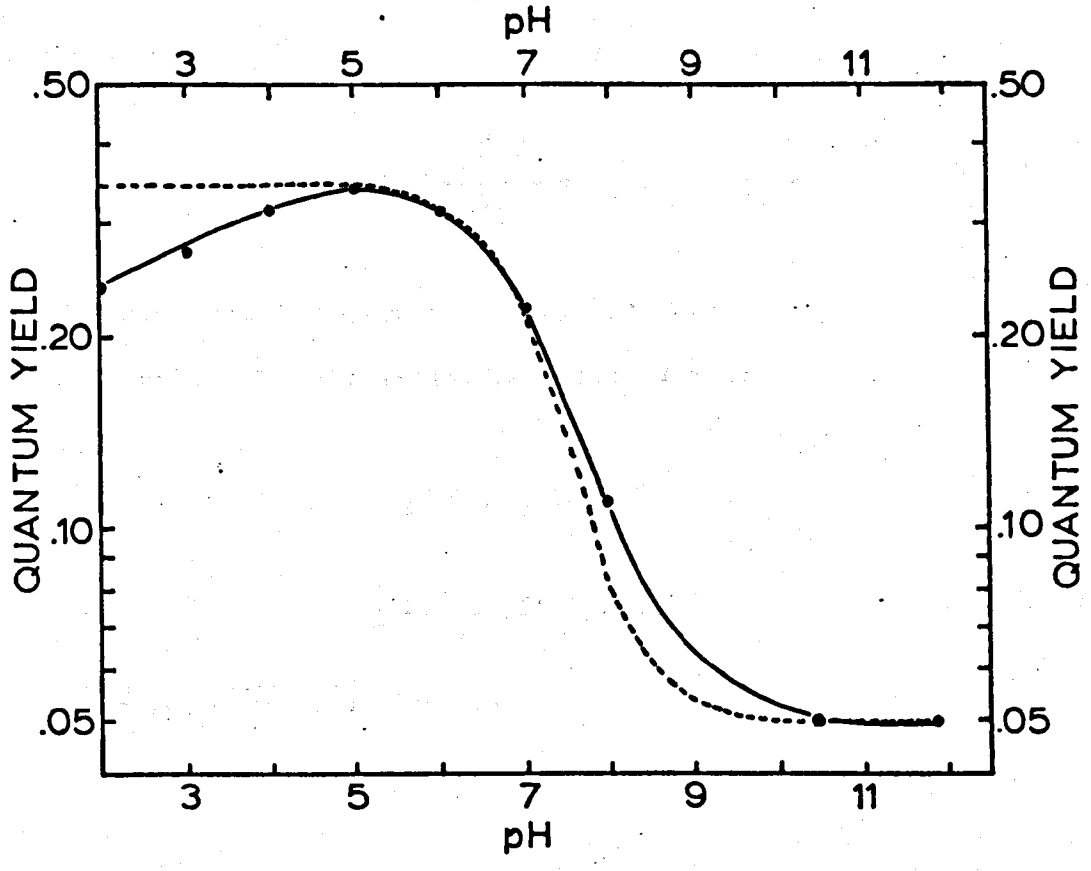

Figure 31. Log ϕ_f of 5MC in EGW at 143K versus solution pH. The dashed line was calculated from the experimetally obtained photophysical parameters of 5MC and an estimated pK_a of 7.0.

143K. The solid line represents the experimental data, while the dashed line was produced by use of the following equation,

$$\phi_f^{obs} = \phi_f 5MC \cdot \frac{A^{5MC}}{A^{TOT}} + \phi_f 5MC^+ \cdot \frac{A^{5MC^+}}{A^{TOT}} \qquad [45]$$

where ϕ_f and A are the quantum yields and absorbances, respectively. Absorption values for the individual species were determined as follows,

$$A^{5MC} = \varepsilon^{5MC} \alpha^{5MC} \qquad [46]$$

$$A^{5MC^+} = \varepsilon^{5MC^+} \alpha^{5MC^+} \qquad [47]$$

where α^{5MC} and α^{5MC} are given by

$$\alpha^{5MC^+} = \frac{[H^+]^2}{([H^+]^2 + K_a[H^+] + K_b K_a)} \qquad [48]$$

$$\alpha^{5MC} = \frac{K_a[H^+]}{([H^+]^2 + K_a[H^+] + K_b K_a)} \qquad [49]$$

Since the value of $K_a K_b$ is ca. 4 orders of magnitude smaller than either of the other two terms in the denominator, the room temperature value of 4×10^{-13} was used for K_b. Quantum yield values of 0.35 and 0.05 were assigned to the cation and neutral species and molar absorptivity coefficients were 7.4×10^3 and 6.2×10^3, respectively. The value of K_a was varied until the theoretical curve

best fit (by visual inspection) the experimental points. A value of 7.0 ± 0.2 was used to produce the curve seen in Figure 32. This value is 2.4 pH units higher than the reported pK_a at 25°C.

Cytidine

In Figure 32 is presented the ABS and FES of cytidine at pH's 4(a), 6(b), 7(c) and 10(d) in EGW at 143K. At pH 4.0, the absorption spectrum is clearly due to the cation species. The excitation spectrum is nearly coincident, with only a slight mismatch apparent. When the pH of the solution is increased to 6.0 (Figure 32), a noticeable amount of neutral character is infused into the ABS spectrum. Note that the maximum is blue-shifted 3-4 nm and the ABS minimum is increased by ca. 30%. No change is seen in the FES at this pH, nor is any apparent at pH 7.0 (Figure 32). However, at this pH the ABS appears to be composite with about 50% contribution from the neutral species. Results from pH 10.0 (Figure 32) show that the absorption is due to the neutral species of cytidine. The excitation has blue-shifted, somewhat, and its minimum now coincides very well with that of the ABS. A fairly large mismatch still remains between the two spectra, however. One which is much greater than that found under the same conditions for 5MC.

Figure 33 displays the quantum yield of cytidine as a function of wavelength in three EGW solutions of different pH values. The bottom (solid) curve in the figure is the quantum yield from a pH 4.0 solution. Quantum yield values increase monotonically across this curve, beginning at .0126 (240 nm) and rising to .033 at 295 nm.

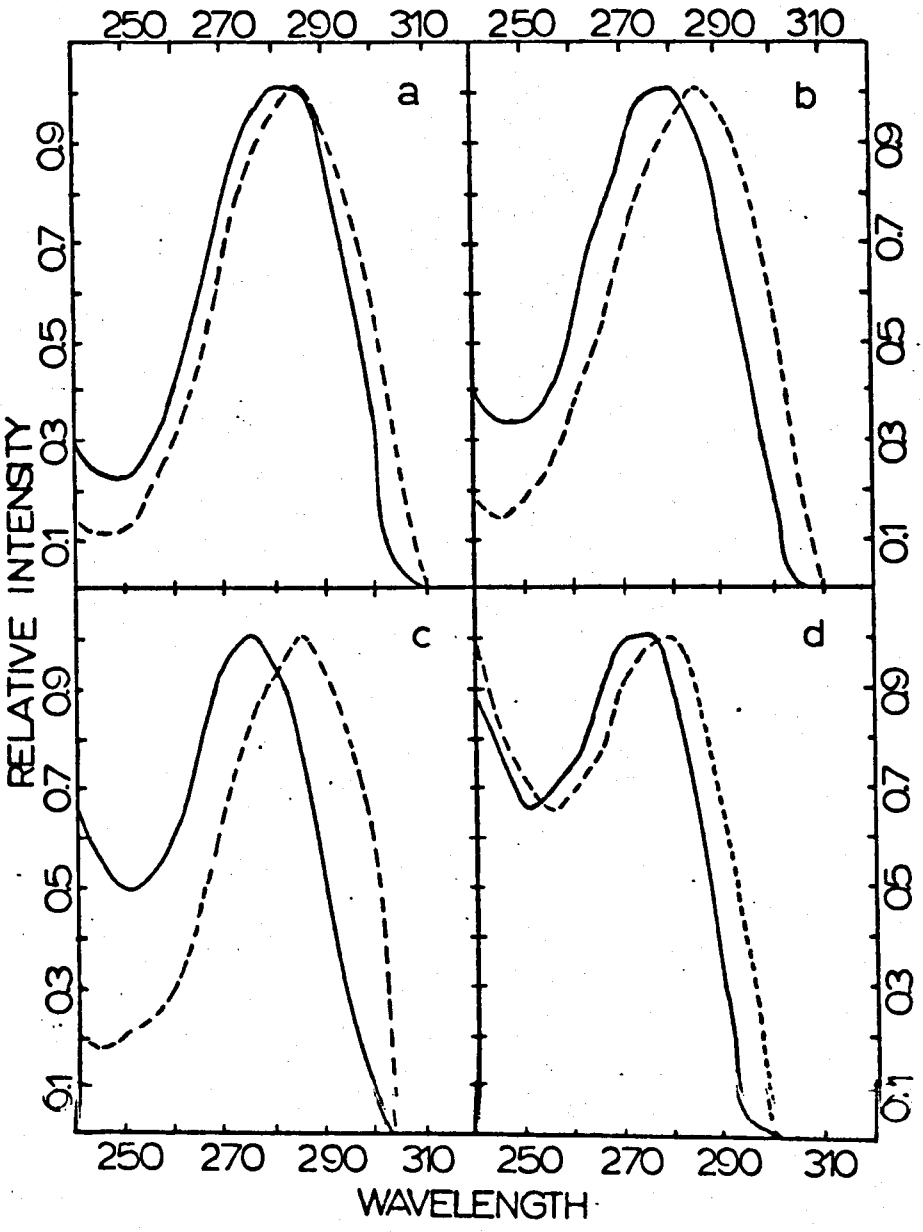

Figure 32. ABS (——) and FES (---) of cytidine at 143K in EGW solutions of pH 4 (a), 6 (b), 7 (c) and 10 (d). λ_f = 330 nm.

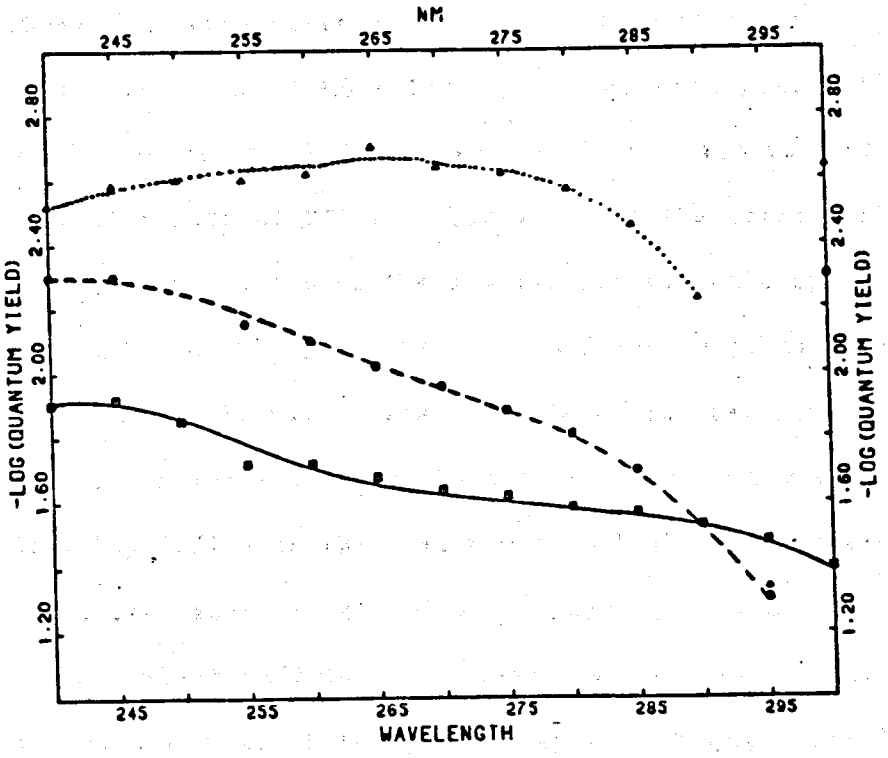

Figure 33. ϕ_f of cytidine at 143K in EGW solutions at pH's 4 (——), 7 (---) and 11.0 (...) versus wavelength of excitation. λ_f = 330 nm.

Similar plots were obtained from pH 2.0, 5.0 and 6.0 solutions, all of which showed the same decreasing quantum yield at higher excitation energies. In pH 7.0 solution, the quantum yield of cytidine at 240 nm is ca. .005 but is seen to increase to .032 or to that of the cation form at 270 nm. The shape of the curve reflects the difference in absorption of the neutral and cationic species of CD. The top curve in this graph was obtained from a pH 11.0 EGW solution. Quantum yield values are fairly constant near the middle of the band, but increase both on the low and high energy ends. This behavior probably indicates the presence of a highly fluorescence minor species, such as residual CD^+ or hydrogen bonded CD molecules. Data which will be shown later (see Figure 34) leads us to believe that the neutralization process is not quite complete at this pH, and thus, that the anomolous tails are caused by presence of the cationic species.

Figure 35 shows a plot of the quantum yield of CD for excitation at 270 nm versus the pH of EGW solutions at 143K. Two curves are presented, one obtained from experimental data (solid line) and the other calculated (dashed line), in the same manner as that for 5MC (see Figure 40). In the acidic region, the experimentally obtained quantum yield is seen to be high, near .023, but tails off below pH 4.0 and above pH 6.0. On the lower end, the decrease in quantum yield could be due to the presence of a doubly protonated species, unobserved at room temperature because of its highly acidic pK_a. Near neutrality, the decrease is most certainly due to the formation of neutral cytidine molecules. The quantum yield is seen to steadily

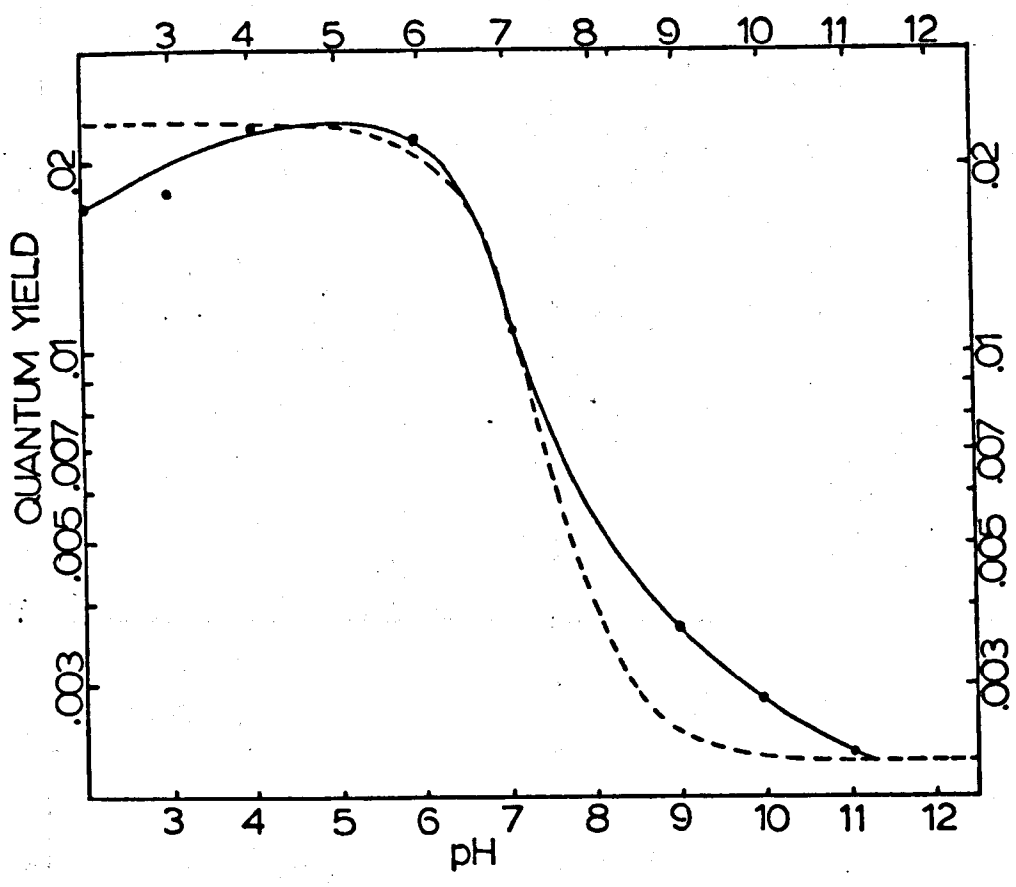

Figure 34. ϕ_f of cytidine in EGW solution at 143K versus pH. Experimental points (——) and calculated values (——) are included. λ_x = 270 nm.

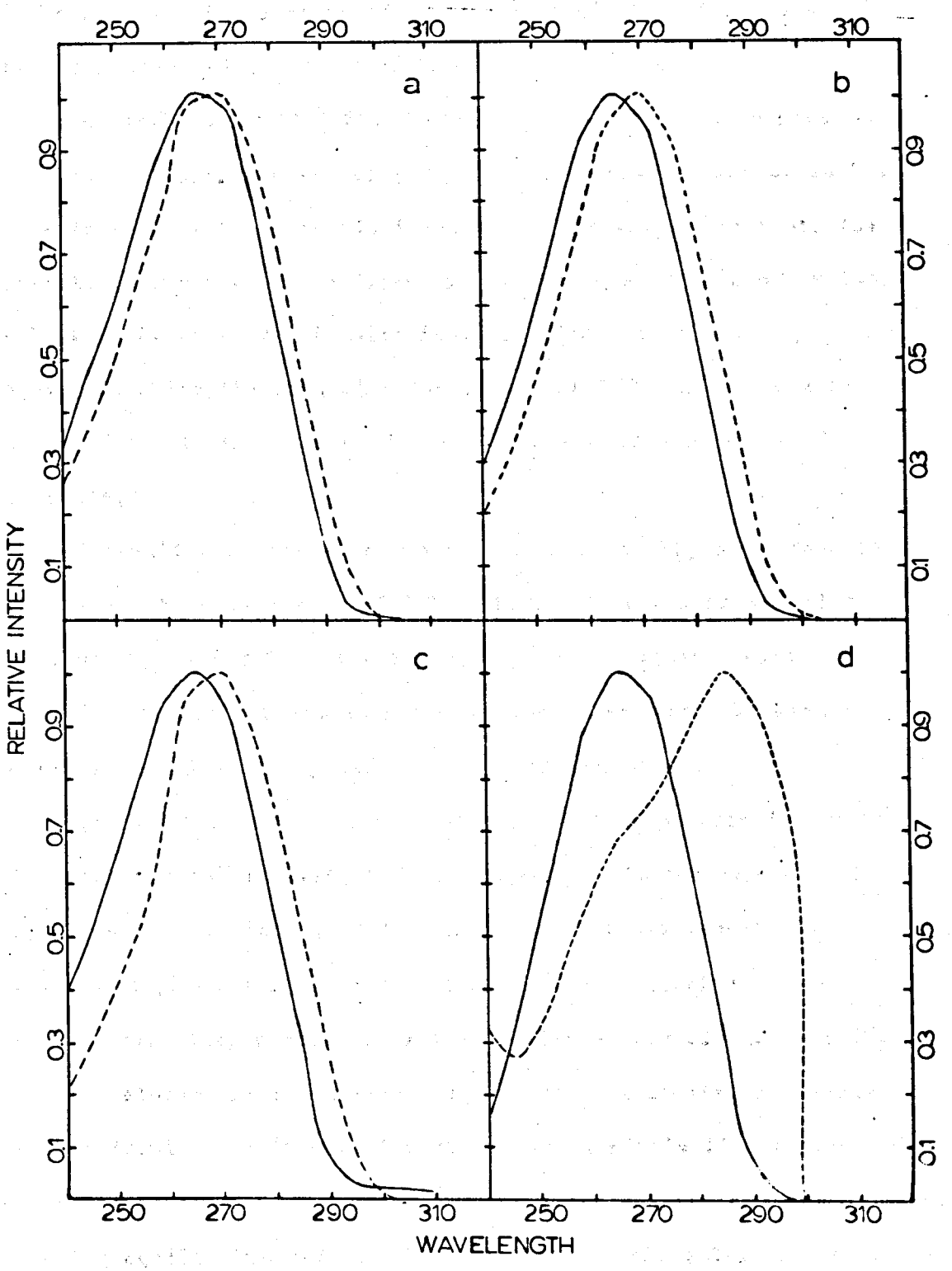

Figure 35. ABS (——) and FES (---) of thymine at 143K in EGW solutions of pH 1.5 (a), 4.0 (b) and 11.94 (d). λ_f = 330 nm.

decrease, reaching a value of .0023 or 10% of the cation ϕ_f at the last experimental point at pH 11.0.

Fox and Shugar (59) found the pK_a of CD to be 4.1 in aqueous solution at 298K. It is quite apparent that the pK_a for CD in EGW solutions at 143K is noncoincident with this value. In fact, the calculated curve shown in Figure 34 was produced from a pK_a value of 6.8, a difference of 2.7 units from that found at room temperature. Again, invoking the reasoning developed for 5MC, this change is to be expected due to the nature of the thermodynamic properties of the molecule.

You will note that the two curves shown in Figure 34 deviate widely in the region from pH 7.0 to 11.0. This result was also obtained by us for 5MC at room temperature in aqueous solution (28) though the effect there is not nearly as dramatic. We have not yet obtained a suitable explanation for this phenomenon.

As this thesis was being written, a paper appeared in the Soviet literature which investigated the anomalous fluorescence behavior of cytidine in EGW glass at 77K (40). These authors report that cytidine's pK_a has a value of 5.9 under their experimental conditions. They further note that a discrepancy of 2-5 nm still exists between the absorption and fluorescence excitation maxima of this molecule even in the pH region where a single fluorescence species exists. This noncoincidence is explained in terms of hydrogen bonding equilibrium between the cytidine and the solvent, e.g. the same argument invoked by Becker (39) in the case of thymine. The data presented here is in quite good agreement with this work with

the exception that we find pK_a of CD to be shifted to a slightly higher value of 6.8. Since our data was obtained under different conditions, the two results can only be viewed as supportive.

Thymine

Since the large anomolous shift in the excitation spectra for 5MC and CD relative to their absorption was explained so well by a shift in pK_a, we extended the work to thymine. Figure 35 displays the absorption and excitation of this molecule at pH's 1.5, 4.0, 8.0 and 11.94. At the low pH, thymine's ABS maxima occurs at 265 nm and its FES spectrum is shifted 3-4 nm to the red from this. Examination of the plots generated at pH 4.0 and pH 8.0 shows very little change from the corresponding spectra at pH 1.5.

In Figure 35 we see the ABS and FES of thymine in pH 11.94 EGW solution. The absorption spectrum is identical to that found in lower pH solutions. However, the excitation is shifted some 20 nm to lower energy.

An early study (13) on the anionic forms of thymine shows that two tautomers are present in basic solution 1(H)-thymine$^-$ and 3(H)-thymine$^-$, each of which are highly fluorescent even at room temperature. Spectra presented in this work were from 0.01 N NaOH where the ABS maximum for thymine was ca. 290 nm.

Shugar and Fox (59) found the pK_a of thymine at 298K to be 9.9. From the scant evidence shown above, it is apparent that this value is incorrect for EGW solutions at 148K. That thymine's absorption spectrum is still dominated by the neutal species at pH 11.94 alerts

us that the pK_a is greater than this value. This is not surprising in light of our previous discussion on the temperature dependency of molecules with high positive ΔH's of ionization.

Quantum yields ($\lambda_f = 265$) for thymine of .034, .026, .023 and .044 were obtained at pH's 1.5, 4.0, 8.0 and 11.94, respectively. Plots of the quantum yields from three of these solutions (pHs 1.5, 8.0 and 11.94) versus wavelength of excitation are shown in Figure 36. You will note that very little difference exists between the curves at 1.5 and 8.0, a fact which supports the notion that thymine exists as a neutral molecule throughout the pH range of 1.5 to 8.0. Since almost all low temperature fluorescence measurements on thymine in EGW were performed in neutral solution, anomolous speciation could not have been the cause of this molecule's slight wavelength of excitation dependent ϕ_f.

Examination of the top curve in Figure 36 reveals that thymine's quantum yield is highly wavelength dependent at pH 11.94. The source of this dependency is most certainly the presence of the thymine anion which is highly fluorescent.

Summary and Conclusions

Each proposed explanation for the wavelength of excitation dependency found in the quantum yields of the DNA bases was examined as to application to 5MC, cytidine and thymine.

Results for thymine rule out all possibilities except that of preferential fluorescence from hydrogen bonded species. Spectra obtained from this molecule in non-aqueous solution at low

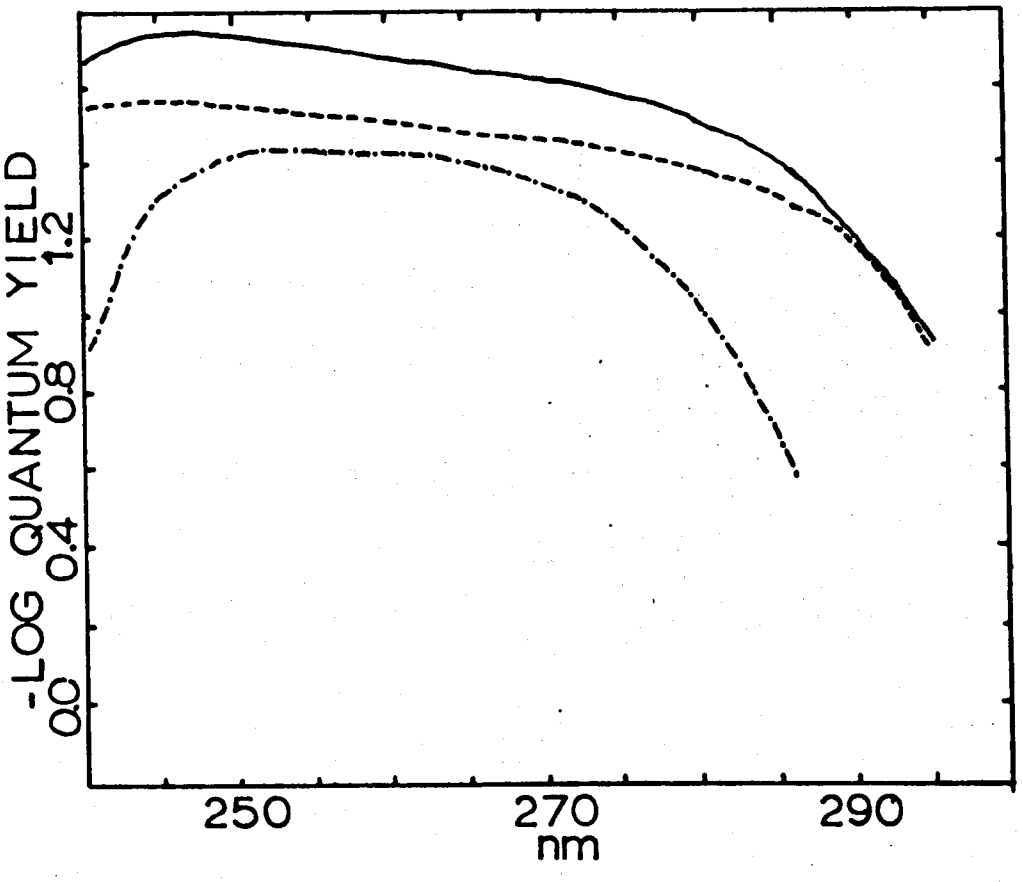

Figure 36. ϕ_f of thymine at 143K in EGW solutions at pH's 1.5 (——), 8.0 (---) and 11.94 (·—) versus wavelength of excitation. λ_f = 320 nm.

temperature showed nearly coincident excitation and absorption. Our results supported earlier findings (39) and, indeed, this proved to be the only reasonable explanation for the wavelength dependency found in the quantum yield of this biologically important molecule. The small amount of mismatch remaining between the ABS and FES of thymine should be experimental error, or possibly a manifestation of competitive deactivational pathways.

Additional experiments performed on thymine in different pH EGW glasses at 143K showed that the pK_a of thymine is shifted at least 2 units higher to around 12.0. However, this shift cannot possibly effect the photophysical properties of thymine in the pH 7 EGW glasses normally employed in fluorescence measurements on neutral thymine.

Fluorescence data was obtained for 5MC in several different solvents at low temperature. Results from non-aqueous solvents were conflicting in many cases. Several spectra obtained from EM glasses at 123K showed perfect matches between the absorption and excitation. However, a number of spectra displayed an anomalous relationship between the absorption and fluorescence excitation of 5MC. These results were correlated to the acidity or lack of it, of the EM solutions.

The cation was found to exist solely or in mixture with neutral 5MC up to pH 9.0 or greater. Quantum yield values were found to be .35 and .05 in EGW glasses at 143K for $5MC^+$ and 5MC. At pH 11.65, a near perfect match between the ABS and FES was found, indicating

that fluorescence is intrinsic to a single emitting species. Also, at acidic pH's (2-6), the ABS and FES of 5MC was found to coincide very well. In addition, the shift of 5MC's fluorescence spectrum with varying excitation wavelength was found to be a consequence of the existence of two emitting species in solution at pH 7.0, each with different fluorescence spectra. At this pH, a rather large phosphorescence occurs near 425 nm. The excitation spectrum of this phosphorescence proved to be a perfect match of the neutral absorption, while excitation of the fluorescence at 330 nm resembled the cation absorption.

It was found that the pK_a of 5MC shifts from 4.6 at 298K in aqueous solution to near 7.0 in EGW at 143K. The consequence is that at pH 7.0, both 5MC and $5MC^+$ are formed in solution, leading to the apparent shift in the excitation spectrum.

In addition, the pH dependency of cytidine's fluorescence in low temperature solution was examined. This molecule proved to exhibit the same shift in pK_a as was the case for 5MC. A plot of ϕ_f vs. pH was produced which showed that the pK_a in EGW glass at 143K was near 6.8. The ABS and FES of this molecule, however did not completely match even in the pH regions where only one species was known to exist. Hydrogen bonding equilibrium, e.g. the theory used to explain thymine's anomolous fluorescence properties, is concluded to be responsible for the remainder of cytidine's fluorescence FES shift. These results are in good agreement with those found independently (41).

TWO PHOTON EXCITATION OF BENZIMIDAZOLE

Results and Discussion

Figure 37 shows the one photon absorption (dashed line) and two photon fluorescence excitaton spectrum (solid line) along with the ratio of two photon excited fluorescence intensity obtained with circularly and linearly polarized light (dark circles) of benzimidazole (BMD). The highest peaks in both spectra are normalized to one and the wavelengths of the OPA spectrum are marked on the upper axis.

At first glance, the features of the two spectra look quite dissimilar. However, their 0 - 0 bands and the first vibrational progressions (the small hump in the TPE at 544 nm and the second peak in the OPA) appear at nearly the same wavelengths. You should also note that the relative heights of these peaks are the same in both spectra.

At energies above that of the second peak, the two spectra seemingly have no features in common. A very intense peak appears in the TPE at 536.5 nm along with a smaller one at 522 nm. Both of these are absent or of much smaller intensity in the OPA. Also, the large band seen in the OPA peaking at 245 nm (490 nm) is not seen in the TPE. Below 440 nm (220 nm), both spectra begin to rise rapidly. Data was collected down to 403 nm in the TPE, at which point

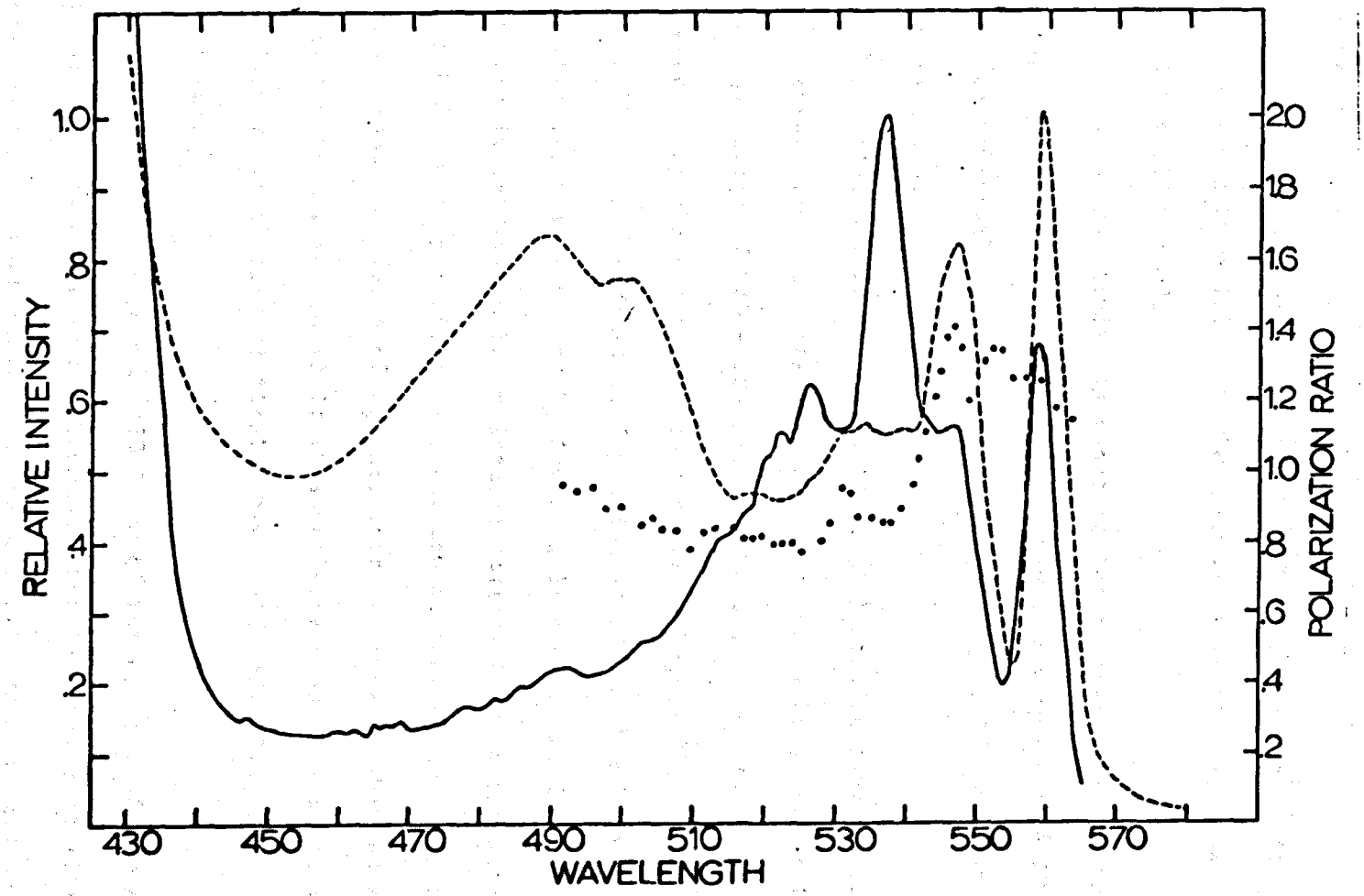

Figure 37. OPA (——), TPE (——) and circular/linear polarization ratios of benzimidazole at room temperature in 50% cyclohexane and 50% isopropanol solution.

the intensity was ca. 5 times that of the 536.5 nm band, and still increasing.

Ratios of circular:linear excited fluorescence intensity are fairly constant from 490 nm to 540 nm, but rise sharply near the red edge of the third peak.

Due to the difficulty in constructing accurate TPE spectra, the relative peak heights in the BMD spectrum may vary up to ± 10%. Also, the polarization ratios presented in Figure 37 could be in error by ± .05.

Experimental (81) and theoretical (82) studies have shown that two separate electronic states account for BMD's UV spectrum in the wavelength range of 240 - 285 nm. The lowest energy band, represented by the first two sharp peaks in Figure 37, is L_b-like in nature. The broad, diffuse band peaking at 245 nm has been dubbed L_a. Note that the use of L_b and L_a for transitions in BMD is incorrect. Their use is only valid for molecules fitting Platt's perimeter model (44) but for making analogy with the transitions of benzene, they will be retained. Bands of L_b character in aromatic systems are invariably well resolved while those arising from ground state to L_a transitions are characteristically broad and only slightly structured.

Peaks 1 (280 nm) and 2 (273.5 nm) of the L_b band of BMD are separated by 816 cm^{-1}, so the third and fourth members of this progression are expected at 267.5 nm and 261.8 nm, respectively. However, due to the broadness of the L_a band, these peaks are quite obscured. Also, the overlap of the two bands makes it impossible to

discern the 0 - 0 transition of the L_a. So, the small bumps seen in the OPA of BMD in Figure 37 between 255 nm and 270 nm could be due to either vibronic or Franck-Condon transitions within the manifolds of either L_b or L_a.

BMD's L_a band is very solvent dependent in that it red-shifts proportionally to the polarity of the solvent. The ABS seen in Figure 37 was taken in 50% isopropanol:50% cyclohexane, so the separation of L_a and L_b are almost at a minimum. When acid is added to BMD solutions to form cations (BMD+), the separation between L_a and L_b becomes even less and, in fact, L_a (due to its broadness) becomes almost degenerate with L_b. This leads to the very curious property of dual emission from BMD+ (83,84), a phonomenon which has been reported for other molecules (85). Callis and Mansanti (84) have viewed the fluorescence of BMD+ and found that two peaks are present in the emission spectrum, one hump with a maximum near 300 nm corresponding to L_b fluorescence, and another peak at 360 nm due to L_a fluorescence. If the acidic solutions, e.g. EGW or glycerol, are cooled to form a rigid glass, the proportion of molecules emitting from the L_b excited state becomes greater than those emitting from L_a.

Published reports on the deconvolution of the L_b and L_a bands of benzimidazole have not been forthcoming, a fact which introduces some difficulty in the upcoming discussion of the TPE of BMD. However, some attempts have been made to distinguish between the L_b and L_a

bands of indole, a molecule which differs from BMD only in its lack of a geometrically opposed nitrogen atom.

Indole's first two UV absorption bands are nearly degenerate. Fluorescence studies (86) of neutral indole have shown that L_a is the lowest excited state in this molecule in water with L_b lying slightly above it in energy. Transition moments of the two bands were found to be oriented at -38° and 56° relative to the long molecular axis and the oscillator strengths are reported to be 0.112 and 0.010 for L_a and L_b, respectively (86). The ratio of these oscillator strengths are ca. 11:1, which is quite questionable in view of the polarized excitation work done by Valuer and Weber (87). Their results show the strength of L_a to be less than 3 times that of the L_b. Strickland, Horwitz and Billups (88) have reported the positions of the 0 - 0 L_a transition of indole. Relying on the property that L_a and L_b shift in opposite directions in different polarity solvents, they have been able to separate the peaks due to L_a transitions from those arising from L_b. In methylcyclohexane, indole shows peaks at 730 cm^{-1}, 973 cm^{-1}, 1310 cm^{-1}, 1723 cm^{-1}, 1973 cm^{-1}, 2673 cm^{-1} and 3423 cm^{-1} above the L_b 0 - 0 transition. Through comparsions with the UV spectra of indole in the gas phase and in perfluorinated hexane, the transitions occurring at 730 cm^{-1} and 1310 cm^{-1} are shown to lie within the L_b manifold. The peak found at 973 cm^{-1} is designated the L_a 0 - 0 transition. Vibrational components of L_a are at 750 cm^{-1}, 1000 cm^{-1}, 1700 cm^{-1} and 2450 cm^{-1} relative to its' 0 - 0.

Figure 38 shows the UV absorption of BMD in cyclohexane (A), 10% isopropanol-90% cyclohexane (B) and 50% isopropanol-50% cyclohexane (C) by volume. The data in curve A shows the L_a maximum to be 5650 cm^{-1} more energetic than the L_b 0 - 0. In the 10% isopropanol solution this maximum has red-shifted 406 cm^{-1} and you will note that a new peak appears at 2841 cm^{-1} to the blue of the L_b 0 - 0 and 2403 cm^{-1} to the red of the L_a maximum. Since the L_a maximum in B is blue-shifted 1821 cm^{-1} from the corresponding peak in indole in methylcyclohexane (relative to L_b 0 - 0), we would expect to find the L_a 0 - 0 of BMD at L_b +2794 cm^{-1} (1821 + 973), or $L_{a(max)}$ -2450 cm^{-1}, that is assuming the L_a and L_b manifolds of the two molecules are the same. That these expected values correlate so closely with those found experimentally lead us to designate the hump in the second absorption minimum as the L_a 0 - 0 transition. The spectrum in C of Figure 38 is the same as that shown in Figure 37 and was included to show that the UV spectrum of the solution used in the TPE studies is indifferentiable from the 10% - 90% isopropanol-cyclohexane spectrum.

Returning to our discussion of BMD's TPE, we see that the first two transitions in the L_b band shown in Figure 37 are quite visible in the TPE. They are separated by 786 cm^{-1}, very close to the 816 cm^{-1} separation seen in the OPA and the polarization ratio, Ω (where $\Omega = F_c/F_l$ and F_c is the fluorescence intensity under circularly polarized excitation and F_l is the corresponding value for linearly polarized illumination) is very high throughout each peak which is indicative that both have the same state symmetry, one which is different than that of the ground state. These transitions,

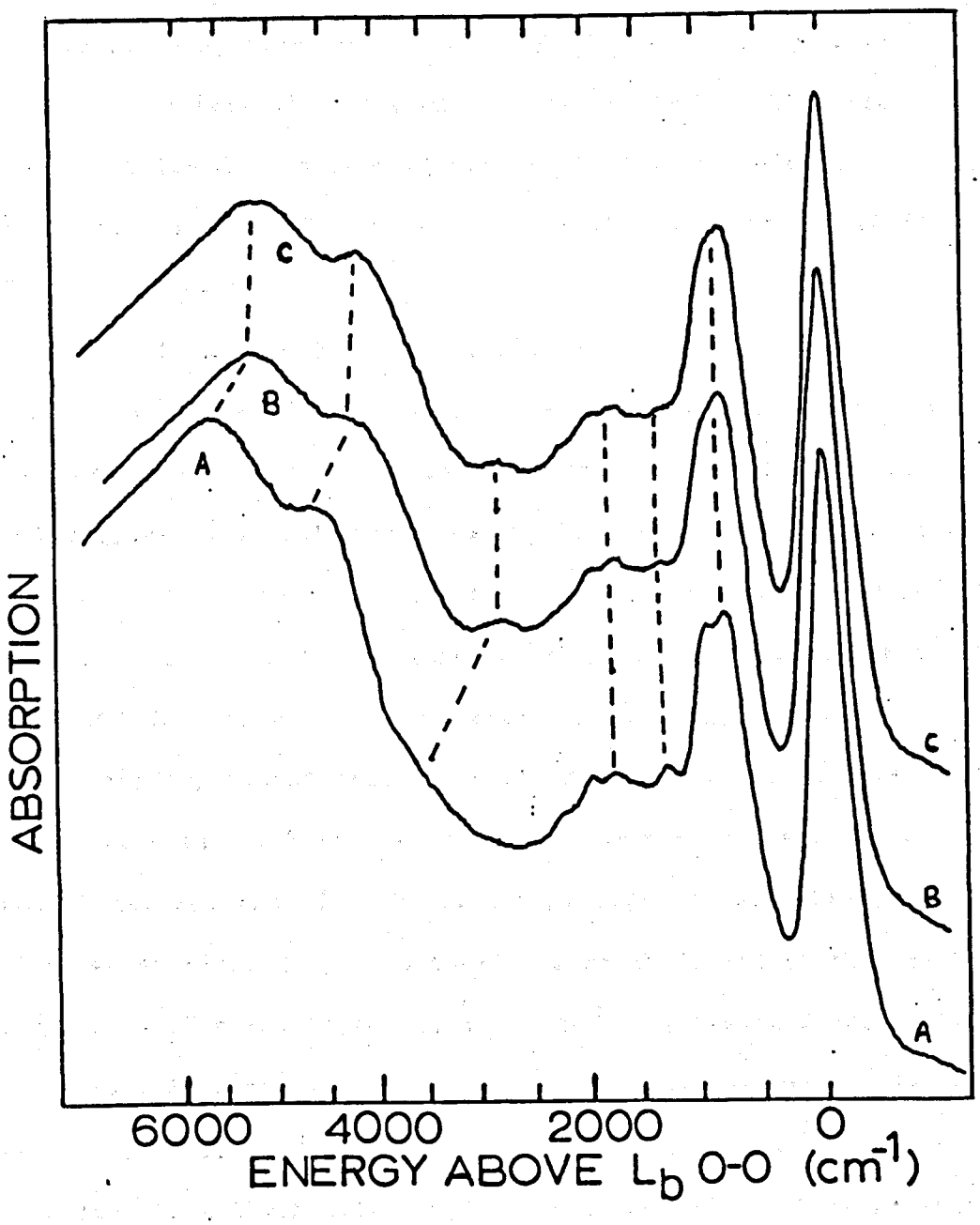

Figure 38. ABS of BMD in cyclohexane (bottom), 10% isopropanol-90% cyclohexane (middle) and 50% isopropanol-50% cyclohexane (top). The x axie represents energy above the L_b 0-0 transition.

therefore, clearly comprise part of the Franck-Condon allowed portion of the L_b band. Viewing the higher energy portion of the TPE, we see that the large L_a component seen in the OPA is entirely missing or is much lower in intensity, proportionally to the L_b. The rise in intensity below 440 nm is most definitely due to one of the strong B-like states of BMD. Thus we are left with the two peaks at 536.5 and 522 nm to explain.

Since the L_a 0 - 0 is expected to occur at 517 nm, L_a transitions can be effectively ruled out as possible candidates for these two peaks. You will note, however that a small hump appears in the OPA spectrum directly underneath the 523 nm TPE peak and that bumps are present below the 536.5 nm transition. Third and fourth members of L_b's Franck-Condon progression should be found at 535 nm and 523.6 nm, respectively. However, these should be lower, proportionally, in intensity than the 0 - 0. We should note, too, that these have not been viewed in the vapor phase spectrum of indole (88). This, coupled with the fact that this circular/linear polarization ratio drops drastically near the onset of the 536.5 nm band, makes it possible to eliminate it being Franck-Condon allowed.

Figure 39 shows the TPE spectrum of BMD along with a plot of the relative intensity of benzene's L_b band, which is known to gain intensity through vibronic coupling. The relative height of the two spectra were found experimentally by taking ratios of the fluorescence intensity of BMD and benzene at several different wavelengths under the same conditions of excitation. These ratios were then corrected for concentration and relative fluorescence

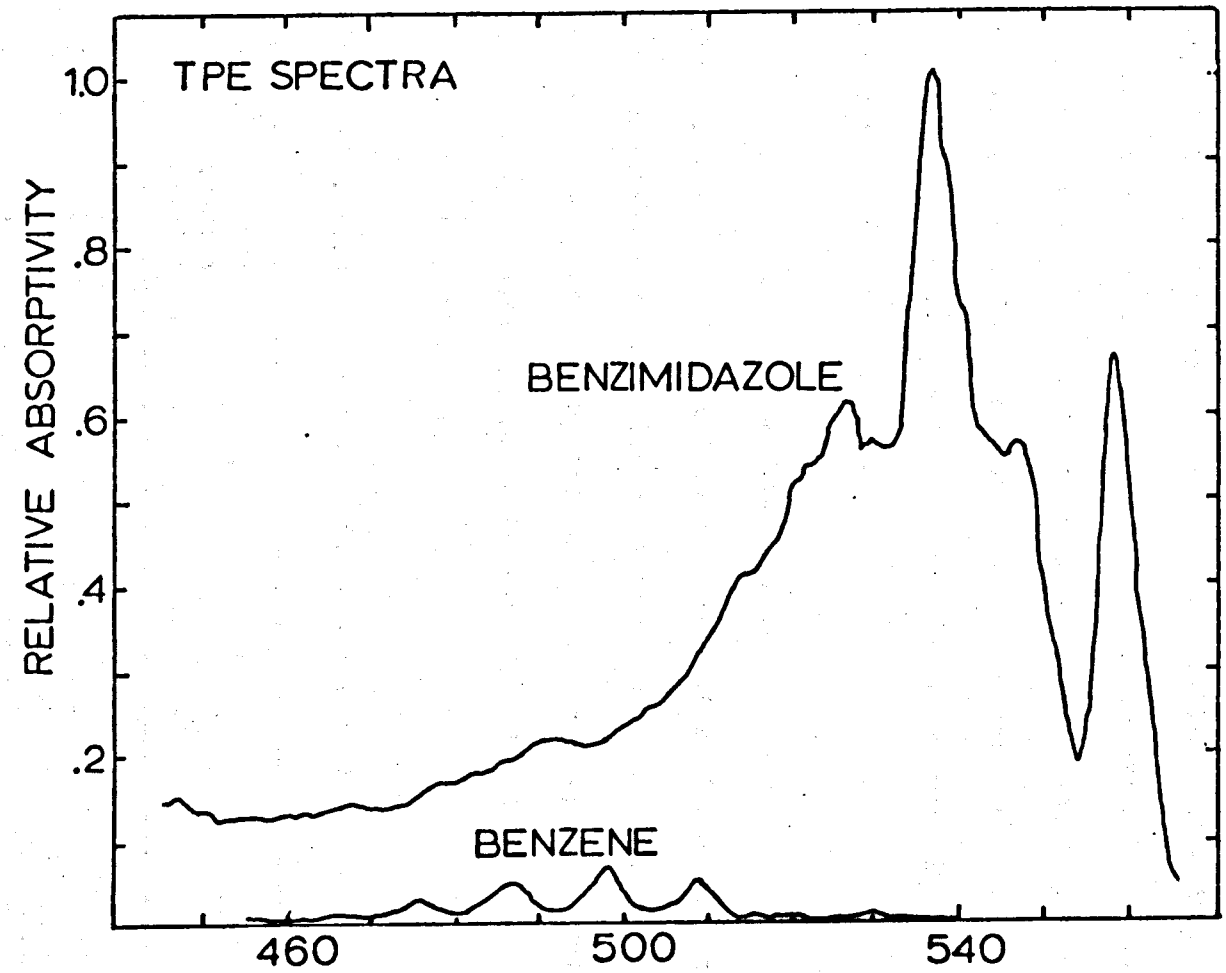

Figure 39. Relative TPE intensity of BMD and benzene.

intensity differences. Admittedly, this ratio could be in error by a factor of two. From the figure, we see that BMD's relative two photon absorptivity is a factor of 10 greater than that of benzene. However, if the 536.5 nm transtion is built on other transitions, the area under the peak is at most twice that of benzene's L_b. Also, this peak occurs at L_b +1524 cm^{-1} which is very close to the $_{14}$ vibrational frequency found in benzene. The second peak, at 523 nm, is much lower in intensity and could be the second peak in the $_{14}$-like progression of benzimidazole.

CNDO Calculations

Table 6 lists the lowest four $\pi \rightarrow \pi^*$ states of BMD and their pertinent spectral data as calculated from CNDOS-CI (89). These calculations were performed by the author on the campus Honeywell 66 computer. Singly excited states only were included in the configuration interaction calculations.

Table 6. Calculated spectral data for benzimidazole.

States	OPA transition wavelength	f_{osc}	δ_G $10^{-43} cm^6$	Ω
L_b	284.8	.046	122.2	1.46
L_a	249.5	.288	341.9	0.96
B	219.2	.289	1502.6	0.72
B	204.5	.783	125.6	1.10

Values of δ_G are found by summing the squares of the two photon tensor elements of a state. The individual tensor elements are obtained by use of the following equation (90),

$$S_{AB} = \sum_i \left[\frac{\langle \psi_o | M_A | \psi_i \rangle \langle \psi_i | M_B | \psi_f \rangle}{E_i - h\nu_1} + \frac{\langle \psi_f | M_A | \psi_i \rangle \langle \psi_i | M_B | \psi_o \rangle}{E_i - h\nu_2} \right] \quad [51]$$

where the subscripts o, i and f are for intermediate and final states, A and B are the cartesian coordinates X, Y and Z, M's are for transition moments between the initial, intermediate and final states, E_i are the eigenvalues of the intermediate states, ψ's are the wavefunctions of the states included in the calculations and sums are over all possible states, initial and final inclusive.

Polarization ratios ($\delta_{cir}/\delta_{lin}$) are obtained through the use of the following equation (92),

$$\Omega = \frac{\delta_{cir}}{\delta_{lin}} = \frac{-2\delta_F + 6\delta_G}{2\delta_F + 4\delta_G} \quad [52]$$

where

$$\delta_F = \frac{\sigma}{30} \sum_A S_{AA} \cdot \sum_B S^*_{BB} = (TrS)^2 \quad [53]$$

$$\delta_G = \frac{\sigma}{30} \sum_A \sum_B S_{AB} S^*_{AB} = Tr(S^2) \quad [54]$$

and

$$\sigma = 4\pi^4 \nu_1 \nu_2 / c^2 \quad [55]$$

where ν_1 and ν_2 are the frequencies (in cm^{-1}) of the two photons being absorbed. The theoretical range of Ω is from 0.0 - 1.5 for

transitions which involve no change in state symmetry, but can only be 1.5, where changes in state symmetry occur.

First, you should note that the predicted wavelengths of the OPA 0 - 0's of L_b and L_a are qualitatively correct. The oscillator strength of L_a is overestimated by a factor of 3 but that of L_b is approximately correct. The most surprising result shown here is that δ_G for the L_a band is predicted by CNDO to be 3 times larger than δ_G for L_b. Since these calculations were performed previous to the experiments, we were quite surprised to find only subtle hints of L_a in the TPE of BMD. Subsequent calculations performed on slightly different geometries of BMD have shown that the TPA intensity of L_a is very sensitive to molecular perturbations. This problem is presently receiving attention and a further discussion will be included in our upcoming publication.

Conclusion

The two photon fluorescence excitation and circular/linear polarizations of benzimidazole were presented and analyzed. An overwhelming majority of the two-photon absorptivity is seen to be due to transitions in the L_b band while L_a, though predicted by CNDO-CI methods to be quite strong, is missing in the TPE spectrum. Two peaks, not seen in the UV spectrum of BMD, are seen in the TPE and these are believed to be vibronic components of the L_b band.

In addition, the 0 - 0 transition of benzimidazole's L_a band in the OPA spectrum is identified, to our knowledge, for the first time. Further studies are now being performed in our lab to more firmly

characterize the TPE of benzimidazole. Transition densities between excited states have been obtained and are in the process of being interpreted in order to find out what states effectively couple with L_b to produce strong vibronic transitions. Also, additional UV absorption spectra will be taken to confirm our assignment of the L_a 0 - 0 and to attempt to view the vibronic transitions seen in benzimidazole's TPE.

LITERATURE CITED

1. Daniels, M., "Photochemistry and Photobiology of Nucleic Acids," Ed. S.Y. Wang, Academic Press, NY (1976); Callis, P.R., "Annual Reviews of Physical Chemistry", 1983 (in press).

2. Daniels, M. and Hauswirth, W. W., Science, 171, 675 (1971).

3. Strickler, S. J. and Berg, R. A., J. Chem. Phys., 37, 814 (1962).

4. Eisinger, J., Photochem. Photobiol., 7, 597 (1968).

5. Callis, P. R., Chem. Phys. Lett., 61, 563 (1979).

6. Morgan, J. P. and Daniels, M., Photochem. Photobiol., 27, 73 (1978).

7. Longworth, J. W., Rahn, R. O. and Shulman, R. G., J. Chem. Phys., 45, 2930 (1966).

8. Borresen, H. C., Acta. Chem. Scand., 19, 2100 (1965).

9. Borresen, H. C., Acta. Chem. Scand., 21, 920 (1967).

10. Borresen, H. C., Acta. Chem. Scand., 21, 2463 (1967).

11. Drobnik, J. and Augenstein, L., Photochem. Photobiol., 5, 83 (1966).

12. Eastman, J. W., Ber. Bunsenges Physik Chem., 73, 907 (1969).

13. Berens, K. and Wierzchowski, K. L., Photochem. Photobiol., 9, 433 (1969).

14. Kleinwachter, Y. and Kondelka, J., Coll. Czech. Chem. Comm., 37, 3433 (1972).

15. Wilson, R. W., Morgan, J. P. and Callis, P. R., Chem. Phys, Lett., 36, 618 (1975).

16. Hauswirth, W. and Daniels, M., Photochem. Photobiol., 13, 157 (1971).

17. Daniels, M., Proc. Natl. Acad. Sci., U.S.A., 69, 2488 (1972).

18. Knighton, W. B., Master's Thesis, Montana State University, Bozeman, Montana (1980).

19. Vigny, P. and Duquesne, "Excited States of Biological Molecules," Ed. J.B. Birks, Wiley-Interscience, NY (1976).

20. Knighton, W. B., Giskas, G. O. and Callis, P. R., J. Phys. Chem., 86, 49 (1982).

21. Wilson, R. W. and Callis, P. R., Photochem. Photobiol., 31; 323 (1980).

22. Spencer, M., Acta. Cryst., 12, 59 (1959).

23. Mezey, P. G. Ladik, J. J. and Barry, M., Theoret. Chim. Acta (Berl.), 54, 251 (1980).

24. Eastman, J. W. and Rosa, E. J., Photochem. Photobiol., 7, 189 (1968).

25. Mezey, P. G. and Ladik, J. J., Theoret. Chim. Acta. (Berl), 52, 129 (1979).

26. Lewis, T. P. and Eaton, W. A., J. Amer. Chem. Soc., 93, 2054 (1971).

27. Callis, P. R. and Simpson, W., J. Amer. Chem. Soc., 92, 3593 (1970).

28. Anderson, B. E. and Callis, P. R., Photochem. Photobiol., 32, 1 (1980).

29. Matsuka, Y. and Norden, B., J. Phys. Chem., 86, 1378 (1982).

30. Fucaloro, A. F. and Forster, L. S., J. Amer. Chem. Soc., 93, 6443 (1971).

31. Sprecher, C. A. and Johnson, W. C., Biopolymers, 16, 2243 (1977).

32. Sutherland, J. C. and Holmquist, B., Ann. Rev. Biophys. Bioeng., 9, 293 (1980).

33. Stewart, R. F. and Davidson, N., J. Chem. Phys., 39, 253 (1963).

34. Eaton, W. A. and Lewis, T. P., J. Chem. Phys., 53, 2164 (1970).

35. Morgan, J. P. and Daniels, M., J. Phys. Chem., 86, 4004 (1982).

36. Abramson, A. S., Spears, K. G. and Rice, S. A., J. Chem. Phys., 56, 2291 (1972).

37. Yamazaki, I., Fujita, M. and Baba, H., Chem. Phys., 57, 431 (1981).

38. In the absence of my advisor, Dr. R. Howald of Montana State University lent guidance and assistance to myself and my lab partner, Tim Aoki.

39. Becker, R. S. and Kogan, G., Photchem. Photobiol., 31, 5 (1980).

40. Rapoport, V. L. and Bakuler, V. M., Bull. Leningrad State Univ. (Physics and Chemistry), 90 (1982).

41. Rapoport, V. L. and Bakulev, V. M., Optics and Spectroscopy, 52, N6, 1054 (1983).

42. Mason, S. F., "The Pyrimidines," Ed. D. S. Brown, Wiley-Interscience, NY (1962).

43. Chen, H. H. and Clark, L. B., J. Chem. Phys., 51, 1862 (1969).

44. Platt, J., J. Chem. Phys., 17, 484 (1949).

45. Murrel, J. N. and Pople, J. A., Pro. Proc. Phys. Soc., (London), A69, 245 (1956).

46. Friedrich, D. M. and Mclain, W. M., Ann. Rev. Phys. Chem., 31, 559 (1980).

47. Mahr, H., "Quantum Electronic: A Treatise," Eds. H. Robin and C. L. Tang, Vol. IA, Academic Press, NY (1975).

48. Goppert-Mayer, M., Ann. Phys., (Leipzig), 9, 273 (1931).

49. Abella, I. D., Phys. Rev. Letters, 9, 453 (1962).

50. Goodman, L. and Rava, R., "Advances in Chemical Physics," Eds. I. Prigogine and S. A. Rice, Vol. 54, Wiley, NY (1983).

51. Callis, P. R., Scott, T. W. and Albrecht, A. C., J. Chem. Phys., 75, 5640 (1981).

52. Callis, P. R., Scott, T. W. and Albrecht, A. C., J. Chem. Phys., 78, 16 (1983).

53. Scott, T. W., Callis, P. R. and Albrecht, A. C., Chem. Phys. Lett., 93, 111 (1982).

54. Melhuish, W. H., J. Opt. Soc. Amer., 52, 1256 (1962).

55. Parker, C. A., "Photoluminescence of Solution," Elsevier, Amsterdam (1968).

56. Aoki, T. I., Ph.D. Thesis, Montana State University, 1982.

57. Bridges, J. W. and Williams, R. T., Biochem. J., 107, 225 (1968).

58. Callis, P. R., Personal communication.

59. Shugar, D. E. and Fox, J. J., Biochim. Biophys. Acta., 9, 199 (1952).

60. Perrin, F., Compte. Rend., 80, 581 (1925).

61. Gill, J. E., Photochem. Photobiol., 11, 259 (1970).

62. Bauer, D. R., Brauman, J. I. and Pecora, R., J. Amer. Chem. Soc., 96, 6840 (1974).

63. Edward, J. T., J. Chem. Ed., 47, 261 (1970).

64. Weber, G., Biochemistry, 51, 145 (1952).

65. Albrecht, A. C., J. Mol. Spectrosc., 6, 84 (1961).

66. Wong, Y. P., J. Amer. Chem. Soc., 95, 3511 (1973).

67. Goddard, J. P., Mezey, P. G. and Csizmadia, I. G., Theoret. Chim. Acta. (Berl), 39, 1 (1975).

68. Czcinirski, R., Lesyng, B. and Pohorille, A., Int. J. Quant. Chem., 16, 605 (1979).

69. Yu, C., Peng, S., Akiyama, I., Lim, J. and Lebreton, P.R., J. Amer. Chem. Soc., 100, 2303 (1978).

70. Barber, D.L. and Marsh, R.E., Acta. Cryst., 17, 1581 (1964).

71. Dreyfus, M., Bensande, O., Dodin, G. and Dubois, J. E., J. Amer. Chem. Soc., 98, 6338 (1976).

72. Johnson, W. C., Jr., Vipond, P. M. and Girod, J. C., Biopolymers, 10, 923 (1971).

73. Gerdi, R., Acta. Cryst., 14, 333 (1961).

74. Weber, G. and Teale, F. W. J., Trans. Faraday Soc., 53, 646 (1957).

75. Birks, J. B., "Photophysics of Aromatic Molecules," Wiley-Interscience, NY (1970).

76. Fisher, G. J. and Johns, H. E., Photochem. Photobiol., 11, 429 (1970).

77. Brown, I. H. and Johns, H. E., Photochem. Photobiol., 8, 273 (1968).

78. Takemura, T., Das, P. K., Hug, G. and Becker, R. S., J. Amer. Chem. Soc., 100, 2626 (1978).

79. For example, see: Itoh, K. and Azumi, T., J. Chem. Phys., 62, 3431 (1975).

80. Weast, R. C., Ed., Handbook of Chemistry and Physics, 9th ed., The Chemical Rubber Company, Cleveland (1971).

81. Passerini, R., J. Chem. Soc., 2256 (1954).

82. Kamiya, M., Bull. Chem. Soc. Jap., 43, 3344 (1970).

83. Kondo, M. and Kuwano, H., Bull. Chem. Soc. Jap., 42, 1433 (1969).

84. Mansanti, J. and Callis, P. R., unpublished results.

85. Suzuki, S., Fujii, T., Imai, A. and Akahori, H., J. Phys. Chem., 81, 1592 (1977) and references therein.

86. Yamamoto, Y. and Tanaka, J., Bull. Chem. Soc. Jap., 45, 1362 (1972).

87. Valeur, B. and Weber, G., Photochem. Photobiol., 25, 441 (1977).

88. Strickland, E., Horowitz, J. and Billups, C., Biochem., 9, 4914 (1970).

89. Ellis, R., Kuehnlenz, H. and Jaffe, H., Theor. Chim. Acta, 26, 131 (1972).

90. Marchesse, F., Seliskar, C. and Jaffe, H., J. Phys. Chem., 72, 4194 (1980).